Molecular Diffusion and Self-Organization on Metal Surfaces: Sub-Phthalocyanine on Ag(111)
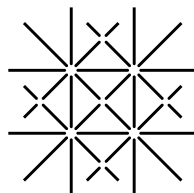
Simon Berner

aus Schafisheim (Aargau)

Basel, 2002

UNI
BASEL

Genehmigt von der Philosophisch-Naturwissenschaftlichen Fakultät auf Antrag von:

Prof. Dr. H.-J. Güntherodt
Dr. T.A. Jung
Prof. Dr. P. Oelhafen

Basel, den 2. Juli 2002

Prof. Dr. A.D. Zuberbühler, Dekan

Abstract

The adsorption and layering of chloro[subphthalocyaninato]boron(III) (SubPc) on Ag(111) has been studied in detail by means of Scanning Tunneling Microscopy (STM) and photo-electron spectroscopy at room temperature. SubPc is a polar molecule with an aromatic 14-π-electron system. An interesting phase behavior is observed for the first molecular layer of SubPc growing on Ag(111). At a coverage below $\approx$ 0.2 monolayer (ML), only a two-dimensional (2D) lattice gas is present, whereas at a coverage in the order of 0.2–0.5 ML two-dimensional condensed molecular islands are in coexistence with the 2D lattice gas. In these condensed islands, the molecules self-organize into well ordered overlayers with a honeycomb pattern which has a low packing density. At a coverage of 0.6–0.9 ML the molecules self-organize into a 2D hexagonal close packed (hcp) pattern. This hcp pattern is observed in coexistence with a dense 2D gas phase. For the honeycomb and the hcp pattern, individual molecules are imaged with sub-molecular resolution. Typically the molecules are imaged as characteristic three lobes. The coexistence of the honeycomb pattern with the 2D lattice gas is studied in detail. A dynamic equilibrium of the condensed honeycomb phase with its gas phase by exchange of molecules is observed. The energy barrier for surface diffusion as well as the condensation energy to form 2D islands is estimated and discussed.

Interesting and unusual features of the ordered molecular overlayers are observed. For each pattern, the honeycomb and the hcp, only two different orientations with respect to the Ag(111) substrate exist. For the honeycomb pattern, the two different orientations have different chirality, although the SubPc molecule itself is achiral. Not only single SubPc molecules show diffusion but also whole ordered islands exhibit mobility. This becomes evident in the observed flipping process of overlayers, where whole condensed islands change their orientation between the two stable orientations of the pattern. In the case of the honeycomb pattern, this constitutes a transition between the two chiral layers. Phase transitions from the gas phase to the condensed hcp phase and vice versa of whole overlayer islands could be controlled by the STM tip. In vacancy islands of the Ag(111) surface produced by sputter defects, it is possible to reversible change the phase of the confined molecular overlayer by tip induced experiments. The two phases, the hcp phase and the gas phase, exist at the same conditions at room temperature. Therefore one of these two phases is thermodynamically not favored and in a metastable state. A microscopic model based on the electric field between tip and sample is proposed for this tip-controlled phase transition.

In addition to the STM experiments the adsorption geometry and the electronic structure of SubPc on Ag(111) is studied by means of photoelectron spectroscopy. It is observed that the intact SubPc molecule is mainly physisorbed on the Ag(111) with the Cl towards the Ag surface. The π-electron system of the molecule undergoes only slight changes upon adsorption on the Ag surface. In general, the observed features of the molecular overlayers are attributed to the charge distribution of SubPc and to its resulting dipole moment.

Contents

Abbreviations

2D	Two dimensional
AES	Auger electron spectroscopy
DFT	Density functional theory
DOS	Density of states
ESCA	Electron spectroscopy for chemical analysis
hcp	Hexagonal close packed
HOMO	Highest occupied molecular orbital
HOPG	Highly ordered pyrolytic graphite
LDOS	Local density of states
LEED	Low energy electron diffraction
LUMO	Lowest unoccupied molecular orbital
MBE	Molecular beam epitaxy
ML	Monolayer
MPc	Metal phthalocyanine
PEEM	Photoemission electron microscope
PTCDA	Perylene-tetracarboxylic-dianhydride
STM	Scanning tunneling microscope
STS	Scanning tunneling spectroscopy
SubPc	Chloro[subphthalocyaninato]boron(III)
UHV	ultra-high vacuum
UPS	Ultraviolet photoelectron spectroscopy
XPS	X-ray photoelectron spectroscopy

1. Introduction

1.1. Motivation and Outline

Richard P. Feynman gave a famous talk "There's plenty of room at the bottom – An invitation to enter a new field of physics" in December 29th 1959 at the annual meeting of the American Physical Society at the California Institute of Technology. In his talk he had the vision to miniaturize machines and computers to the atomic scale and to "arrange the atoms the way we want". This talk can be considered as the start of 'nanotechnology'. Nanotechnology refers to the ability to control individual atoms and molecules, to build machines or electronic devices in the nanometer scale. There is an increasing number of research activities going on in nanoscale science and technology. Applications for nanotechnology could potentially change a variety of fields ranging from medicine, computers, machines to materials and objects not yet imagined.

A primary motivation for nanotechnology stems from the desire to continue Moore's law. Gordon E. Moore, co-founder of the Intel company, predicted already in 1965 that the number of transistors per integrated circuit will double every couple of years [1]. Surprisingly, he predicted this law only a couple of years after the invention of the first planar integrated circuit and yet Moore's law kept valid till present with doubling the number of transistors every 18 month. With conventional 'top-down' methods in semiconductor industries, i.e. lithography techniques, Moore's law will halt in about 10 years. Scaling down the lithography process is not only a matter of fabrication costs, but also of reaching fundamental physical limits [2, 3][1].

A new and promising approach to miniaturize the structures is the so-called 'bottom-up' technique. The 'bottom-up' technique is based on the formation of functional devices by special designed molecular building blocks. The ultimate limit of a functional device, e.g. a switch or transistor, can be considered as a single molecule. Consequently, with molecular electronics much smaller structures are feasible than with conventional semiconductor techniques based on the 'top-down' approach. A molecular rectifier has been proposed already in 1974 [4] and single molecule transistors could be realized a few years ago [5, 6]. A recent highlight in molecular electronics is the demonstration of logic circuits with field-effect transistors based on single carbon nanotubes [7]. However, the goals of the 'bottom-up' approach using molecular electronics are aiming very high and many difficulties have to be solved to achieve the goals. There are three major problems to tackle: designing the functional devices, contacting these devices and arrange them in a controlled manner. A lot of progress

---

[1]The narrowest feature in silicon devices is the gate oxide. Fundamental physical limits are reached in about 10 years when the thickness of the gate oxide is in the order of 1 nm. At this thickness, current will penetrate though the gate oxide causing the chip to fail.

has been achieved in supramolecular chemistry in the last years [8, 9]. The basic concept of supramolecular chemistry is to assemble molecular building blocks by intermolecular bonds. With the use of supramolecular chemistry or specially designed molecules [10] functional devices can be generated. Besides the necessity to contact and control a high number of functional devices, single molecules can change their properties upon adsorption on surfaces, e.g. porphyrin molecules undergo different conformation on different substrates [11]. The contacting of a molecule in the nanometer scale can completely change the characteristics or functionality of the molecule. This is for instance observed in the different charge transport behavior through a molecule depending on the metal-molecule contacts [12]. Therefore, the functional devices have to be designed in such a way that they can be contacted without disturbing their functionality. In other words the functional devices are the molecules including the contacts. In order to obtain a high number of functional devices on a small area, the arrangement of the molecular building block has to be controlled precisely. For this purpose, molecular self-assembly is a very promising approach. Molecular self-assembly has been defined by Whitesides as "the spontaneous association of molecules under equilibrium conditions into stable, structurally well-defined aggregates joined by non covalent bonds" [13]. Self-assembly is governed by the inter-molecular interactions, the molecule-substrate interaction and the thermal energy. Therefore this process runs in parallel. Due to the self-organization mechanism a high quality of the layers is achieved.

With the invention of the Scanning Tunneling Microscope (STM) in 1981 it became possible to study conducting surfaces in real space on an atomic scale. The STM is well suitable for the investigation of molecular phenomena on surfaces, e.g. adsorption, thin film growth and overlayer structures. Besides the imaging of surfaces, the STM also has the ability to interact with the surface at the atomic scale. With the STM, Feynman's vision to "arrange the atoms the way we want" has become possible, as shown by the manipulation of single atoms [14] and molecules [15] on surfaces and the construction of artificial structures [16]. Large organic molecules are considered as potential building blocks for molecular electronics. Therefore it is of high interest to investigate their behavior and properties on surfaces. Copper-phthalocyanines are among the first organic molecules which have been studied with the STM [17, 18]. In this PhD thesis, substituted phthalocyanine (SubPc), a polar molecule with an aromatic 14-π-electron system, has been investigated in detail on Ag(111). Interesting and unusual phase behavior is observed for the first monolayer (ML), as studied by means of room temperature STM and photoelectron spectroscopy. Special experiments have been carried out which address the nucleation and stability of the ordered layers. In account of the permanent dipole moment of SubPc, new phenomena of overlayer islands are observed upon investigation with the STM.

The outline of this thesis is as follows. In Chapter 2, the experimental methods and set-up are described. A brief introduction into STM and photoelectron spectroscopy is presented. The ultrahigh vacuum (UHV) system and particularly the molecule deposition system are sketched. Finally, the sample preparation is described.

In Chapter 3, the different overlayer structures are described and discussed. The chapter starts with the description of the two ordered superstructures formed by self-organization. These ordered structures coexist in a dynamic equilibrium with a molecular gas phase,

which is studied in detail. At the end of the chapter a phase diagram of SubPc on Ag(111) is sketched.

Chapter 4 deals with the adsorption behavior of SubPc on Ag(111). The combination of photoelectron spectroscopy and STM leads to a detailed understanding of the adsorption geometry and mechanism. The appearance of the SubPc in the STM images for different tunneling conditions is discussed as well.

Chapter 5 reports on coordinated orientation changes of ordered overlayers. This chapter starts with a brief introduction into island diffusion. The ability for the change in orientation originates in the balance of the inter-molecular interactions and the substrate-molecule interaction in conjunction with the thermal energy at room temperature.

Chapter 6 deals with phase transitions from a molecular gas phase to a condensed phase controlled by the STM tip. A model for this interesting and reversible tip-induced condensation and evaporation is presented and discussed.

Finally, the main results are summarized and concluded in Chapter 7. This chapter ends with a perspective to possible experiments proceeding this work.

In Appendix A an additional ordered superstructure of SubPc/Ag(111) is presented. This pattern could not yet be reproduced and is therefore only presented in this appendix.

1.2. SubPc Molecule

In the following some of the properties of metal phthalocyanines (MPc) and chloro[sub-phthalocyaninato]boron(III) (SubPc) in particular are presented. MPc are organic molecules used as functional dye molecules [19, 20]. Regular MPc molecules consist of a four-fold π-conjugated macrocyclic ring with four isoindoline groups. Copper Pc has already been imaged in the very early stages of investigation of organic molecules with the STM [17, 18]. However, the SubPc molecule, which was studied in detail in this PhD project, differs from the usual four-fold symmetric MPc. In the case of SubPc the central metal atom is replaced by a boron-chlorine unit connected to three instead of four isoindoline groups [21–24]. Therefore the molecule has a C_{3v} symmetry with an aromatic 14-π-electron system. The geometric and electronic structure of the SubPc molecule were calculated with ab-initio density functional theory (DFT) by S. Ivan[2]. The calculations were performed with the B3LYP exchange-correlation function and the 6-31Gd basis set using the Gaussian98 program package [25]. The calculations complete previous ones done by semi-empirical Hartree-Fock calculations at the AM1 level [23, 26].

Figure 1.1 shows the shuttlecock shape of SubPc. The bond length between the central B and axial Cl is 1.8 Å and the distance between the centers of peripheral benzene rings is 7.6 Å. The total height of the molecule is ≈ 5 Å and the diameter ≈ 13 Å. An excess of negative charge is found on the electro-negative atoms which surround the electron deficient boron (Fig. 1.1d). This charge is compensated by an electron deficit localized mainly at the six central carbon atoms. Therefore the SubPc is a polar molecule with the negative charge

---

[2]The calculations were performed by S. Ivan in the group of Prof. B. Giese at the Institut für Organische Chemie, St. Johanns-Ring 19, CH-4056 Basel.
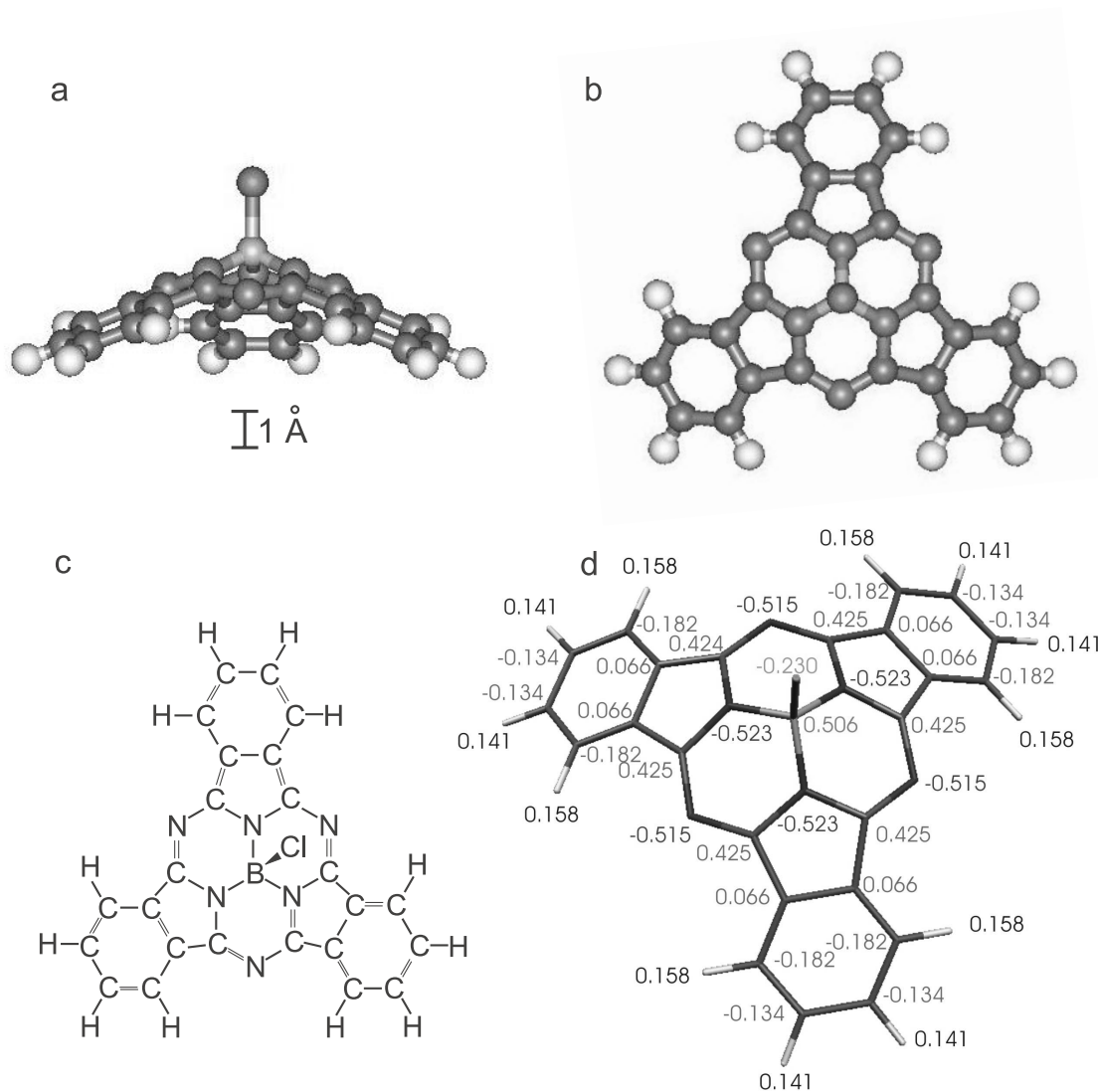
Figure 1.1.: SubPc molecule. (a) Side view and (b) top view of the calculated geometric structure. The scale bar is valid for (a) and (b). (c) Chemical Structure. (d) Effective atomic charges determined by a Mulliken population analysis.

at the Cl and the positive charge in the phthalocyanine core. This results in a calculated axial permanent dipole moment of 1.0 eÅ, which compares well to the experimental value of 1.1 eÅ [23]. All occupied molecular orbitals were calculated and additionally unoccupied orbitals located up to several eV above the LUMO. The calculated HOMO-LUMO gap for a SubPc molecule is 2.7 eV, where the HOMO-LUMO gap for SubPc measured by fluorescence in a dimethylholamide solution is 2.2 eV [26]. Thus, the fluorescence of SubPc is in the visible range of the spectrum.

2. Experimental Methods and Set-up

In this chapter an introduction to the experimental methods and the experimental set-up is presented. The STM was the main analytical tool in this PhD project for studying the adsorption of SubPc on Ag(111). An introduction into STM is given in section 2.1. Chemical analysis of the sample surface and measurements of the valence band were done by photoelectron spectroscopy. In section 2.2, a brief introduction of the basic ideas of photoemission is presented. All preparation and characterization steps of the samples were performed in-situ in the NANOLAB at the University of Basel. This UHV system is described in section 2.3. The deposition system for molecular layers, which was built-up at the beginning of this PhD project is shown in more detail in section 2.4. Finally the preparation of the samples is described in section 2.5.

2.1. Scanning Tunneling Microscopy

In the following a short introduction into the basic measurement principles of STM (section 2.1.1), its theory (section 2.1.2) and its application for imaging of adsorbates (section 2.1.3) is presented.

2.1.1. Introduction

Scanning tunneling microscopy was invented in 1981 at the IBM Research Laboratory in Rüschlikon by Gerd Binnig and Heinrich Rohrer. In 1986 they were honored with the Nobel Price for the invention of the STM. The basic principle of the STM is the quantum mechanical tunneling of electrons through the potential barrier between the surface of a conducting sample and a sharp metal tip at a distance around 10 Å [27][1]. Applying a bias voltage between the tip and the sample results in a net tunnel current. The corrugation of the sample surface results in a variation of the tunneling current, while scanning the tip over the surface by means of a piezo-electric tube. Two different imaging modes are distinguished. In the constant current mode, the tip sample distance is adjusted by a feedback loop in order to keep the tunneling current constant. In this mode the z-displacement[2] of the tip is recorded and one obtains a so called topographic image[3]. In the constant height mode the z-position of the tip is kept constant and the variation of the tunneling current is recorded.

---

[1] The STM had its predecessor in the Topografiner of R. Young et al. [28].

[2] z is definded as the direction perpendicular to the sample surface.

[3] The term topograhic image is misleading since one obtains rather a surface of constant local density of states. Thus the image reflects a mixture of the topography and the electronic structure of the sample (section 2.1.2).

The constant height mode allows faster scanning, whereas the constant current mode usually yields better resolution.

Binnig and Rohrer were the first to resolve with the STM monatomic steps and surface reconstruction [29] and demonstrated as well that real space images with atomic resolution can be obtained on metal [30, 31] and on semiconductor surfaces [32]. The invention of STM marks a breakthrough for the investigation of surfaces and adsorbates on an atomic level. In addition the STM is also useful to study dynamic processes, e.g. diffusion and thin film growth. Apart from imaging, the STM tip is a tool for manipulation of single atoms [14] and molecules [15] on surfaces and allows the construction of artificial nanostructures [16].

2.1.2. Basic Theory of STM

An exact theoretical description is extremely difficult or even impossible due to the low symmetry of the tip with its almost unknown shape and exact chemical composition. Therefore it is a challenge to model the tip and sample states and their evanescence into the tunneling gap accurately. An overview on the theory in STM can be found in textbooks [33, 34] or in a recently published review article by Drakova [35].

Starting from the one-dimensional tunneling through a potential barrier one can already explain the most important features of STM [33]. In quantum mechanics, an electron moving with energy E in $+z$-direction into a classical forbidden region ($z > 0$) with potential V ($E < V$) is described by an exponentially decaying wavefunction

$$\psi_{(z)} = \psi_{(0)}e^{-\kappa z}, \qquad \kappa = \sqrt{2m(V - E)}/\hbar \tag{2.1}$$

Thereby, m is the electron mass and $\hbar$ the Planck constant. According to equation 2.1 there is a nonzero probability to penetrate a localized barrier, i.e. the well-known quantum mechanical tunneling effect. In a next step we assume a one-dimensional metal-vacuum-metal tunneling junction with work function ϕ being the height of the potential barrier. Applying a bias voltage U between the two metals results in a net tunneling current. The tunneling current is directly proportional to the number of states on the sample surface within the energy interval $[E_F - eU, E_F]$[4] and their intensity at the location of the tip ($z = d$).

$$I \propto \sum_{E_n = E_F - eU}^{E_F} | \psi_n(d) |^2 \tag{2.2}$$

For low bias voltages U the tunneling current is given by:

$$I \propto U\rho_S(z = 0, E_F)e^{-2\kappa d}, \qquad \kappa = \sqrt{2m\phi}/\hbar \tag{2.3}$$

Here it is assumed that the density of states does not vary significantly within the energy interval $[E_F - eU, E_F]$ and can be written in terms of the local density of states (LDOS) $\rho_S(z, E)$ at the Fermi energy E_F. Equation 2.3 implies already the main features of STM. The exponential decay of the tunneling current leads to the high resolution in the tip-sample

---

[4] E_F is the Fermi energy.

displacement. Typically the current decays about one order of magnitude per Å. The other important result derived from equation 2.3 is the following: For low bias voltages U a constant current STM image is a map of the constant LDOS at the Fermi energy at the position of the tip surface and thus reflects the electronic structure of the sample surface.
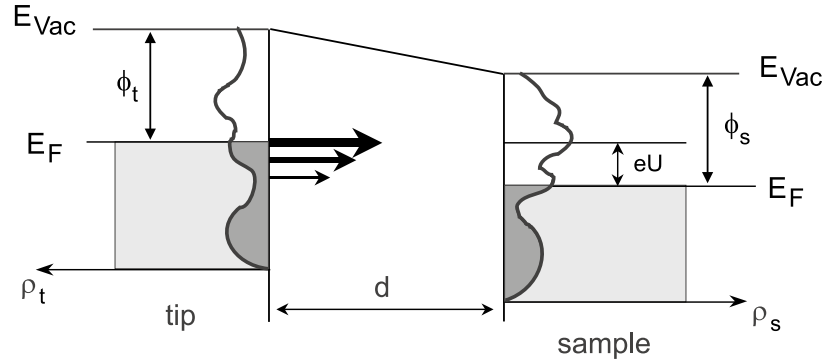

Figure 2.1.: Schematic energy diagram for tunneling from tip to sample, which are separated by a distance d, for a positive bias voltage U applied to the sample. The density of states for the tip and the sample are indicated as ρ_t, ρ_s respectively. The size of the arrows in the gap indicates the probability for a tunneling event depending on the transmission coefficient.

Already in 1961 Bardeen introduced a way to calculate the tunneling current between two metal plates [36]. He solved the stationary Schrödinger equation for the two subsystems and calculated the transfer rate for an electron from one electrode to the other by time-dependent perturbation theory. The concept from Bardeen was first applied to the tip-sample geometry by Tersoff and Hamann in the so-called s-wave approximation [37, 38]. Thereby the tip is approximated by spherical symmetry and can be described by a s-wavefunction. Thus the tunneling current is given by the following expression [39]:

$$I(U,d) \propto \int \rho_s(E, z=0)\rho_t(E-eU)T(E,U,d)[f(E-eU)-f(E)]dE \qquad (2.4)$$

with the transmission coefficient

$$T(E,U,d) = exp(-\frac{2d\sqrt{m}}{\hbar}\sqrt{\phi_s + \phi_t - 2E + eU}) \qquad (2.5)$$

Here ρ_t is the density of states (DOS) of the tip, ρ_s the LDOS of the sample at its surface at the lateral tip position (x,y), d the tip-sample distance[5] and $f(E)$ the Fermi-Dirac distribution[6]. Therefore the tunneling current is proportional to the convolution integral of the

---

[5] d is defined as the distance between the surface and the center of curvature of the tip.
[6] $f(E) = [1 + exp((E-E_F)/kT)]^{-1}$

LDOS of the sample and the tip as expected from Fig. 2.1. For small bias voltages $U \ll \phi_{s,t}$ and for an approximation of the Fermi-Dirac distribution as a step function[7], equation 2.4 simplifies to

$$I(U,d) \propto U \rho_t(E_F) \rho_s(E_F, z = 0) e^{-2\kappa d}, \qquad \kappa = \sqrt{m(\phi_s + \phi_t)}/\hbar \qquad (2.6)$$

This equation is very similar to equation 2.3 and even the same result is obtained if the DOS of the tip is constant around the Fermi energy E_F. Consequently, also in the approximation of Tersoff and Hamann, a constant current STM image reflects the surface of constant LDOS of the sample. However, for metals the LDOS at E_F generally reflects the surface topology in good agreement, whereas for adsorbates the LDOS can be completely different than the topology. On the other hand, the dependence of the tunneling current on the surface LDOS can be used to obtain spectroscopic information on the local electronic structure of the surface [35, 40]. Chemical sensitivity is revealed by resonant tunneling into (or out of) characteristic electronic states of atoms or molecules of the sample surface. A review on chemical imaging is given by Jung et al. in [41].

2.1.3. Imaging Adsorbates with the STM

A simple height interpretation of constant current STM images is not valid for many adsorbates on surfaces. For instance, CO appears on Cu(211) as a protrusion or depression depending on the proximity of neighboring molecules and the modification of the tip with CO adsorbed on it [42]. Also in the case of organic molecules with an extended π-electron system the height interpretation is not necessarily straightforward. Porphyrin molecules are imaged as protrusions or depressions depending on the substituents [43].

Before the first successful STM experiments with clearly resolved organic molecules were reported [17, 18, 44], it was not sure whether molecular imaging is possible at all. As stated in section 2.1.2, within the s-wave approximation of Tersoff and Hamann, the tunneling current is proportional to the LDOS at the Fermi energy. Since most organic molecules have a large energy gap between the highest occupied molecular orbital (HOMO) and the lowest unoccupied molecular orbital (LUMO), one might expect that organic molecules are not visible in the STM for low bias voltages. The pioneering work for the interpretation of the contrast mechanism for a single adatom on a metal surface was performed by Lang [45–47]. His results showed that the results from Tersoff and Hamann are also valid for an adsorbed adatom. Thus the adatom is imaged as a protrusion or depression depending on its modification of the LDOS at the Fermi level. Based on Lang's theory Eigler and coworkers [48] for the first time quantitatively discussed what makes an "insulating" atom visible with STM in the case of Xe adsorbed on Ni(110). The Xe is imaged as a 1.5 Å high protrusion in the STM, although the gap between the highest occupied Xe5p states and the lowest Xe6s states is approximately 12 eV in the gas phase. Physisorption causes weak mixing of the Xe6s state with the metal substrate states, resulting in a strong broadening of the atomic resonance. Nevertheless, the contribution to the density of states at the Fermi

---

[7]For not too high temperatures the Fermi-Dirac distribution can by approximated by a step function.

level is low and can not explain the observed corrugation of Xe atoms in STM. However, the Xe6s resonance extends considerably further out into the vacuum than the bare surface wave functions, which leads to the "visibility" of the Xe in the STM.

A physisorbed molecule on a metal surface remains a potential well with its discrete energy levels. Therefore the tunneling process through the molecule can be described in terms of a double barrier model with the molecule as an additional potential well between the tip and the sample [49]. An increased tunneling probability is expected when the LUMO or the HOMO of the molecule are near the Fermi level of the tip and resonant tunneling through the potential well of the molecule is possible. For calculating an STM image of an adsorbate in general, the knowledge of the electronic structure of the sample surface and the tip is a prerequisite. Various levels of approximation are used to calculate the electronic structure and the resulting tunneling current.

A detailed discussion of different theoretical approaches to the contrast mechanism of adsorbates in STM is given in a recent review by Sautet [50].

2.2.   Photoelectron Spectroscopy

In the following a brief introduction into photoelectron spectroscopy is presented. Photoelectron spectroscopy is a complementary method to STM and provides additional information about the electronic structure of the sample surface. In contrast to STM, photoelectron spectroscopy is a method which integrates over the sample surface and therefore no lateral resolved information is obtained[8]. The basic effect for photoelectron spectroscopy is the photoelectric effect, i.e. the emission of an electron out of a material due to irradiation with light. The photoelectric effect was already discovered in 1887 by Hertz [51] and theoretically explained by Einstein in 1905 [52].

The kinetic energy E_{kin} of a photoelectron emitted from a solid is given by energy conservation:

$$E_{kin} = h\nu - E_b - \phi \qquad (2.7)$$

where $h\nu$ is the energy of the incident photon, E_b the binding energy of the electron relative to the Fermi energy and ϕ the work function of the solid.

For photoelectron spectroscopy the sample is irradiated with monochromatic light. By detecting the number of photoelectrons for each kinetic energy $N(E_{kin})$ one obtains a mapping of the occupied energy levels of the probed solid and therefore information about its DOS (Fig. 2.2). Usually two energy regimes are distinguished. In X-ray photoelectron spectroscopy (XPS) the energy of the incident photon exceeds ≈ 100 eV, whereas for ultraviolet photoelectron spectroscopy (UPS) the photon energy is below ≈ 100 eV. With XPS the binding energies of the core levels are determined which allows the determination of the chemical composition of the sample. Different chemical environment of an adsorbate, or a

---

[8]XPS has an ultimate spatial resolution in the order of 1 μm and is therefore still integrating over many molecules. The XPS system of the NANOLAB has a spatial resolution in the order of 4 mm in diameter. With a Photoemission electron microscope (PEEM) a spatial resolution down to 20 nm is achieved, which is still integrating over many molecules.
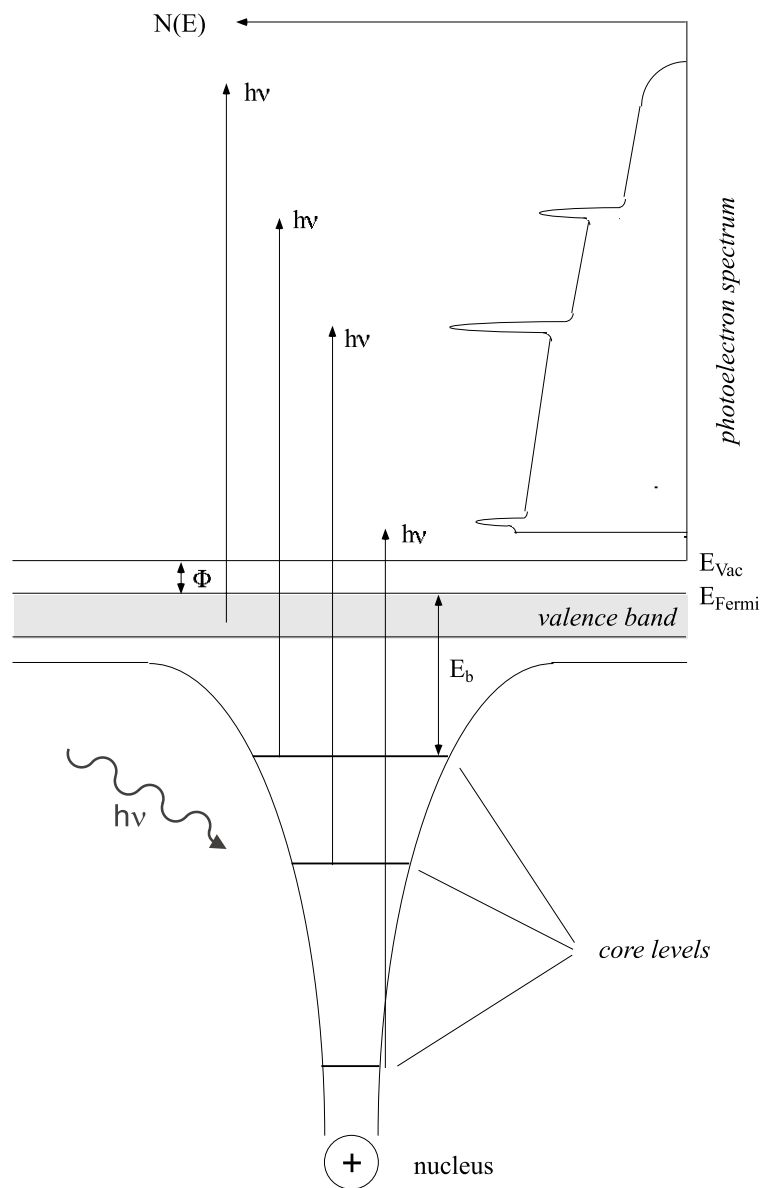
Figure 2.2.: Schematic diagram of the principle of photoelectron spectroscopy. The relation between the occupied energy levels of a solid and the corresponding photoelectron spectrum is outlined (from [53]).

species in general, leads to slightly different binding energies of the core levels. This energy difference is called a 'chemical shift'. Consequently, information from the interaction of an adsorbate with the substrate is obtained by measuring its chemical shift of the core levels [54]. UPS is used to obtain information about the DOS of the valence band and states close to the Fermi energy. Therefore the changes of the valence band upon adsorption of molecules and the occupied molecular orbitals can be measured with UPS. The surface sensitivity of photoelectron spectroscopy is given by the short mean free path of the photoelectrons which

is for UPS 1–2 ML and for XPS in the order of 3–8 ML [55].

A detailed description of photoelectron spectroscopy is given in the book of Hüfner [54].

2.3. UHV System

All experiments presented in this PhD thesis were performed in the NANOLAB. The NANOLAB is a versatile UHV system, which allows different in-situ preparation and characterization methods. A sketch of the whole UHV system is shown in Fig. 2.3. In order to avoid the coupling of oscillations of the building to the UHV system, the NANOLAB is located in the basement of the Physics Department and the whole UHV system is mounted on pneumatic feet. The system consists of seven connected chambers, each with its own pumping system comprising of a combination of turbo, ion getter and titanium sublimation pumps. Depending on the chamber the base pressure is in the 10^{-11} mbar or in the low 10^{-10} mbar range. The fast entry air lock allows to insert new samples into the UHV system without breaking the vacuum in the main system. The samples are mounted on modified VG stubs and are transferable in the whole UHV system by a sophisticated transfer system. The single crystals are mounted on stubs which are equipped with an internal filament. These stubs can be heated up to 1100 K.

For the preparation of the metallic substrates standard facilities for sputter/annealing cycles and for the growth of metallic films by electron beam evaporation are existing. The deposition system for the molecular layers, which was built within this PhD project, is described in section 2.4 in more detail.

For the sample analysis different methods are available. The prime instrument used in this work was the STM, which is a powerful tool for investigating adsorbed layers in real space. The home-built STM is working at room temperature and is described in more detail in [56]. It is mounted on an Eddy-current damping system and is equipped with an in-situ pre-amplifier in order to keep the noise in the tunneling current on a low level. As scanning tips electrochemically etched W-tips are used. The tips can be cleaned in-situ by electron bombardment. The sample bias voltage is applied with respect to the tip i.e. negative (positive) bias corresponds to tunneling from occupied (into unoccupied) electronic states of the sample. All STM images presented in this thesis have been acquired in constant current mode, recording the variation of the tip-sample separation, which is presented as greyscale STM image. Analysis of the electronic structure of the sample surface is performed in a VG ESCALAB MKII. The chemical composition of the sample surface is determined by core level analysis with Auger electron spectroscopy (AES) or XPS. The X-ray source is a non-monochromatized Mg/Al twin anode. The photon energies of the Mg K_α and Al K_α lines are 1253.6 eV and 1486.6 eV, respectively. UPS is performed using a non-monochromatized He gas discharge line source. The main line of the lamp is HeI$_\alpha$ (21.2 eV) whereas the lamp can be optimized to run with HeII$_\alpha$ (40.8 eV). The electrons emitted from the sample are detected in a spherical 150° analyzer with three channeltron electron counters. A commercial rear view low energy electron diffraction (LEED) is attached to the UHV system for the investigation of the crystallographic structure of the sample surface.

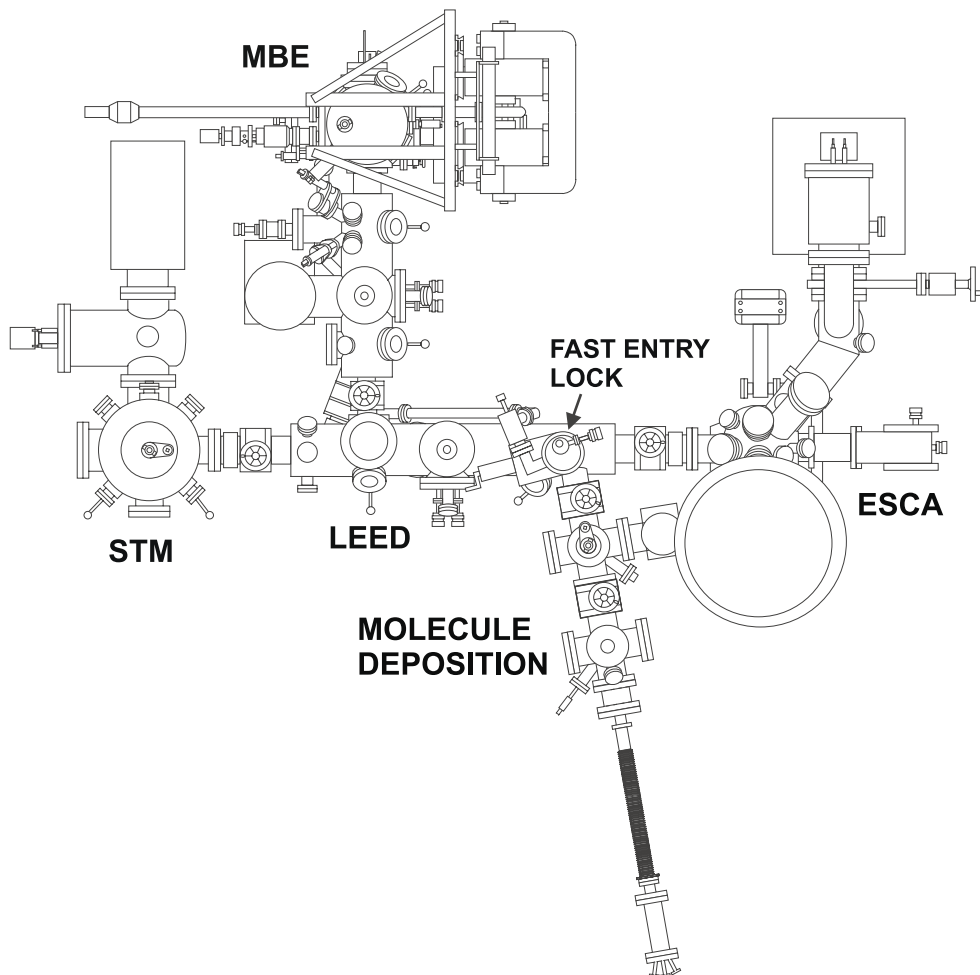More details about the UHV system can be found in [57–59].

Figure 2.3.: Schematic topview of the NANOLAB multi-chamber UHV system. Notation: molecular beam epitaxy (MBE), electron spectroscopy for chemical analysis (ESCA).

2.4.   Molecular Deposition System

At the beginning of this PhD thesis, the molecular deposition system was constructed and attached to the existing UHV system. Figure 2.4 shows a sketch of the two UHV chambers of the deposition system. The left chamber houses the evaporation stage and the quartz micro balance, the right one a mass spectrometer for masses up to 100 atomic units. The right chamber is also used to keep the substrate in a low pressure during adjustment of the desired evaporation rate.

The evaporation stage, the quartz micro balance and the manipulator are custom built for the special purposes of the deposition of sub-monolayers of molecules (Fig. 2.5). The stage can be loaded with four molecule evaporators and thus with four different kind of molecules. It is possible to sublime the molecules simultaneously or successively. The evaporators are
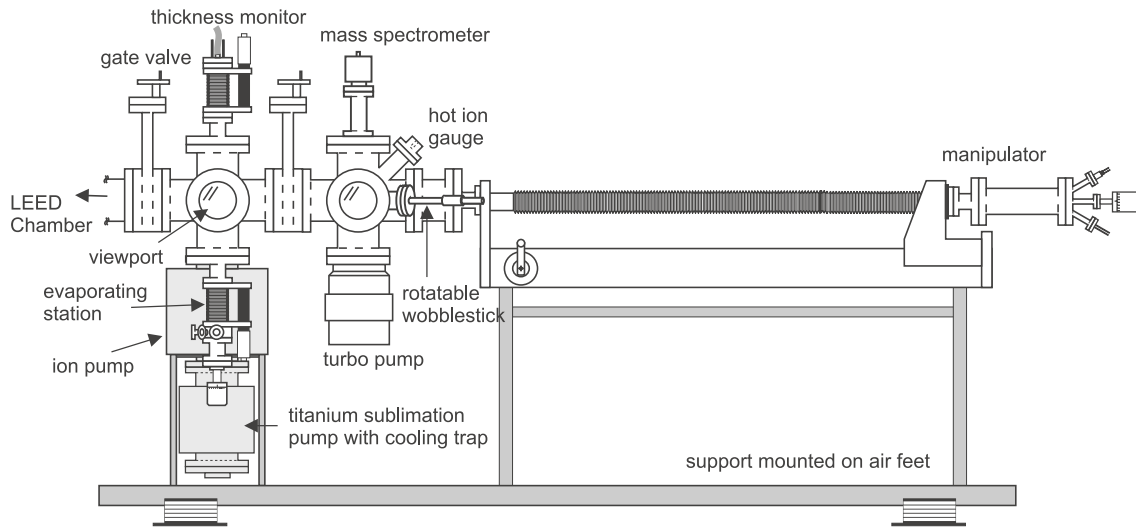
Figure 2.4.: Schematic side view of the molecule deposition setup. The deposition system is on the left side connected to the 'LEED Chamber'.
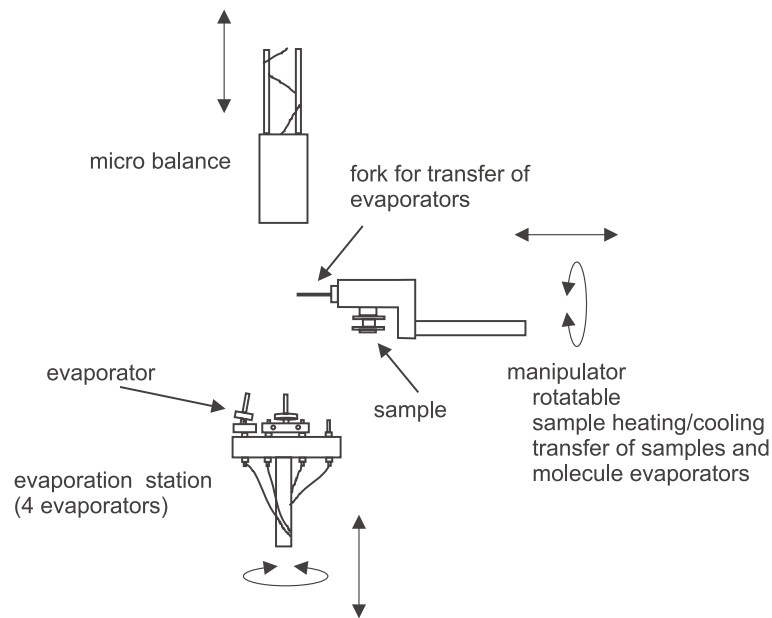
Figure 2.5.: Schematic sketch of the main parts for the molecule deposition, which are custom-built. For evaporation onto the sample the manipulator is moved above the evaporation stage.

small button heaters with a crucible made of tantalum. The molecules are filled as a powder into the crucible and are sublimed by heating the button heater. The crucible collimates the molecular beam in the direction to the sample. The manipulator is used for the transfer of the samples to the LEED chamber as well as for the transfer of the molecule evaporators from the fast entry air lock to the evaporation stage. In this way new molecules are brought

into UHV without breaking the vacuum, allowing an efficient handling of various molecules in UHV. The manipulator is equipped with two different heating systems. One system uses the internal filament of the stub and reaches a temperature in the order of 1100 K. In this case the temperature is measured by an optical pyrometer. The other heating system is integrated in the front part of the manipulator and is used for the accurate heating of the sample during deposition of the molecular layers. With this heating system a temperature of 650 K can be reached while the temperature is measured with a thermocouple on the manipulator close to the sample. Using liquid nitrogen the sample can be cooled down to a temperature of 120 K. During molecule deposition the sample is placed with the rotatable manipulator above the evaporation stage. The molecular evaporation rate is detected before and after deposition onto the sample by means of the quartz micro balance. The water cooled micro balance detects rates down to 0.1 nm per minute and therefore allows the reproducible deposition of molecular layers with sub-monolayer coverage down to a few percent. The error in the thickness of the molecular layers is in the order of 10–20% of the layer thickness.

2.5. Sample Preparation

Most of the experiments were performed with Ag(111) films as substrates. The Ag(111) films were prepared by UHV sublimation of Ag onto cleaved mica [60]. The 120–150 nm thick Ag layers were deposited at a rate of 0.1–1 nm per second onto the substrate held at 570 K. After the deposition the Ag(111) films were annealed at 570 K for 60 minutes. The quality of these films were checked by LEED, XPS and STM. From the LEED pattern it is apparent that silver grows in the (111) direction with domains differing by the rotational orientation. The contamination of the Ag(111) films was checked by XPS. The main contamination is carbon, which is below 0.03 ML C. In STM images it is found that the films exhibit atomically flat terraces with a mean terrace width of 100–150 nm separated by monatomic step edges. However, in some areas also higher roughness was found on the samples. The Ag(111) films were used for several experiments in a row. Molecular layers were removed by cycles of argon ion etching (600 eV, 1 μA, 18 minutes, 300 K) and annealing (570 K, 30 minutes) in order to regain atomically clean Ag(111) substrates. For the experiments on the tip induced phase transition (Chapter 6) sputter vacancies were introduced to the substrate. After the usual cleaning procedure by sputter/anneal cycles as described above, the sample was sputtered with 600 eV and a sample current of 1 μA for 90 seconds at a sample temperature of $T = 320$ K without post annealing. This procedure leads to monatomic vacancy islands with diameters in the range of 30–80 nm.

Some of the experiments were performed on a Ag(111) single crystal. The single crystal was cleaned by cycles of argon ion sputtering (1 keV, 2.3 μA, 30 minutes, 300 K) and annealing (800 K, 30 minutes). The last anneal cycle was kept shorter in time at a lower temperature. The main contamination of the single crystal is carbon which is below 0.1 ML C as determined by XPS.

The SubPc layers were deposited with a rate of 0.2–0.8 nm per minute while the Ag(111) substrate was kept at room temperature. During the deposition of the SubPc layer the pressure raised to $5 \cdot 10^{-9}$ mbar. For the STM measurements the thickness of the layers were

kept below one monolayer whereas in photoelectron spectroscopy experiments also layers with a thickness of several monolayers were studied.

3. Superstructures and Phase Behavior of SubPc on Ag(111)

In the following, the different overlayer structures of SubPc on Ag(111) are presented. Two different ordered superstructures are observed for increasing sub-monolayer coverage: a honeycomb pattern characterized by a low packing density (section 3.1) and a hexagonal close packed (hcp) structure (section 3.2). This two ordered overlayers are in coexistence with a 2D molecular gas phase. The coexistence is studied in detail for the honeycomb pattern and its gas phase (section 3.3). Finally, a schematic phase diagram of SubPc on Ag(111) is proposed (section 3.4).

3.1. Honeycomb Pattern: A Chiral Structure Made of Achiral Molecules

STM measurements on samples with a SubPc coverage of approximately 20-50% of a hcp-monolayer[1] reveal 2D ordered islands. In these islands the molecules self-organize in a 2D crystalline overlayer with a hexagonal honeycomb pattern characterized by a low packing density (Fig. 3.1). The molecules are imaged as protrusions with a height of ≈4.5 Å for positive sample bias voltages around 1 V. In high resolution STM images individual SubPc molecules are resolved as triangular structures with characteristic three lobes. In Fig. 3.1b the structure of SubPc is outlined within a 2D island as observed in the STM. The appearance of the SubPc in STM images is discussed in more details in section 4.2, where the lobes are identified as the isoindol groups.

The inter-molecular distance of the honeycomb pattern measured from the STM images is 17.9 ± 1.0 Å leading to a packing density of 0.24 molecules/nm^2. A full layer of the honeycomb pattern corresponds to 0.7 ML of the hcp pattern. The inter-molecular distance of the honeycomb pattern is much larger than the average inter-molecular distance of ≈7.8 Å in a SubPc crystal [21, 22]. In Chapter 4 it is shown that the SubPc molecule adsorbs with the Cl towards the Ag(111) substrate and the B-Cl axis perpendicular to the Ag surface. In this configuration an enlarged inter-molecular distance for a 2D layer compared to the average distance in a 3D crystal is expected because of the asymmetry of the molecule with its much larger width compared to its short height along the B-Cl axis. In addition the repulsive interaction between the parallel dipole moments of adjacent SubPc molecules further increases the inter-molecular distance. The dipole moment of an adsorbed SubPc is perpendicular to the Ag surface and pointing away from it. The image charges of the SubPc molecule which are formed in the metallic substrate lead to an image dipole. This image

---

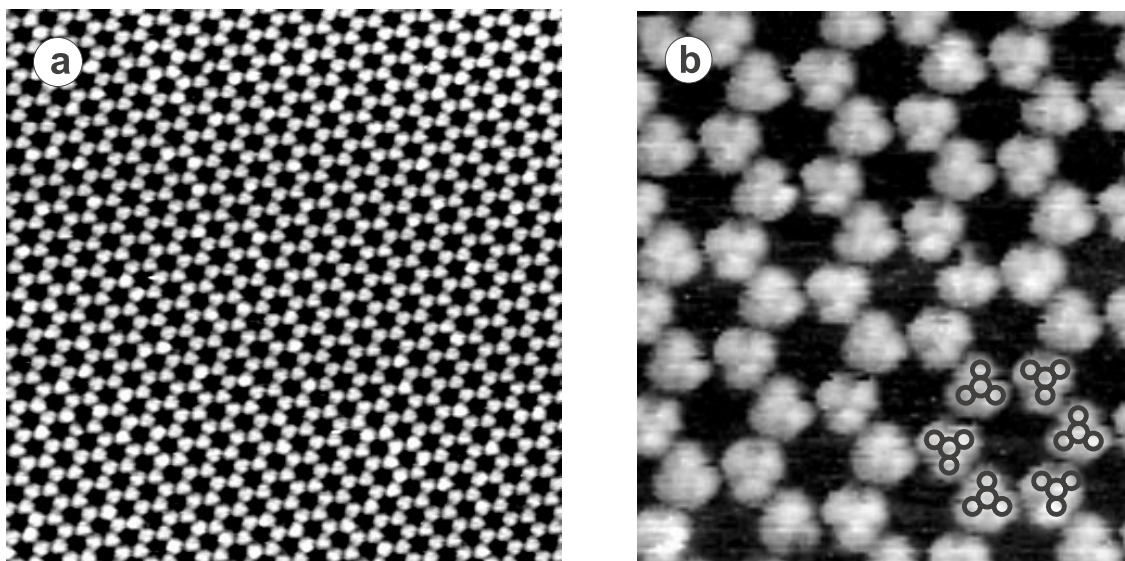[1] All SubPc coverage refer to the full monolayer of the hcp structure.

Figure 3.1.: STM images of the 2D honeycomb overlayer of SubPc on Ag(111). (a) scan range 56x56 nm, $I = 10$ pA, $U = 1.2$ V; (b) scan range 14x16 nm, $I = 10$ pA, $U = 0.7$ V. Single molecules are observed with sub-molecular resolution. The internal structure of the SubPc molecules is outlined at the bottom right (drawn to scale). The dark region in the center of the honeycomb pattern represents the underlying silver substrate.

dipole has the same direction as the SubPc dipole and leads to a reinforcement of the total dipole moment [61] and thus of the repulsive interaction of the adsorbed molecules.

Two different orientations of the honeycomb pattern with respect to the Ag(111) substrate are observed. Figure 3.2 shows a domain boundary between two domains of different orientations. The mismatch angle of these two orientations is $9° \pm 1°$ [2]. The experimental observation that only two different orientations of the honeycomb pattern exist, implies that besides the inter-molecular interaction also the molecule-substrate interaction is crucial for the formation of this crystalline overlayer. In case of dominating inter-molecular interactions and a negligible molecule-substrate interaction more equivalent orientations of the overlayer pattern have to be observed than only two.

The two different orientations of the overlayer structure have different chirality although the SubPc molecules and the Ag(111) surface are achiral. This becomes evident from high resolution images resolving the individual orientation of SubPc molecules. It is important to note that each molecule is rotated with respect to the honeycomb pattern which leads to the observed chirality. The chirality of the two different orientations is defined in the text as follows: Left (right) chirality whether the 'legs' (phenyl rings) of the molecules point to the left (right) side of the central vacancy (Fig. 3.3). The domain on the left hand side in Fig. 3.2 has right chirality and is the mirror domain of the one on the right hand side which has left chirality. The observed structure in Fig. 3.1b is identified as a domain with

---

[2]The error in the angle is estimated by taking advantage of the symmetry of the pattern and therefore of known angles.
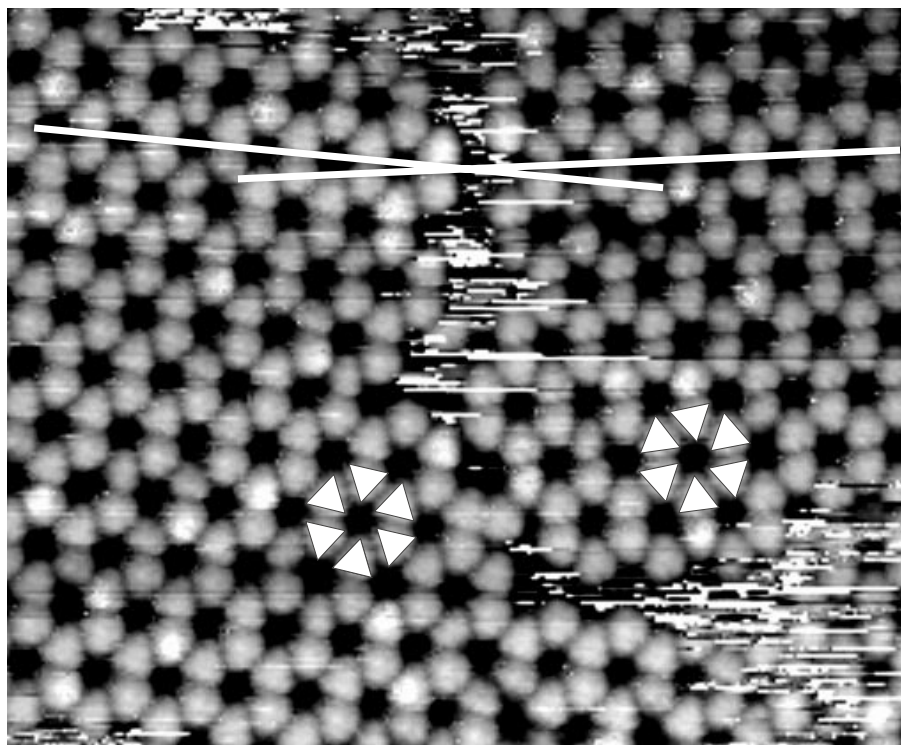
Figure 3.2.: STM image of a domain boundary of the two possible orientations of the honeycomb pattern (range 39x32 nm, $I = 30$ pA, $U = 1.3$ V). The mismatch angle of the two domains is indicated by the white lines. SubPc molecules simplified as triangles are drawn into the image for both domains showing that the two orientations of the honeycomb pattern are chiral.

left chirality. Consequently, the achiral SubPc molecules self-organize into islands which have enantiomorphic structure. The inter-molecular distance of 17.9 ± 1.0 Å in the case of SubPc on Ag(111) is larger than the inter-molecular distance of 13 Å which is observed for the square lattice of SubPc on Cu(100) [62]. The larger inter-molecular distance in the case of SubPc on Ag(111) and geometrical arguments exclude that the rotation of the SubPc molecules with respect to the honeycomb pattern is caused by steric repulsion. In this structure of the honeycomb pattern the distance between the 'legs' of two adjacent SubPc molecules is enlarged due to the rotation of the SubPc molecules. This is potentially caused by the repulsive electrostatic interaction of the 'legs', since their H-atoms carry positive partial charges (Fig. 1.1). Furthermore, the N atoms of the phthalocyanine macrocycle carry negative partial charges and therefore the rotation of the SubPc molecules is energetically favored because the distance of the 'legs' is enlarged and the 'legs' get next to the N atoms. Thus, the rotation of the molecules with respect to the honeycomb pattern can be derived from the charge distribution of single molecules. Consequently, both interactions, the inter-molecular and the molecule-substrate interactions, are crucial for the formation of the SubPc honeycomb pattern on the Ag(111) surface. Self-assembly of achiral molecules into chiral structures has been reported in recent STM studies for Langmuir-Blodgett films [63], liquid

crystals [64] and for benzoic acids [65].

Figure 3.3 presents a proposed model of the superstructure of SubPc on Ag(111) which is based on symmetry arguments. The molecules in the honeycomb pattern have the same contrast and the same sub-molecular structure for both orientations of the overlayer. With the assumption that each molecule is located at an equivalent adsorption site a model of the molecular superstructure is proposed. From the STM measurements the inter-molecular distance and the angle between the two possible orientations of the superstructure is used. The resulting superstructure of SubPc on Ag(111) is a $\sqrt{111} \times \sqrt{111}R \pm 4.7°$ (2 SubPc) overlayer, where the center of a molecule is located above a silver atom (on top site) and the phenyl rings on hollow sites. Two SubPc molecules are needed for each unit cell in order to represent the honeycomb structure. The two orientations of the pattern are $\pm 4.7°$ rotated with respect to the $[1\bar{1}0]$ direction of the Ag(111) substrate. This proposed model fits very well with the experimental data: The inter-molecular distance is 17.7 Å and the angle between the two domains is 9.4°, compared to 17.9 ± 1.0 Å and $9° \pm 1°$ measured in the STM images, respectively. Also the rotation of each molecule within the proposed lattice corresponds to the experimentally observed orientation.
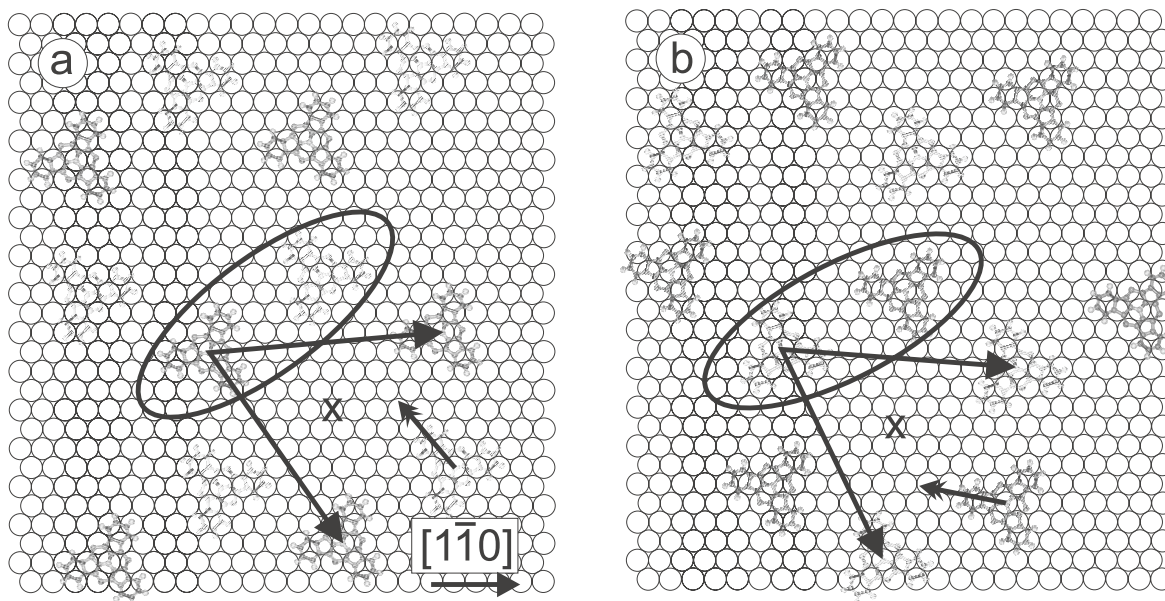
Figure 3.3.: Proposed model of the honeycomb pattern. The basis consisting of two SubPc and the corresponding Bravais vectors are drawn into the model for (a) the orientation with right chirality and (b) for the orientation with left chirality. For the molecule at the bottom right the chirality is shown by an arrow. For right chirality (a) the 'legs' of the molecule point to the right hand side of the center of the honeycomb (marked by a cross) as indicated by the arrow. For left chirality (b) the 'legs' point to the left hand side.

3.2. Hexagonal Close Packed Pattern

The SubPc molecules self-organize in a 2D hcp pattern for coverage in the order of 0.6–0.9 ML. Figure 3.4 shows STM images of the hcp layer where individual SubPc molecules are resolved with sub-molecular resolution. For positive sample bias around 1 V, the molecules are imaged as protrusions consisting of three lobes with a height of ≈ 4.5 Å exactly as they are observed in the honeycomb pattern[3]. The inter-molecular distance measured from STM images is 18.9 ± 1.0 Å and therefore slightly larger than the one of the honeycomb pattern. The packing density for the hcp pattern is 0.34 molecules/nm² which is 42% higher compared to the honeycomb pattern. Two possible orientations of the hcp pattern with respect to the Ag(111) substrate are observed, like in the case of the honeycomb pattern. The mismatch angle of these two orientations is $15° \pm 1°$. By a simple rotation of the overlayer pattern the two orientations are brought to identity because the axis of the molecules are in line with the axis of the hcp pattern. Consequently, the two superstructures have no chirality. From the experimental observation that only two orientations of the hcp pattern with respect to the Ag(111) substrate are observed, it is concluded that also for the hcp pattern the molecule-substrate interaction plays an important role.

The difference between the honeycomb and the hcp pattern is more profound than just a missing molecule in each 'honeycomb'. The SubPc molecules in the hcp pattern are aligned in rows where each SubPc is pointing with its 'legs' to an outer N atom of the phthalocyanine macrocycle of the next molecule. In this configuration the distance between the repulsive 'legs' of two adjacent molecules is increased and the 'legs' are pointing to the electron-rich N of the phthalocyanine macrocycle of neighboring molecules. This configuration is expected to be energetically favored because of the charge distribution of the SubPc (Fig. 1.1d). Consequently, the inter-molecular interactions and the molecule-substrate interactions seem to be crucial for the formation of the hcp pattern as already observed in the case of the honeycomb pattern.

Overview images (e.g. Fig. 3.4a) show many defects in the hcp layer. However, high resolution STM images (Fig. 3.4b) show that these defects are not vacancies, but are filled with molecules of a different apparent height. These molecules have the same shape as the other molecules but approximately only half of their height. Therefore these molecules are denoted in the following as 'small' molecules. The reason for these 'small' molecules is attributed to a different LDOS compared to the others. According to the theory of Tersoff and Hamann (section 2.1.2) a different LDOS leads to a different apparent height in the STM image. The difference in the electronic structure is attributed to a slightly different bond of the molecule to the Ag substrate. The possibilities that the 'small' molecules are caused by imaging artefacts or decomposed molecules are ruled out. In Fig. 3.4b two real vacancies are visible and exclude therefore that the 'small' molecules are due to a double tip. The same apparent height of the SubPc molecules for the hcp and honeycomb pattern rules out the possibility of a double layer in the images of Fig. 3.4. Also a decomposition of the SubPc molecules is unlikely, since the amount of 'small' molecules is in the order of 5-12% whereas the purity of the molecules is >99%. Furthermore, no 'small' molecules are observed

---

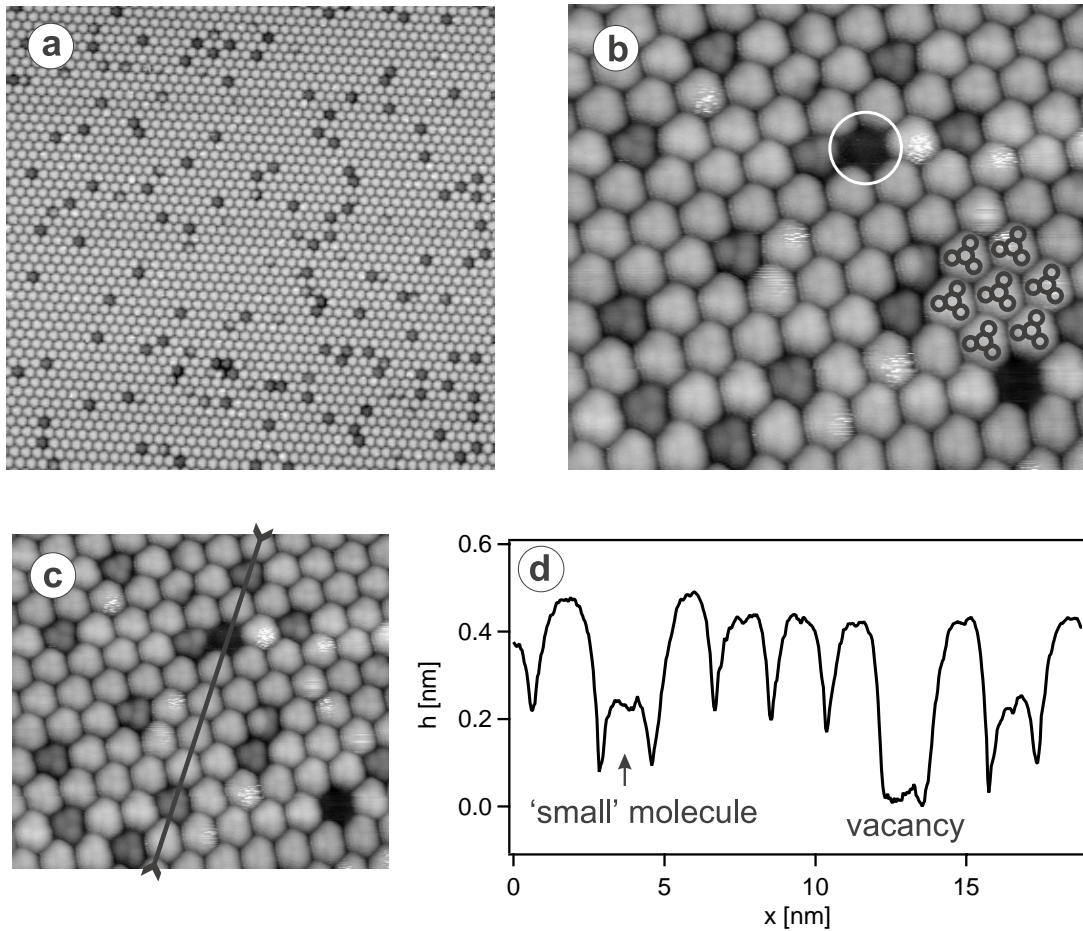[3]The appearance of the SubPc molecules in the STM images will be discussed in more detail in section 4.2.

Figure 3.4.: STM images of the 2D hcp overlayer of SubPc on Ag111. (a) scan range 86x82 nm, $I = 20$ pA, $U = 1.0$ V; (b) scan range 20x18 nm, $I = 10$ pA, $U = 1.0$ V. Individual SubPc molecules are imaged with sub-molecular resolution. The internal structure of SubPc is outlined on the right hand side. Note that there are only two vacancies in this image, where one of them is marked by a white circle. The minor apparent height of some molecules is due to a local change of their electronic structure. (c) Same STM image as (b), the black line shows the location of the cross section shown in (d). (d) The difference in the apparent height for the 'small' molecules is clearly visible in cross sections.

in the honeycomb pattern. Therefore the different apparent height of the 'small' molecules is attributed to a different electronic structure, which is also supported by preliminary STS measurements (dI/dU maps)[4] at different bias voltages. These measurements indicate that the 'small' molecules have a lower differential conductivity (lower LDOS) than the others. The relative height difference between the 'small' molecules and the others undergoes only slight variations in the range of 0.3–2 V positive sample bias voltage. It is worth to note that these 'small' molecules are slightly rotated with respect to the molecular rows of the

---

[4]Scanning Tunneling Spectroscopy (STS) gives information about the sample LDOS by measuring the differential conductance dI/dU [35].

hcp pattern. This rotation of the 'small' SubPc molecules along the B-Cl axis leads to a slightly different adsorption geometry (Fig. 3.5), which might cause the different apparent height. Stress relaxation in the molecular layer could be a possible reason for the rotation of the 'small' molecules. In the case of C_{60} on various metals different apparent height for the C_{60} have been observed [66–68]. This difference in the apparent height is attributed to electronic differences caused by surface interactions, where a mixture of subtle different chemical bonding and adsorption geometry takes place [66–69]. A different explanation for the 'small' SubPc molecules in the hcp pattern is that these molecules are located on a Ag-vacancy site and are therefore topographically lowered. However, this explanation is very unlikely since no 'small' molecules are observed in the honeycomb pattern.

In overview images most of these 'small' molecules show high mobility while some of them are pinned to their adsorption site. In principle, there are two possible types of mobility of the 'small' molecules. One possibility is that the 'small' molecules themselves are mobile and diffuse around. The second possibility is that all the molecules remain on their adsorption site and only the different bonding types diffuse, causing always different molecules to appear as 'small' molecules. For the second possibility no molecule transport is involved. However, for small STM image frames[5] the mobility of the 'small' molecules is significantly reduced. Consequently, the diffusion of the 'small' molecules is influenced by the STM tip, where a small scan frame leads to less mobility.

It is interesting to note that the slight rotation of the 'small' molecules with respect to the molecular rows in the hcp pattern leads to a symmetry breaking of the two different orientations of the hcp pattern (Fig. 3.5). This symmetry breaking arises because all the 'small' molecules of one orientation of the hcp pattern are rotated to the same direction, whereas the 'small' molecules in the pattern with the other orientation are rotated exactly to the other direction. Consequently, the two orientations of the hcp pattern have different chirality if the 'small' molecules are taken into account.

In Fig. 3.5, a model of the superstructure of SubPc on Ag(111) is proposed. This model for the hcp pattern is based on the same symmetry arguments as in the case of the honeycomb pattern. From the STM measurements the inter-molecular distance and the angle between the two possible orientations of the hcp pattern is used. The resulting superstructure of SubPc on Ag(111) is a $\sqrt{43} \times \sqrt{43}R \pm 7.6°$ overlayer. The two orientations of the pattern are $\pm 7.6°$ rotated with respect to the $[1\bar{1}0]$ direction of the Ag(111) substrate. This proposed model fits very well with the experimental data: The inter-molecular distance is 19.1 Å and the angle between the two domains is 15.2°, respectively 18.9 ± 1.0 Å and $15° \pm 1°$ measured in the STM images. It is important to note that the proposed models for the honeycomb and the hcp pattern are self consistent since the molecules are in both models on the same adsorption sites.

A single molecule has threefold symmetry whereas the Ag(111) surface has six fold symmetry. This allows for the hcp pattern to nucleate in four possible orientations on the Ag(111) surface: For each of the two experimentally observed directions of the pattern two molecular orientations are possible. In Fig. 3.5 the molecules can not only have the indicated

---

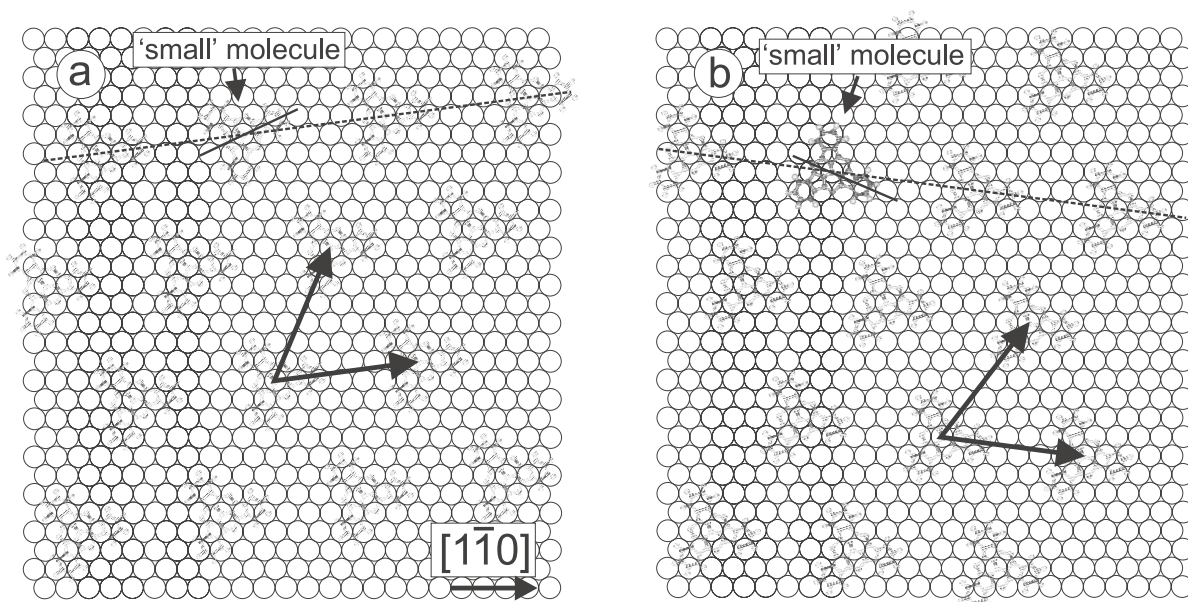[5]Image frames in the order of 30x30 nm or smaller.

Figure 3.5.: Proposed model of the hcp pattern. The Bravais vectors for the two possible orientations (a) and (b) are indicated. In (a) the 'small' molecules are slightly rotated to the left side with respect to the molecular rows. In (b) the 'small' molecules are rotated exactly to the opposite side with respect to the molecular rows. Therefore the hcp pattern exhibits chirality if the 'small' molecules are taken into account.

orientation but can also be turned 180°. Experimentally all these different orientations are observed.

3.3. 2D Molecular Solid-Gas Equilibrium

The SubPc molecules form islands with honeycomb (hcp respectively) pattern, but not all the molecules condense to these islands. A fraction of the molecules remain mobile and form a 2D molecular gas phase which is in coexistence with the condensed phase. In section 3.3.1 a basic introduction in surface diffusion is presented. In section 3.3.2 the experimental findings on the solid-gas coexistence of SubPc are discussed in detail.

3.3.1. Introduction to Surface Diffusion

The mobility and interactions of adsorbates on metal surfaces affect island nucleation and layering and therefore influence the structure and properties of grown layers. The lateral random-walk diffusion of a single adsorbate[6] on a surface is determined by the corrugation of the potential energy surface (surface potential) of the adsorbate-substrate complex and

---

[6]For single adsorbate diffusion often the term migration is used in stead of diffusion.

by the kinetic energy available for hopping between stable adsorption sites [70, 71]. This kinetic energy arises from thermal energy exchange with the substrate.

If the thermal energy of the adsorbed molecule is small compared to the corrugation of the surface potential, one can consider the adsorbed molecule as localized in a minimum of the surface potential. The locations of the minima form a regular lattice compatible with the substrate symmetry. Each molecule has to overcome the energy barrier imposed by the corrugation of the surface potential in order to hop to an adjacent minimum and thus participate in the diffusion process (see figure 3.6a). The lattice gas model has been successfully used to represent adsorption in such systems [61, 72]. The hopping rate ν of isolated molecules depends on the temperature T and the energetic barrier between two adjacent sites, i.e. the diffusion barrier E_d, via the Boltzmann factor:

$$\nu = \nu_0 \cdot exp\left(-\frac{E_d}{kT}\right) \qquad (3.1)$$

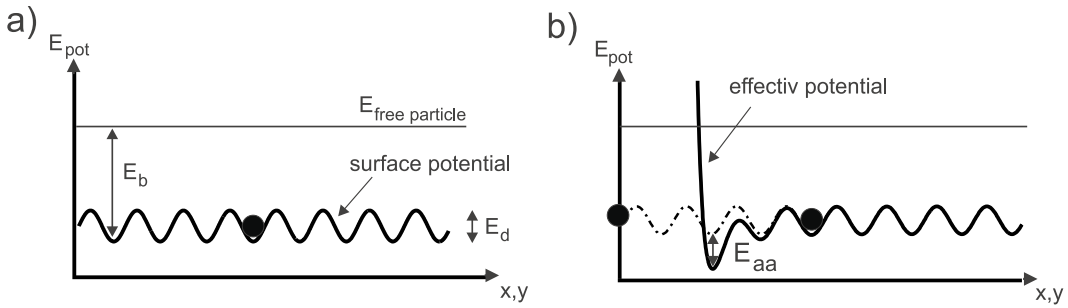ν_0 is the attempt frequency for penetration of the barrier.

Figure 3.6.: a) Schematic potential energy surface experienced by an adsorbed molecule. The notation is as follows: E_d energy barrier for diffusion, E_b adsorption energy (binding energy). b) Schematic potential energy surface for an adsorbed molecule interacting with another molecule located at the origin. E_{aa} is the inter-molecular interaction energy.

The potential energy surface for an adsorbed molecule in the presence of another adsorbate can be approximated as the superposition of the inter-molecular interaction and the surface potential of the molecule-substrate complex (see Fig. 3.6b). As a consequence of these deformations of the surface potential the diffusion barrier is locally reduced or increased in the case of repulsive or attractive interaction, respectively. For simple cases this inter-molecular interaction E_{aa} can be described by the two particle Lennard-Jones-Potential. This leads to a 2D overlayer formation in the case of attractive interaction and E_{aa} significantly larger than the thermal energy kT.

Diffusion coefficients for individual adsorbates are experimentally accessible by different methods [70]. Using FIM it is possible to measure the migration of single adatoms [73], but FIM is limited to very stable adsorbates due to the high electric field which is necessary for imaging. The STM it is well suitable to study diffusion processes of individual adsorbates on surfaces [74–77]. Here particular care has to be taken to eliminate the influence of the

scanning tip on the observed mobility, for instance as shown in the case of Sb dimers on Si(100) [74].

3.3.2. Experimental Observation and Study of a 2D Molecular Solid-Gas Equilibrium

In addition to the condensed honeycomb islands two more regions can be distinguished in STM images. In Fig. 3.7 an STM image with a coverage of approximately 0.3 ML is shown. On the terrace next to the condensed island noisy streaks appear in the scan direction. The tip excursions perpendicular to the sample hint at a mobile adsorbate component. In areas with mono atomic substrate steps bunched together (noted by s in Fig. 3.7) the SubPc molecules are stably adsorbed in a less regular pattern. Most of the molecules adsorbed on the step edges have round shape which implies slightly different bonding to the substrate compared to molecules of triangular shape on the terrace.

The noisy pattern next to the condensed islands corresponds to molecules on the same terrace which exhibit mobility on the time scale of one scan line. This is supported by Fig. 3.8: The height profiles of the excursion of the tip scanning in constant current mode are similar for condensed and mobile molecules. The similar widths of the profiles leads to the conclusion that the residence time for a mobile molecule is comparable to the time required to scan over a molecule (roughly 10 ms). Therefore pushing and pulling of molecules by the tip are not significant. This is in contrast to the trapping mechanism of molecules in the tunneling junction as observed by Böhringer et al. for Anthracene and PTCDA[7] on Ag(110) [78, 79]. Comparing subsequent scan lines reveals perfect correlation in the condensed islands compared to essentially no correlation in the noisy regions. Therefore we identify the observed regions with a 2D-condensed phase, a 2D-gas phase and molecules pinned at step edges. According to the scan line analysis the molecules in the gas phase are stably adsorbed for a certain time but tend to hop to nearby adsorption sites. Consequently, the gas phase can be described in terms of the 2D lattice gas model. For symmetry reasons it is expected that the molecules adsorb at equivalent sites with respect to the periodicity of the Ag(111) lattice. This is consistent with our measurements since the molecules adsorb at many equivalent sites, not only the honeycomb lattice sites, when observed in the gas phase.

Additional evidence for this 2D molecular lattice gas is obtained from time-lapse imaging sequences. In the STM images of figure 3.9 the time evolution of the border line of an island is shown. This border moves as a function of time as expected for the condensed phase being in dynamic equilibrium with the gas phase. However, the size of an island does not significantly change over several hours as observed in time-lapse imaging sequences of whole islands. Coexisting islands and 2D gas phase have been observed for various scan and tunneling parameters[8]. None of these parameters had an influence on the behavior of the coexistence. Even after a few days the coexistence of the condensed phase and the gas phase is still observed. Therefore, these two phases coexist in a 2D thermodynamic equilibrium at room temperature. In addition it is observed that the gas phase is confined to terraces,

---

[7]PTCDA: Perylene-tetracarboxylic-dianhydride

[8]Scan parameters: scan range 13–120 nm, scan speed 65–260 nm/s; tunneling parameters: bias voltage 0.7–1.7 V, tunneling current 10–100 pA.
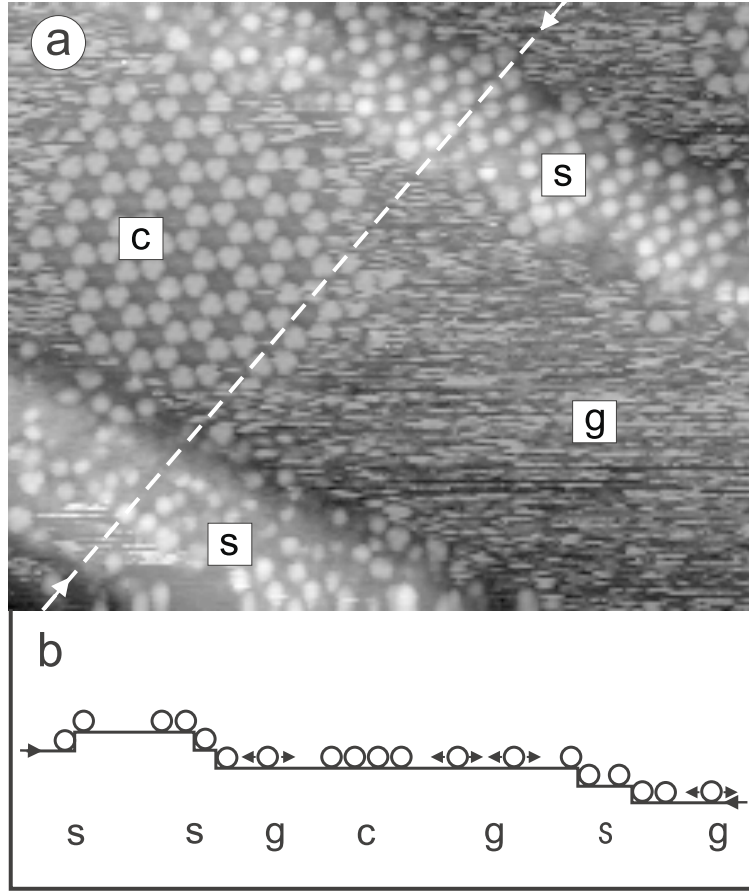
Figure 3.7.: (a) STM image showing the coexistence of different patterns of SubPc adsorbed on Ag(111) (scan range 54.3x44.0 nm; $I = 12$ pA, $U = 0.85$ V). On the left-hand side of the image a condensed island with a honeycomb pattern (c) is present, whereas next to the condensed island a noisy streak pattern (g) is visible. At the left bottom corner and in the top right bunched step edges of the Ag(111) substrate (s) cross the image. These steps are decorated by SubPc molecules which are pinned by the interaction with the steps. The dashed white line represents the location of the schematic cross section shown in (b).

e.g. the noisy streaks in Fig. 3.7 are not crossing the decorated step edges. However, in thermodynamic equilibrium of the 2D condensed phase and the 2D gas phase, also a gas phase is present on top of the condensed phase in the second layer [80]. The ratio between the densities of the two gas phases in the first and second layer, respectively, is given by [80]

$$\frac{n_1}{n_2} = exp\frac{E_{b1} - E_{b2}}{kT} \tag{3.2}$$

where n_1, n_2 are the densities of the first layer and the second layer, respectively and E_{b1}, E_{b2} are the binding energies of the first and the second layer, respectively. According to this formula, a slightly smaller binding energy of the second layer leads to a significant lower density. Consequently, it is expected that the gas phase in the second layer has a much lower
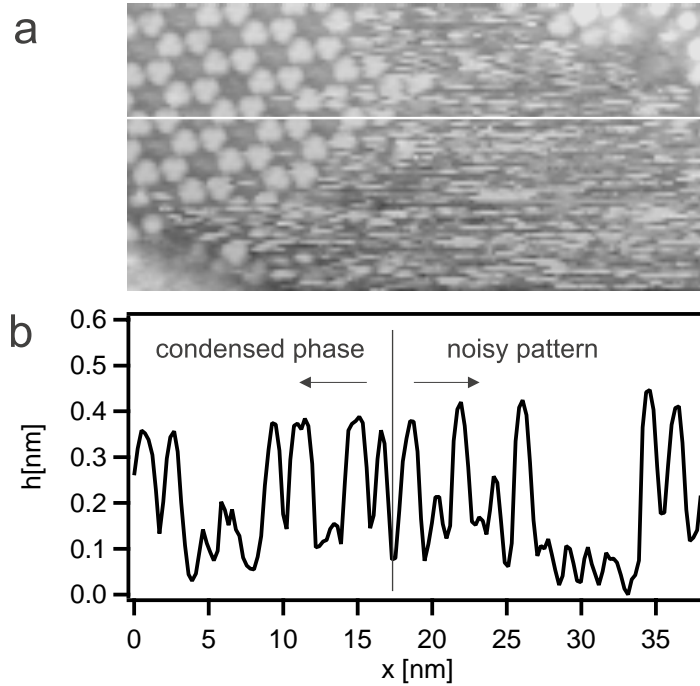
Figure 3.8.: (a) Sub image taken from figure 3.7a (scan range 38.4x18.9 nm; $I = 12$ pA, $U = 0.85$ V). The white line shows the location of the cross section shown in (b). (b) Cross section in the fast scanning direction (x direction). In this line section single molecules are clearly visible and exhibit a characteristic shape which is similar for molecules in the condensed phase and in the noisy pattern. This strongly suggests that in the latter case molecules hop to adjacent adsorption sites but that the residence time on a particular adsorption site is comparable to the time required by the scanning tip to pass over a single molecule.

density than the one in the first layer and is therefore not visible in STM images.

In contrast to the molecules in the lattice gas most of the molecules at the step edges are stable adsorbed and did not move in time lapse imaging sequences. The step edges are usually preferred adsorption sites due to charge redistribution inducing an electrostatic dipole moment [81, 82]. This charge redistribution is called Smoluchovski effect [83]. Since the SubPc molecules on the step edges are stably adsorbed in a less regular pattern the molecule-substrate interaction plays a dominant role over the molecule-molecule interaction and the thermal energy.

Semi quantitative conclusions can be obtained by comparing our experiments with the lattice gas model. In the simplest case the probability P that a molecule remains at a given adsorption site after a certain time τ is

$$P_\tau = exp(-\nu_s \tau) \tag{3.3}$$

when no multiple jumps are taken into account [77]. In order to obtain the hopping rate ν_s^g for the SubPc gas phase a statistical analysis of the experimental data was performed. P_τ for different τ is obtained from comparing the forward and the corresponding backward scan
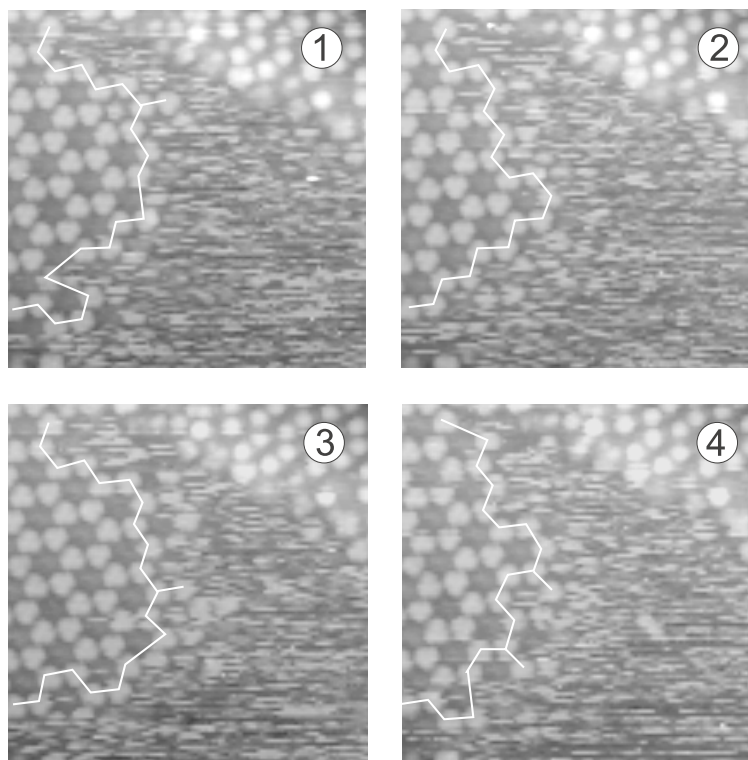
Figure 3.9.: In this sequence of STM images the time evolution of a condensed molecular island is shown as a function of time. The white line connects the outermost molecules and serves as a guide to the eye. The images are taken one after the other with an interval time between two images of 3 minutes 26 seconds (scan range 25.8x25.8 nm; $I = 12$ pA, $U = 0.85$ V).

lines close to the reversing point of the tip with respect to molecular jumps. 62 different molecular jumps have been analyzed, taking into account only molecules close to the reversing point[9] in order to decrease the systematic error due to multiple jumps. The hopping rate of a SubPc molecule in the 2D lattice gas is determined to $\nu_s^g = 31 \pm 10$ s^{-1} at room temperature. In these experiments the total surface coverage was in the order of 0.3 ML. Therefore neighboring sites may be occupied and hinder random jumping of the molecules. Thus the estimated hopping rate in the limit of coverage $\theta \to 0$ can be different, particularly for interacting molecules [84–86]. Using equation 3.1 for the hopping rate an estimate for the diffusion barrier E_d is obtained. Assuming a standard attempt frequency $\nu_0 = 10^{13}$ s^{-1} [61] the diffusion barrier E_d is calculated to $E_d = 0.7 \pm 0.2$ eV. The relatively large error in the diffusion barrier is due to the uncertainty in the attempt frequency for which a lower limit of 10^{10} s^{-1} and an upper limit of 10^{16} s^{-1} were assumed [71]. This result for the diffusion barrier compares to the one for decacyclene on Cu(110), where the diffusion barrier has been determined to $E_d = 0.74 \pm 0.03$ eV [77]. Thus, a reasonable value for the diffusion barrier is obtained. Nevertheless, the result should be considered as semi quantitative due to the finite

---

[9]Molecules close to the reversing point of the tip correspond to a small time frame.

value for the coverage θ and the use of a standard attempt frequency. Despite the solid-gas coexistence is observed at different tunneling and scan parameters tip artefacts can not be ruled out. It is known from other examples that the scanning tip can affect the hopping rate of adsorbates [74, 87, 88]. Also in the case of SubPc on Ag(111), tip induced experiments have been successful in the case of higher molecular coverage (Chapter 6)[10].

The condensation energy E_{cond} is the energy difference for a molecule in the condensed phase compared to the one in the gas phase. The entropy in the gas phase is higher than in the condensed phase and hinders complete molecular condensation. The experimental observations imply that molecules are exchanged between the condensed phase and the gas phase, besides being in thermal equilibrium. The appropriate thermodynamic quantity which takes this exchange and the entropy into account is the Gibbs free energy, which is equal in the gas phase and in the condensed phase.

From a statistical analysis of a few STM images similar to the one described above the hopping rate ν_s^c for a molecule on the border of a condensed island (the molecules which are marked by the white line in figure 3.9) is determined to $\nu_s^c = 0.019 \pm 0.010$ s^{-1}. Assuming that the attempt frequency ν_0 does not change for a molecule in the gas phase with respect to the condensed phase, it is possible to get a rough estimate of the condensation energy:

$$E_{cond} = kT \cdot \ln \frac{\nu_S^g}{\nu_S^c} \tag{3.4}$$

Thus the condensation energy E_{cond} for a molecule on the border of the condensed phase is $E_{cond} = 0.19 \pm 0.02$ eV, with a statistical error due to the error in the hopping rates. This condensation energy E_{cond} is in the same range as the calculated C_{60}-C_{60} interaction. The binding energy at the equilibrium distance for two C_{60} is calculated to 0.3 eV [89]. However, this result for the condensation energy of SubPc has to be considered as semi quantitative due to the finite value of θ and the approximation that the attempt frequency is the same in both phases.

The relative values of the diffusion barrier, the condensation energy and the thermal energy are crucial for the observed coexistence behavior. A much higher condensation energy would cause complete condensation, e.g. no gas phase would be present. If the condensation energy and the diffusion barrier are smaller than the thermal energy all the molecules would form a 2D gas phase. In the case of SubPc adsorbed on Ag(111) the relative values of the diffusion barrier and the condensation energy result in a phase equilibrium at room temperature[11].

2D solid-gas equilibrium and surface melting processes of adatom layers have previously been reported [61, 72], also by STM studies [90–93]. Adsorbed molecules have additional internal degrees of freedom, which go beyond those of single atoms. However, in the condensed

---

[10]For a SubPc coverage of ≈ 0.7 ML tip induced experiments have been successfully carried out. A reversible phase transition of the hcp pattern and a 2D mobile phase could be controlled by the STM tip (Chapter 6). In the case of the low coverage honeycomb pattern similar trials with tip-induced experiments have been performed without success.

[11]Also the hcp pattern is observed in coexistence with a dense molecular gas phase. However, it was difficult and sometimes even impossible to see single molecular events in the gas phase.

phase the orientation of individual SubPc molecules is visible, and molecular rotation is there-fore frozen. In the SubPc gas phase a rotation or other internal motions of the molecules can not be ruled out [94]. In addition to possible changes of internal degrees of freedom upon diffusion and condensation, changes in conformation are also possible [11]. One may foresee that such additional degrees of freedom may cause characteristic deviations from the ideal lattice gas behavior. Using temperature-dependent STM techniques, some of this behaviour could be explored to give similar information about molecular adsorption and diffusion as specific heat measurements have provided about phase transitions in bulk materials. The system presented here, SubPc adsorbed on Ag(111), appears to be a good model system to study such effects.

3.4.   Proposed Phase Diagram for SubPc on Ag(111)

The SubPc overlayers with varying sub-monolayer coverage were measured by STM. For instrumental reasons the studies presented in this thesis were restricted to room temperature. Therefore the here presented STM results represent only a section taken at room temperature from the phase diagram. In Fig. 3.10 the proposed phase diagram is sketched and shows the features observed in the STM at positive sample bias. For coverage below ≈ 0.2 ML mobile molecules were observed to form a 2D lattice gas. A coexistence of the honeycomb pattern with a 2D lattice gas is observed for coverage in the order of 0.2–0.5 ML, whereas for coverage of 0.6–0.9 ML the hcp pattern is observed in coexistence with the 2D lattice gas. Consequently, the hcp pattern in coexistence with the 2D gas phase is thermodynamically favored at 0.7 ML compared to a full monolayer of the honeycomb pattern, which corresponds to 0.7 ML of a hcp monolayer. It is quite possible that new phases will be observed at different temperatures than room temperature making the phase diagram more complicated than the one sketched in Fig. 3.10. The exact phase behavior around 0.5 ML is still contradictory and different results were obtained on different samples. It is not yet clear whether there is a phase transition from the honeycomb pattern directly to the hcp pattern or, more likely, the honeycomb pattern decays at ≈ 0.5 ML to a 2D gas phase and at 0.6 ML the hcp pattern is formed. On large terraces a coexistence of the honeycomb pattern and the hcp pattern was never observed. On samples with many small terraces[12] however hcp and honeycomb pattern have been observed on different terraces. The border effect of the step edges could lead to a favored pattern depending on the width and form of the terraces. Furthermore, for one single deposited SubPc layer a new overlayer pattern was observed even at room temperature. This only once observed double row pattern is presented in appendix A and is not further considered, since it could not yet be reproduced. This additional pattern implies that a more complicated phase diagram has to be expected and that the formed molecular layers could also depend on additional parameters than only the coverage θ and the temperature. The layers could also depend on the quality of the substrate, i.e. the impurities and defects, or on the molecular rate during deposition. However, upon annealing the sample, the overlayer pattern forms the thermodynamically favored phase[13]. For both patterns, the honeycomb

---

[12]Terrace width in the order of 30–40 nm

and the hcp, no changes in the overlayer pattern were observed upon annealing to 360 K. Consequently, these two layers are expected to be thermodynamically favored.
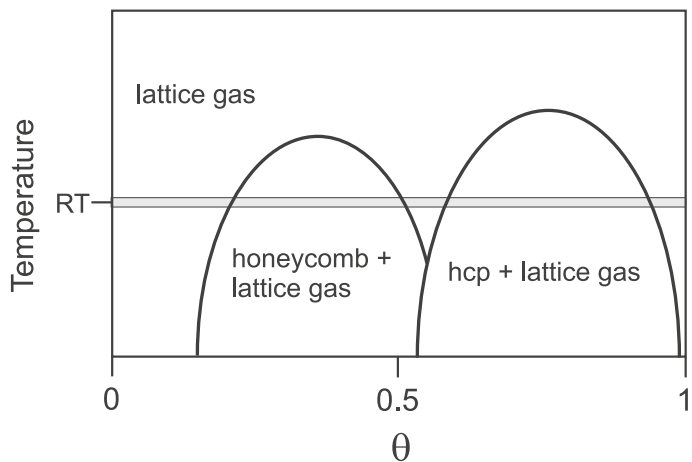

Figure 3.10.: Schematic sketch of the proposed phase diagram of SubPc/Ag(111) in the T–θ plane. The grey bar represents the studied regime at room temperature (RT). The reader should be aware that the phase diagram presented here is only schematic and may not represent all the features.

In order to determine the overlayer structure of the molecular layers LEED experiments have been performed as well. But these experiments did not succeed and it was not possible to determine the patterns. Different problems arised when trying the LEED experiments. The Ag(111) films were not single crystalline, which makes the interpretation of the LEED pattern more difficult. Another problem is that for imaging the large structures of the SucPc overlayers relatively small electron energies[14] are needed [95], which is a high demand on the LEED set-up. Another major problem is that the electron beam from the LEED gun probably damages the molecules or the overlayer pattern. On one molecular sample subsequent STM experiments have been performed and a destruction of the overlayer pattern has been observed. Thus, for successful LEED experiments a good LEED set-up, which allows the use of low electron energies and currents is a mandatory.

In lattice gas models the phase diagrams have been studied in detail by Monte Carlo simulations as a function of different pair and triple interactions [84–86, 96]. In models with either attractive or repulsive nearest neighbor interaction, only one ordered phase is observed for both cases [84, 85]. Ordered phases with distinctly different symmetry are observed for nearest neighbor repulsion in conjunction with next nearest neighbor attraction and three-body interaction [96]. The system O/W(110) was extensively studied by experiments [97–99] and by Monte Carlo simulations [100–102]. In the case of O/W(110) two different ordered

---

[13]Provided that the molecules have enough thermal energy to overcome the activation barrier to form the thermodynamically favored phase.

[14]In order to observe the first order of the diffraction pattern an electron energy of $\approx$ 20 eV or below is needed.

layers are observed for increasing coverage. A combination of attractive and repulsive inter-actions leads to this non-trivial phase behavior[15]. Also in the case of SubPc it is expected that a combination of attractive and repulsive two and more-body interactions lead to the observed phase behavior. In addition to the attractive van der Waals interaction, a re-pulsive interaction due to the parallel dipole moments of adsorbed molecules takes place. Furthermore, repulsive or attractive interactions occur depending on the relative angle of two interacting molecules due to the inhomogeneous charge distribution. The interaction between two molecules depends on their relative angle since the H atoms of the 'legs' are charged positive whereas the N atoms are charged negative (Fig. 1.1d). Consequently, the 'legs' repel each other and a favored position is found if the 'legs' point to the N of the neighboring phthalocyanine macrocycle. This configuration is observed for the honeycomb as well as for the hcp pattern. The balance between the condensation energy in the 2D islands and the entropy in the 2D gas phase leads to the coexistence of these two phases at room temperature.

The observed behavior of SubPc on Ag(111) differs from the one of C_{60} on Ag(111). For C_{60}/Ag(111) only one ordered phase is observed [67], whereas for SubPc/Ag(111) two ordered phases are observed. This difference in the phase diagram is expected to arise from the more complicated interactions between the SubPc molecules compared to the interactions between the highly symmetric C_{60} molecules.

---

[15]In the Monte Carlo simulations it was found that attractive first and fifth neighbor interaction and repulsive second neighbor, third neighbor and trio interactions give the best match with the experiments [100].

4. Adsorption Geometry and Electronic Structure of SubPc on Ag(111)

In the following the adsorption geometry of the SubPc molecules on the Ag(111) surface is determined and possible binding mechanisms are addressed (section 4.1). In section 4.2 high resolution STM data of SubPc and STM images at different tunneling conditions are discussed.

4.1. Adsorption Geometry and Binding of SubPc to Ag(111)

XPS measurements on molecular films with various thickness ranging from sub-monolayer coverage to several layers have been performed. In Fig. 4.1 the evolution of the Cl2p core level peak for increasing film thickness is shown. Compared to the film with a thickness of 13 ML a large shift of the Cl2p peak by 1.6 eV to lower binding energy is observed for the layer with sub-monolayer coverage. The film with a thickness of 2.3 ML reveals a similar spectrum as the one with a thickness of 13 ML. The main difference between the spectra obtained for these two films is the small shoulder at 198 eV binding energy observed at 2.3 ML coverage. Thus, for a layer thickness of 13 ML SubPc bulk-like signals are dominating the XPS spectrum due to the surface sensitivity of XPS (section 2.2). As a consequence, the measured Cl2p peak for the layer with 13 ML corresponds to the peak which would be obtained from bulk SubPc. On the other hand, only 2D growth is observed in the STM experiments of sub-monolayer coverage and therefore every SubPc molecule is directly adsorbed on the Ag(111). Thus, for sub-monolayer coverage the XPS measurements are sensitive to the SubPc-Ag interaction. Compared to the film with a thickness of 13 ML the C1s and the N1s core level peaks shift only slightly to lower binding energies (shift of 0.2-0.3eV) at sub-monolayer coverage, which is in contrast to the large shift of the Cl2p peak. The shift in the C1s and N1s peaks for the thickness above 1 ML is mainly attributed to charging effects upon irradiation of the layers, which will be discussed later on. Therefore, the observed core level shift of the Cl2p peak for sub-monolayer coverage is attributed to a chemical shift due to an interaction of the Cl with the Ag substrate. The binding energy of this peak is in good agreement with the one obtained from Cl/Ag as measured by Briggs and coworkers [103]. Consequently, the Cl in the SubPc interacts with the Ag substrate and therefore the SubPc is adsorbed with the Cl towards the substrate. The chemical shift is attributed to a partial electron charge transfer from the Ag substrate to the Cl of the SubPc as the peak shifts to lower binding energy by the interaction with the Ag substrate. This is consistent with the chemical shift which is expected from the respective electronegativities of Ag and Cl.

Complementary UPS measurements have been performed on SubPc layers with various thickness. In Fig. 4.2 the evolution of the UPS spectra measured with HeI excitation is
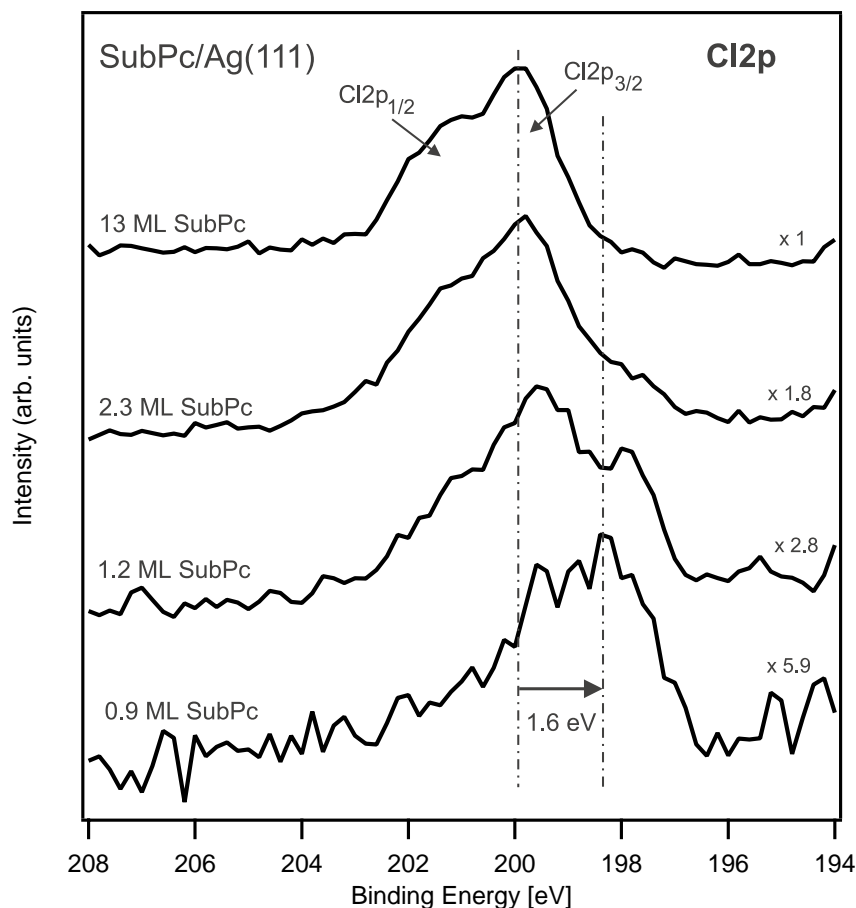
Figure 4.1.: XPS spectra of the Cl2p peak for increasing coverage measured with MgK_α excitation. A chemical shift to lower binding energy is observed for sub-monolayer coverage.

presented for different coverage. In addition to the HOMO located around 1.8 eV binding energy (denoted as HOMO in Fig. 4.2) molecular orbitals with a higher binding energy are visible as well in the spectra. Besides the HOMO, the peak around 9 eV binding energy (denoted as MO4 in Fig. 4.2) is easy to identify even for sub-monolayer coverage, since no features of the Ag(111) valence band are located in this energy region. For the UPS spectra below 1 ML the features of the Ag(111) substrate contribute significantly to the spectra. The main change in the UPS spectra with increasing layer thickness is the vanishing of the Ag features and the shift of the peaks from the SubPc orbitals to higher binding energies, as observed for the films with a coverage higher than 1 ML. However, the shape of the molecular features in these spectra remain almost unchanged. Because of the high surface sensitivity of UPS, only SubPc molecules without interaction to the Ag substrate are measured for the film with a thickness of 13 ML. Thus the measured spectrum corresponds to the spectrum which would be obtained from bulk SubPc. In Fig. 4.2b the shift of the different spectra is compensated in order to match the position of the HOMO for each coverage. In this figure

it is evident that only small changes in the SubPc features occur in the UPS spectra for the different SubPc coverage. In all the UPS spectra the energy difference $\Delta E_{HOMO-MO4}$ from the HOMO to the MO4 are equal within their errors (table 4.1). Furthermore no partial filling of the LUMO upon adsorption of the SubPc on the Ag(111) surface could be observed. This excludes a charge transfer from the Ag to the LUMO of the SubPc molecule. The partial electron charge transfer from the Ag to the Cl of the SubPc, which is observed in the XPS measurements seems to be localized at the Cl. The frontier orbitals of the π-electron system appear not to be affected by this charge transfer and do not lead to a significant change in the electronic structure of SubPc. However, there is a hint for an interaction between the Ag substrate and the SubPc: The main peak of the Ag4d valence band at 5 eV binding energy vanishes to a greater extent than the two peaks around 6 eV binding energy[1].
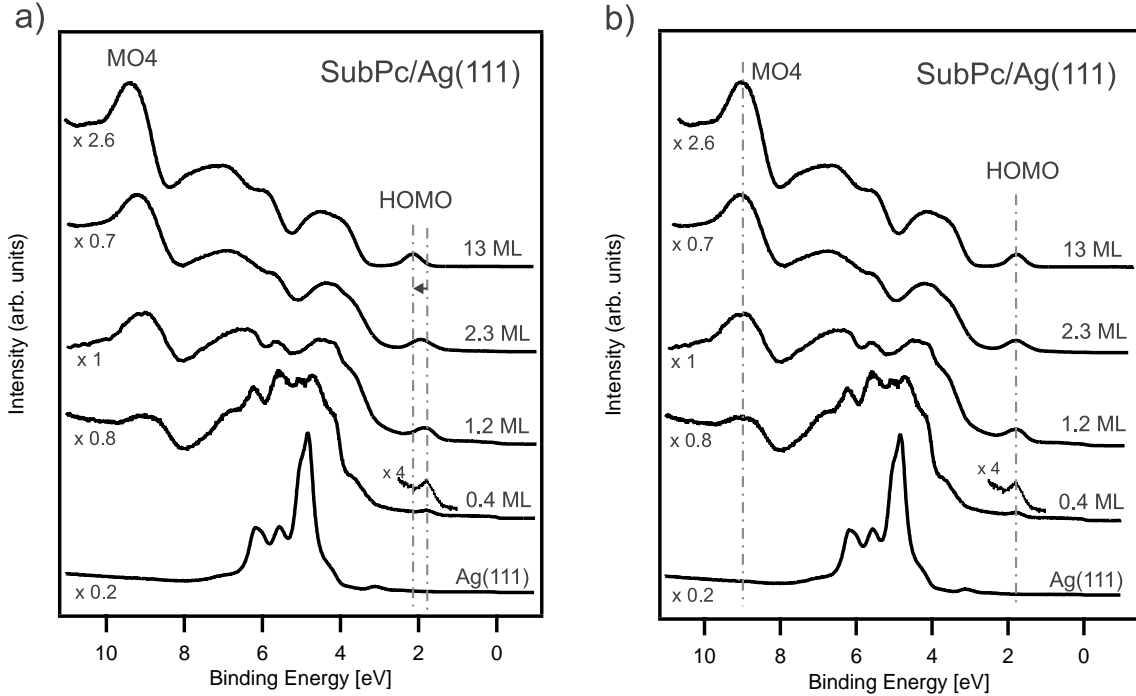
Figure 4.2.: UPS spectra of SubPc on Ag(111) for different thickness measured with HeI excitation. For the clean Ag(111) substrate the Ag4d valence band is mapped. (a) A shift of the spectra to higher binding energies is observed for higher thickness. This is attributed to charging effects of the molecular layer. (b) The same spectra as in (a), but the shift is compensated by matching the HOMO for all thickness. Apart from the disappearance of the Ag features only small changes are observed for the different layers. In particular, the energy difference between the HOMO and the MO4 is equal for all layers. The binding energies are given with respect to the Fermi energy E_F.

It is expected that the observed shift of the binding energies of the molecular orbitals for increasing coverage is not due to a charge transfer from the Ag(111) substrate to the

---

[1]For a layer having no interaction to the substrate, an uniform attenuation of the substrate features is expected with increasing layer thickness.

SubPc. UPS measurements are even more surface sensitive than XPS [55]. Therefore the shift in the whole UPS spectra from the film with a thickness of 2.3 ML to the one with 13 ML can hardly account for the charge transfer from the Ag substrate to the molecular film. The shift of the UPS spectra for the 'thick' molecular layers can be explained by the charge screening in the metallic substrate or by a charging of the molecular layer upon irradiation. For molecular layers in close proximity of a metal surface a photoemission hole in the molecular layer leads to an image charge in the metallic substrate, which screens the initial hole. Bulk SubPc is non-conductive and therefore the screening of a photoemission hole is poorer than for a thin molecular layer on a metal surface. As a consequence, higher binding energies are observed for the orbitals of the bulk material compared to a thin film on a metallic substrate. Such shifts due to screening effects in the photoemission spectra are also observed for C_{60} on metallic substrates [104, 105]. In addition, the shift in the UPS spectra could also arise from charging of the molecular layer upon irradiation. The irradiation induced emission of photoelectrons leads to a positive charging of the sample and thus to a shift of the peaks in the spectra to higher binding energies[2].

There is no evidence for decomposition of the SubPc molecule upon adsorption on Ag(111) as only small changes are observed in the UPS spectra for different thickness. In a 'gedanken experiment' the decomposition of the SubPc due to a split off of the chlorine seems be a feasible process. Cl chemisorbs on the Ag substrate with a sticking coefficient in the order of unity upon Cl_2 exposure at room temperature [103]. Furthermore, ab-initio DFT calculations reveal that the isolated SubPc molecule is stable as a cation without the Cl, i.e. as a +1e charged ion (in the following denoted as $[SubPc]^+$). The calculations for the neutral SubPc without the Cl did not converge and thus no stable configuration was obtained. The calculations of the SubPc molecule without the Cl were performed by S. Ivan with the Gaussian98 program package [25] (section 1.2). According to these calculations all molecular orbitals of the $[SubPc]^+$ shifted to higher binding energies, e.g. the shift of the HOMO is 3.36 eV. Figure 4.3 shows the DOS of the calculated SubPc and $[SubPc]^+$, respectively and the binding energies of the different molecular orbitals. Additionally, the DOS graph obtained by broadening the orbitals by a Gaussian function is drawn into the figure. The width of the Gaussian function is chosen to be the same width as the one of the HOMO in the measured UPS spectra. In these DOS graphs the HOMO and the MO4 can clearly be identified and related to those in the UPS spectra. Besides the shift of the orbitals to higher binding energies in the case of the $[SubPc]^+$, a characteristic decrease in the energy difference $\Delta E_{HOMO-MO4}$ of 360 meV is calculated. In the UPS spectra neither a shift of the spectra to higher binding energy, nor a decrease of $\Delta E_{HOMO-MO4}$ upon adsorption of SubPc on the Ag substrate is observed (table 4.1). This is a clear evidence against a decomposition of SubPc upon adsorption.

The change of the work function upon SubPc adsorption was determined by UPS with HeI

---

[2]Charging effects usually occur more pronounced in UPS than in XPS measurements. The X-rays penetrating through the thin Al-window in front of the X-ray source produce photoelectrons and thus secondary electrons. A certain amount of these electrons hit the sample and partially compensate the charging upon irradiation by the X-rays. In addition, the difference in the mean free path of the photoelectrons for UPS and XPS can lead to different charging effects.
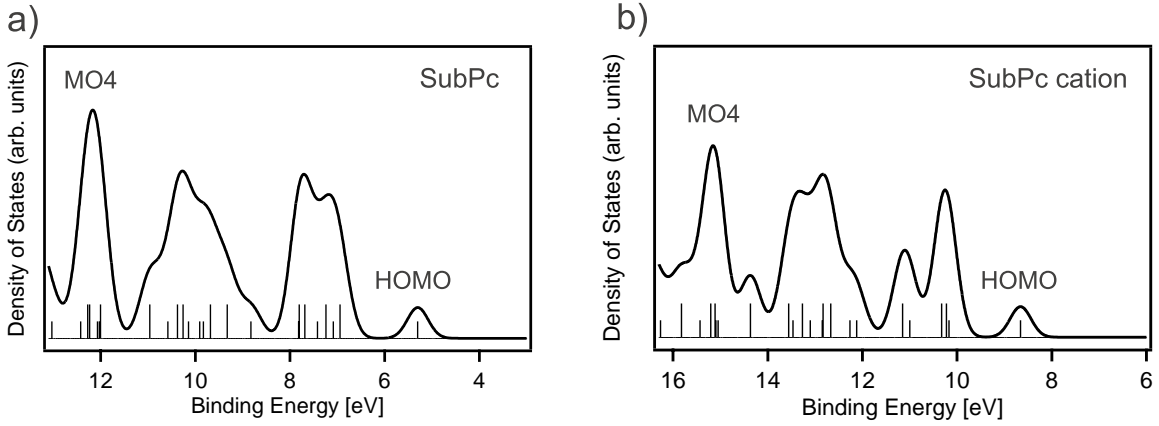
a)   b)

Figure 4.3.: Calculated density of states for (a) the SubPc and (b) the SubPc cation ([SubPc]$^+$). The calculated energies of the individual orbitals are indicated. The graph was obtained by a convolution of the orbitals with a Gaussian function. The Gaussian function is chosen by adapting the width of the calculated HOMO to the width of the HOMO measured by UPS. The resulting structure is similar to the UPS spectra and the HOMO and MO4 can be identified.

	BE HOMO [eV]	BE MO4 [eV]	$\Delta E_{HOMO-MO4}$ [eV]
0.4 ML SubPc	1.78 ± 0.03	8.90 ± 0.10	7.12 ± 0.10
1.2 ML SubPc	1.83 ± 0.02	8.98 ± 0.03	7.14 ± 0.04
2.3 ML SubPc	1.93 ± 0.02	9.09 ± 0.03	7.16 ± 0.04
13 ML SubPc	2.16 ± 0.02	9.27 ± 0.03	7.11 ± 0.04
calculated SubPc	5.30	12.17	6.87
calculated [SubPc]$^+$	8.66	15.17	6.51

Table 4.1.: Binding Energies (BE) of the HOMO and the MO4 for different coverage in comparison with values calculated for SubPc. The energy difference $\Delta E_{HOMO-MO4}$ between the HOMO and the MO4 is equal in all UPS spectra. For the SubPc cation a shift of the HOMO of 3.36 eV to higher binding energy as well as a decrease of $\Delta E_{HOMO-MO4}$ by 0.36 eV is calculated. The binding energies of the UPS measurements are related to the Fermi energy E_F of the Ag(111), whereas the binding energies for the SubPc and [SubPc]$^+$ are calculated for the free molecule and therefore relate to the vacuum energy E_V.

excitation. The work function was measured by applying a negative voltage of $U = -10$ V to the sample in order to cover the whole width ΔE of the spectra including the low energy cut off of the emitted photoelectrons. The work function is then determined using the Einstein equation (equation 2.7).

$$\phi = h\nu - \Delta E \qquad (4.1)$$

The obtained values are listed in table 4.2 and reveal a decrease of the work function upon SubPc adsorption. An extrapolation of the values measured at sub-monolayer coverage to 1 ML leads to a decrease in the work function of $\Delta \phi \approx -1$ eV. This is in agreement with the value observed at 1.2 ML under the assumption that the decrease is maximal at

1 ML and that molecules exceeding 1 ML reduce the dipole moment of the molecular layer[3]. A reduction of the work function is expected for the adsorption of the SubPc with the chlorine towards the Ag substrate. In this configuration the permanent dipole moment is perpendicular to the Ag surface pointing away from it. Therefore, the surface dipole of the metal is reduced leading to a reduction of the work function [61]. According to a simple model where the dipoles of the adsorbed molecules are treated as a parallel plate capacitor, the change of the work function is given by [106]:

$$\Delta\phi = e \cdot p \cdot N_A/\epsilon_0 \tag{4.2}$$

In this equation p is the dipole moment, N_A the number of dipoles per surface area and ϵ_0 the permittivity of free space. The calculated dipole moment of SubPc is 1.0 eÅ (section 1.2) which leads to a decrease of $\Delta\phi = -0.58$ eV for 1 ML using equation 4.2. However, an image dipole is formed in the metallic substrate due to the SubPc dipole. Because the SubPc dipole is perpendicular to the surface, the image dipole has the same orientation, which leads to a reinforcement of the total dipole moment [61] (Fig. 4.4). Therefore the dipole moment per molecule is doubled on a metallic substrate leading to a change in the work function of $\Delta\phi = -2 \cdot 0.58 = -1.16$ eV. This value is in agreement with the measured reduction of the work function of $\Delta\phi \approx -1$ eV. For a more accurate treatment of the calculated change in the work function one has to take into account that the electric field at the site of a particular dipole is modified by all the surrounding dipoles [106]. However, the deviation of the experimental and the calculated changes in the work function could also be due to the partial charge transfer from the Ag substrate to the SubPc molecule as observed in the XPS measurements. This charge transfer leads to an induced dipole moment between the transferred charge and its image charge. This resulting dipole moment points against the surface (Fig. 4.4) and would therefore reduce the total dipole moment of the molecule. To sum up, the work function measurements give additional evidence that the SubPc is adsorbed intact with the Cl towards the Ag(111) surface.

	ϕ [eV]	$\Delta\phi$ [eV]
Ag(111)	4.60 ± 0.02	
0.4 ML SubPc	4.22 ± 0.02	-0.38 ± 0.03
0.5 ML SubPc	4.13 ± 0.02	-0.47 ± 0.03
1.2 ML SubPc	3.77 ± 0.02	-0.83 ± 0.03

Table 4.2.: Work functions measured for SubPc layers on Ag(111). A decrease of the work function is observed upon SubPc adsorption.

In summary, the intact SubPc molecule is mainly physisorbed on the Ag(111) substrate with the Cl towards the Ag surface (Fig. 4.5). It is expected that the binding forces are due to van der Waals interaction and the attractive force of the SubPc and its mirror charges in the metal substrate. In addition there is a chemical bond between the Ag and the Cl of the

---

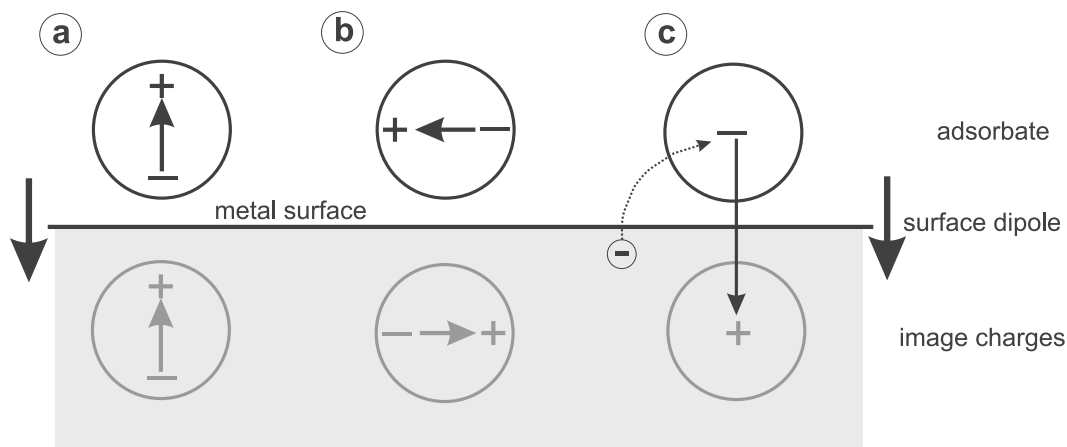[3]This is assumed since bulk SubPc has a net dipole moment of zero [22].

Figure 4.4.: Sketch of adsorbate dipole moments in the vicinity of a metal surface. The surface dipole moment of the metal is indicated by the arrows on both sides of the sketch. The metal bulk is shaded light grey and the image charges in the metal are drawn in grey. (a) The induced image dipole reinforces the adsorbate dipole moment for a dipole aligned perpendicular to the surface. (b) In case of a dipole moment parallel to the surface a counter dipole is induced in the metal. (c) An electron charge transfer from the metal to the adsorbate induces a dipole moment pointing towards the surface.
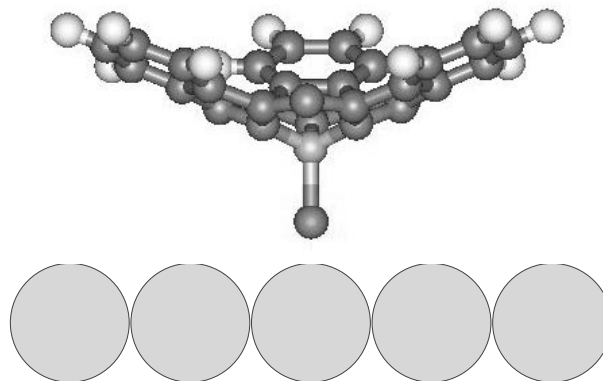
Figure 4.5.: Schematic sketch of the geometry of SubPc adsorption on Ag(111). The SubPc adsorbs with the Cl towards the Ag surface. From symmetry arguments it is concluded that the molecule adsorbs on an on-top site (Chapter 3).

SubPc. However, the frontier orbitels of the π-electron system of the molecule seems not to be affected by this chemical bond, since no significant changes in the UPS spectra were observed, when going from sub-monolayer to multilayer coverage. Especially no partial filling of the LUMO is observed. In the case of C_{60} on Ag(111), the molecules are chemisorbed on the surface which results in changes of the UPS spectra for sub-monolayer coverage compared to multilayer coverage [107]. The charge transfer of about 0.8 e^- per C_{60} leads to a partial filling of the LUMO, which is observed as a peak around the Fermi energy E_F [107]. Thus,

it is concluded for the SubPc on Ag(111) that the molecules are mainly physisorbed. The center of the SubPc molecule (the Cl) is adsorbed on an on-top site of the Ag(111), as deduced from symmetry arguments in Chapter 3. However, a modification of the substrate upon adsorption of the SubPc can not completely be ruled out. Due to the high stability of silver chloride (AgCl), the Cl atoms could replace Ag atoms of the topmost surface layer. In this configuration the Cl would be surrounded by 9 silver atoms instead of only one in case of an on-top adsorption. Reconstructions or modifications of the substrate upon adsorption of an organic molecule were observed in recent studies for various molecule-metal systems [11, 108, 109].

4.2. STM Images of SubPc Under Different Tunneling Conditions

In STM images with positive sample bias in the order of $U = 0.6$–2 V the SubPc is imaged for the honeycomb and the hcp pattern with an apparent height $h \approx 4.5$ Å. The apparent height decreases for bias voltages smaller than 0.6 V. At a voltage below 0.2–0.3 V the molecules are not imaged anymore and only noisy images are obtained[4]. The increase of the apparent height at a voltage of 0.6 V is associated with resonant tunneling into the LUMO for higher bias voltages. The HOMO-LUMO gap of the adsorbed SubPc molecule is therefore estimated to 2.4 eV[5], which is in agreement with the gap of 2.2 eV determined in a dimethylholamide solution [26]. In high resolution data the SubPc molecules are imaged with sub-molecular resolution. Each molecule is imaged as three protrusions having the same height with a slight depression in the center of the molecule (Fig. 4.6). The distance between the center of two protrusions is 8.3 ± 1.0 Å as measured in the STM data. This corresponds to the distance between the center of two phenyl rings in the SubPc which is 7.6 Å (section 1.2). Consequently, these STM images support the findings from the photoemission data that the SubPc is adsorbed with the Cl towards the Ag surface because the three 'legs' are imaged as protrusions and the center of the molecule as a slight depression. The same height of all three protrusions suggests that the B-Cl axis is perpendicular to the Ag surface. However, a wobbling of the molecule with the B-Cl axis to different sides on a time scale much faster than the one accessible by the STM can not be ruled out. This wobbling process would also lead to protrusions with the same height in the STM images, if the B-Cl axis is perpendicular to the Ag surface in time average[6]. The DFT calculations for the SubPc revealed that the molecule has a small intensity from the LUMO at the Cl. Thus, in the case of the Cl pointing away from the surface the molecule is expected to be imaged as a protrusion in the center of the molecule for positive sample bias because of the tunneling into the LUMO. Yanagi et al. found different adsorption geometries for the SubPc on Si(111)-(7x7) [26]. In their STM images they observed molecules with three protrusions and some with only one central protrusion and attributed these different shapes to Cl down adsorption, Cl up adsorption

---

[4]The apparent height and the critical voltages can differ for different tips.

[5]The binding energy of the HOMO of 1.8 eV (from UPS) and the location of the LUMO of 0.6 eV above the Fermi energy (from STM) leads to a HOMO-LUMO gap of 2.4 eV.

[6]Such a time average of a dynamic process is for instance observed with STM for the Si(100) dimer buckling [110].
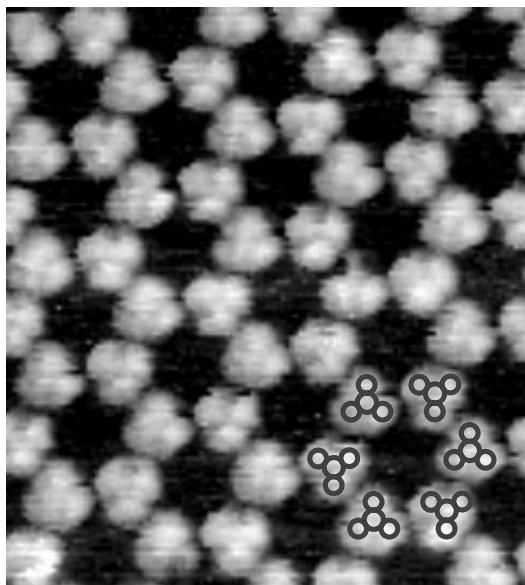
respectively.

Figure 4.6.: STM high resolution pictures of SubPc on Ag(111) in the case of the honeycomb pattern. Individual SubPc molecules are imaged as three protrusions. The internal structure of the molecule is outlined at the bottom right (scan range 14x16 nm; $I = 10$ pA, $U = 0.7$ V).
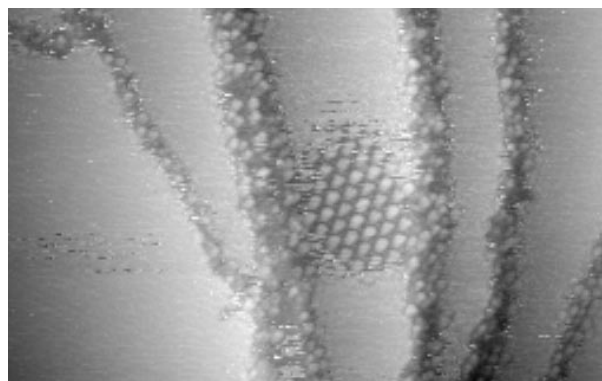
Figure 4.7.: STM image of SubPc on Ag(111) obtained by imaging with negative sample bias. In the center of the image a small island with hcp pattern is present. Next to the island and on the other terraces the molecules form a dense 2D gas phase (scan range 90x56 nm; $I = -10$ pA, $U = -1.5$ V).

For negative sample bias voltages the behavior of the SubPc layers on Ag(111) changes in the STM. The honeycomb pattern could only be imaged with a weak negative sample bias between -0.1 and -0.3 V. For this bias range the same behavior with the coexistence of the condensed honeycomb pattern and the 2D gas phase is observed as for positive sample bias.

For higher negative sample bias ($U < -0.3$ V) no individual molecules could be resolved on terraces anymore, where also by resonant tunneling out of the HOMO no ordered pattern is obtained. The step edges remain decorated with single molecules being resolved, whereas on terraces only a 2D gas phase is observed. It is important to note that the terraces are neither empty nor the molecules "invisible" for the STM, although in some cases almost no corrugation on the terraces is found. In Fig. 4.7 an image with negative sample bias in the case for the hcp pattern is presented. A small island with the hcp pattern remained in this image. From a height comparison of the hcp pattern and its surrounding, it is concluded that the terraces are covered by a dense 2D gas phase and are not empty. It worked only in a few cases to get images of stable hcp islands over a longer period of time. In most cases all the islands with hcp pattern disappeared after scanning a few images with negative sample bias and only 2D gas phase remained on the terraces.

The different behavior of the SubPc layers for positive and negative sample bias is attributed to the permanent dipole moment of the SubPc which experiences a force in the inhomogeneous electric field of the tip. This force acting on the dipole moment of the SubPc leads to directional diffusion towards or away from the tip depending on the polarity of the applied bias voltage. This simple model is described in Chapter 6 and leads to a higher mobility of the SubPc molecules in case of negative bias voltage.

5. Coordinated Change in Orientation of Whole Overlayer Islands

For the honeycomb and the hcp pattern a change in orientation of the overlayer pattern between the two respective orientations is observed. In section 5.1 an introduction in the microscopic mechanisms of island diffusion is presented. The experimental findings on the change in orientation of the overlayer islands are presented in section 5.2.

5.1. Introduction to Island Diffusion

The adatom and island diffusion on surfaces are important for thin film and crystal growth. An island migrates because statistic fluctuations at its border cause shifts in the location of its center of mass. Different mechanisms for island diffusion in a lattice model are: perimeter diffusion, evaporation-condensation of atoms on the border and migration of vacancies across the island [111, 112].

In the perimeter diffusion mechanism, individual adsorbates move around the perimeter of the island and cause center of mass diffusion. This behaviour is expected to be observed at lower temperatures, where the diffusion barrier along the island periphery still permits the adsorbate to move along the island, while a higher barrier prevents the adsorbate to evaporate from the edge to free 2D motion. For systems which are in coexistence with a 2D gas phase, the evaporation from the island is more favorable and the evaporation-condensation of adsorbates may cause the island to diffuse. The evaporation-condensation process is also relevant for systems where the barrier for detachment from the island is low compared to the perimeter diffusion barrier.

The diffusion coefficient D of an island with the number N of adsorbates can be described by an Arrhenius law [112–115]:

$$D \sim N^{-\alpha} \cdot exp\Big(-\frac{E_a}{kT} \Big) \tag{5.1}$$

where E_a is the activation energy for island diffusion and kT the thermal energy. For the island size a simple scaling law is valid [111, 112]. The temperature independent exponent α depends on the diffusion mechanism: for perimeter diffusion $\alpha = 3/2$, for evaporation-condensation $\alpha = 1/2$.

Island diffusion has been experimentally observed for instance for Ag clusters on Ag(100) [116] as well as for vacancy island diffusion, for instance in the case of Ag(111) [117].

5.2.   Experimental Observation and Discussion of Coordinated Flipping of Overlayer Islands

In STM measurements of SubPc on Ag(111) the orientational change of whole overlayer islands in the case of the hcp and the honeycomb pattern is observed. As discussed in Chapter 3, for each pattern, the honeycomb and the hcp, only two stable orientations of the superstructure are observed. The flipping process between the two orientations of the SubPc islands occurs in a reversible manner. Figure 5.1 shows this flipping process for the hcp pattern[1]. The orientation of the central island changed from Fig. 5.1a to the subsequent image Fig. 5.1b. In Fig. 5.1c the flipping process occurred during scanning the image. The time scale of the flipping process is usually in the order of one scan line and in this case in the order of five scan lines (time per line 0.6 s). It is important to note that for this rotational flipping each molecule has to move and to rotate in order to form the pattern with the new orientation. For the hcp pattern a weak tendency is observed that small islands have a higher probability for the flipping process. Besides the island size, the border effects of the island and the step edges of the silver substrate seem to play an important role. A misfit of the molecular island and the step edges could lead to stress in the layer or to molecule positions which are not favored by the pattern and the substrate. The shape of the step edges and the molecular coverage can lead to a stabilisation or destabilisation of an adlayer through registry effects at the boundary.

Figure 5.2 shows STM images of the orientation change for the honeycomb pattern. The three pictures are obtained one after the other with an interval time of approximately 3 minutes. The flipping process in Fig. 5.2b occurred within one single scan line (0.3 s). In case of the honeycomb pattern the flipping process is accompanied by a chirality change, since the two orientations have different chirality. Consequently, a change in orientation is a phase transition between the two chiral layers. In Fig. 5.2a a vacancy in the molecular pattern is visible which disappeared in the next image Fig. 5.2b. This vacancy gives additional evidence for the high level of mobility in such layers. For the honeycomb pattern only very few islands exhibited this flipping process and no characteristic tendency for the flipping probability as a function of the size of the island could be observed.

Hardly any movement of the center of mass of the island in such a flipping behavior is observed. However, it is a collective diffusion phenomenon and has to be treated as a special case of island diffusion. In a floating layer model[2] a substantial part of the central island in figure 5.2 would have to cross the step edge. This can not be supported from our STM time lapse imaging series. Here inter-terrace diffusion would lead to correlated number density changes on neighboring terraces. This has not been observed for either honeycomb or hcp layers. In addition, it is not possible to bring the honeycomb pattern to overlap by

---

[1]The central island in Fig. 5.1 is on a lower height level than the surrounding terraces. This vacancy island in the Ag(111) is not because of sputter defects. It is because a grain boundary of the Ag(111) substrate is crossing the image from the left hand side to the top side. Therefore the SubPc pattern on the top left has different orientation than the other islands.

[2]In the picture of a floating layer model, the whole island is expected to stick together and to diffuse as an entity on the substrate.
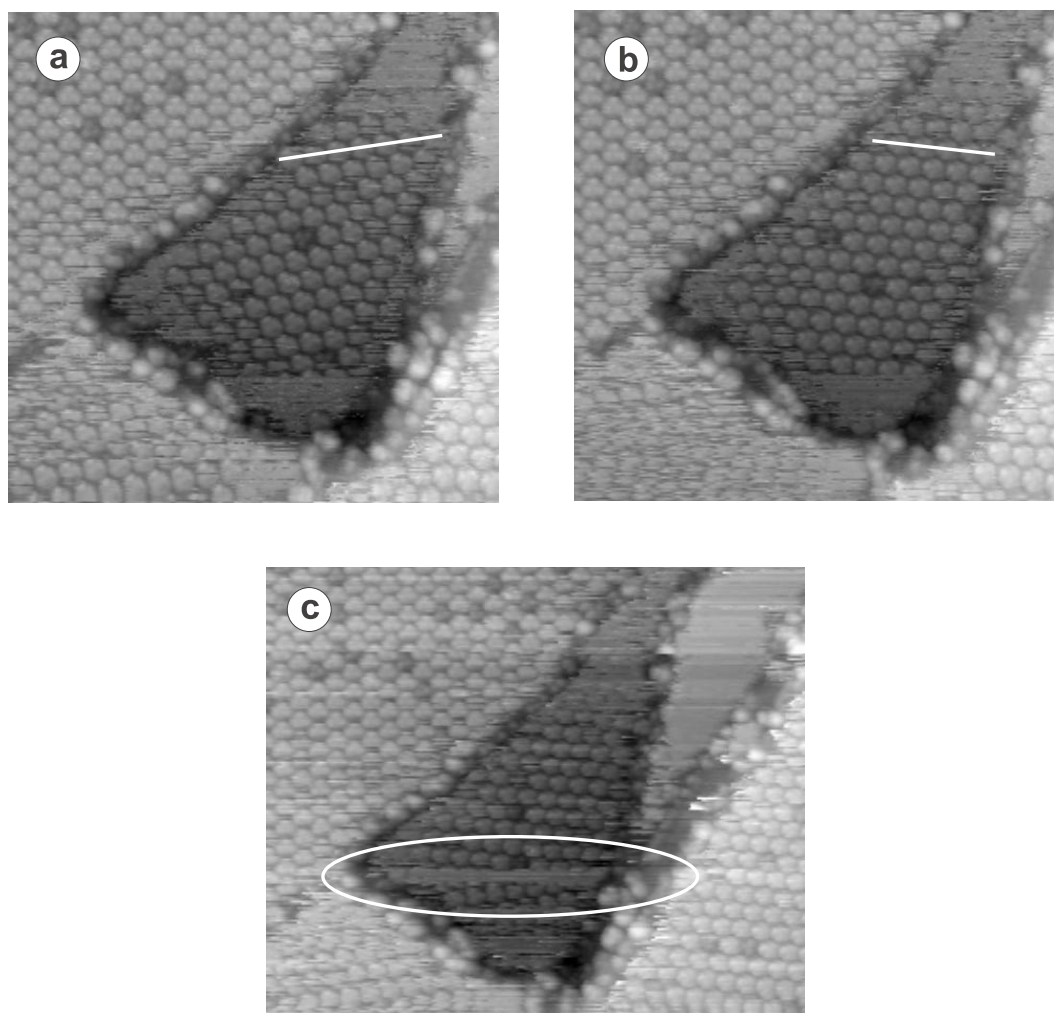
Figure 5.1.: Change in orientation for an island with hcp pattern. The central molecular island flips its orientation between the subsequent STM images (a) and (b). The white line in the images shows the orientation of the island and acts as a guide to the eye. The time interval between the two images is 2 minutes 30 seconds (scan range 39x39 nm; $I = 20$ pA, $U = 1.5$ V). In image (c) the flipping process occurred during scanning the image. The time scale of the flipping process is in the order of seconds (scan range 56x43 nm; $I = 20$ pA, $U = 1.5$ V).

a simple rotation due to its chiral layers. Therefore a floating layer model in the case of SubPc islands on Ag(111) is ruled out. The experimental finding that only two orientations for the honeycomb and the hcp pattern are observed, implies that the molecule-substrate interaction is important. Therefore the system has to be treated in terms of a lattice model as observed in section 3.3 for the lattice gas phase.

The proposed mechanism in terms of a lattice model in analogy to the evaporation-condensation mechanism is the following: Detachment of a small cluster from the original island or formation of a new cluster from the 2D molecular gas phase with different orientation than the original island. This cluster formation could even be assisted or induced by the
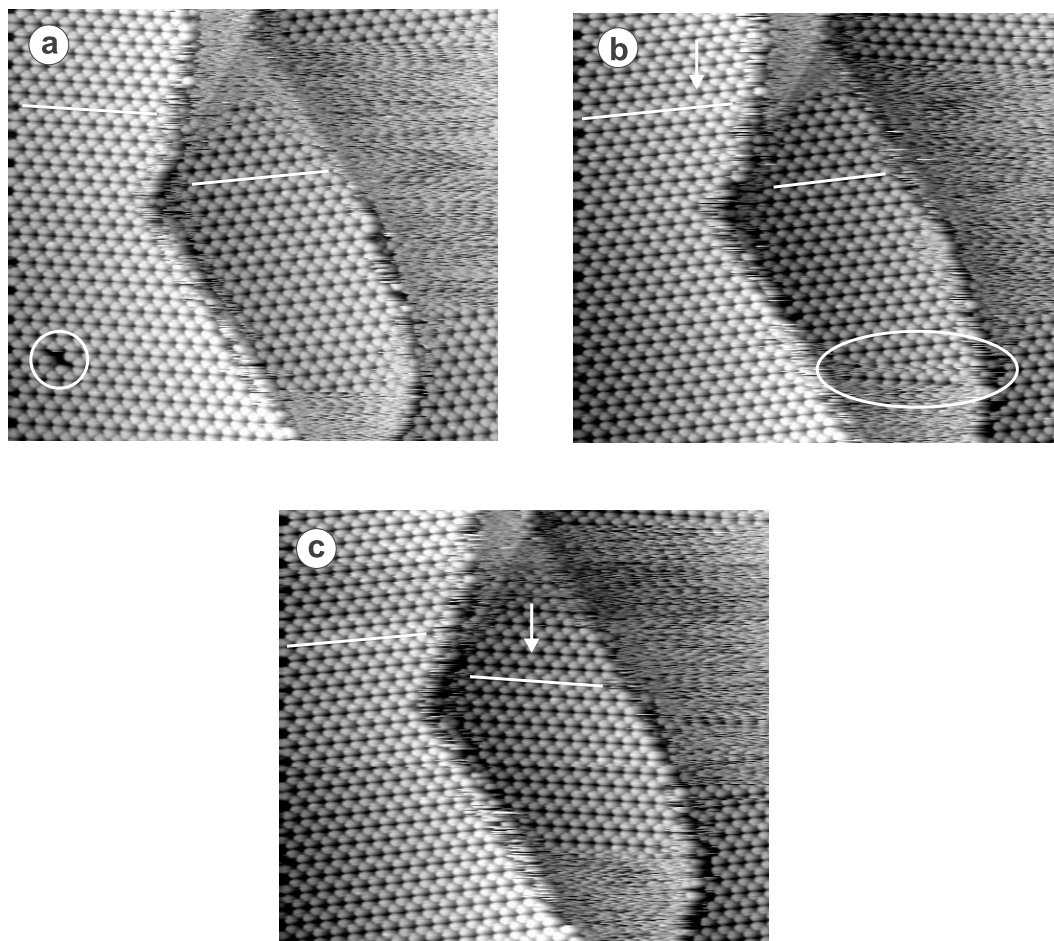
Figure 5.2.: Flipping process for the honeycomb pattern. The three STM images are taken one after the other with a time interval of approximately 3 minutes. From (a) to (b) the large island on the left hand side flipped its orientation, whereas from image (b) to (c) the central island flipped. The white lines indicate the orientation of the patterns. A change in orientation is marked by the white arrows. The vacancy in (a) (marked by the white circle) disappears from (a) to (b), which shows the dynamics of single molecules in the overlayer pattern. The central island flips its orientation in (b) during scanning (marked by the white ellipsoid) (scan range 90x79 nm; $I = 20$ pA, $U = 2.2$ V).

scanning tip (compare also Chapter 6). This would lead to a domain boundary between the original island and the newly formed cluster where the boundary propagates with a certain probability through the whole island while changing its orientation. Since the island is in coexistence with a dense 2D gas phase it is expected that the main mechanism for island diffusion in this crack is due to the evaporation-condensation mechanism. This suggestion is supported by figure 5.1 which shows a gas phase during the change of orientation. Perimeter diffusion may enhance and accelerate the process.

Only very few examples on changes in orientation of overlayer islands are reported in the literature. Rabe and Buchholz observed in the case of octadecanol on HOPG flipping

of small molecular domains [118]. These domains are surrounded by other domains and the configuration after the flipping of the domains appeared to be more stable. The authors did not report about a reversible flipping behavior of such domains. In the work of Lüthi et al. islands of C_{60} on NaCl(001) could be moved by the action of the probing tip of a scanning force microscope [119]. Different modes of motion, such as translation and rotation, were observed. In their work the motion of the C_{60} islands is clearly tip assisted. The change in orientation of the SubPc islands on Ag(111) occurs spontaneously between two subsequent images or during scanning an image. However, this reversible flipping process might be influenced by the scanning tip. To my knowledge the observed flipping behavior between the two stable orientations of the SubPc islands is a new phenomenon. The balance of the molecule-substrate, the inter-molecular interaction and the thermal energy are in such a way that the molecular islands are in coexistence with a 2D molecular gas phase at room temperature. Furthermore, whole islands are not completely stable and tend to rotate between the two stable orientations in a coordinated fashion.

6. Phase Transitions Locally Controlled by the STM-Tip

For SubPc coverage in the order of 0.7 ML a coexistence of the 2D hcp phase and the 2D molecular gas phase is observed[1]. On large terraces the hcp pattern is formed (section 3.2) while in confined areas, e.g. narrow terraces[2] or in corners of two joining steps, a dense 2D gas phase is observed (Fig. 6.1). These experimental findings suggest that on large terraces the hcp pattern is favored, whereas in confined areas the gas phase is dominating. In order to better understand the role of lateral confinement on the formation of molecular phases additional confined areas have been introduced onto the substrate. Such confined areas are introduced to the Ag(111) by the creation of sputter defects, i.e. monatomic vacancy islands with diameters in the range of 30–80 nm (section 2.5). In these confined regions interesting and unusual phase behavior of the molecular layer is observed.

Molecular layers (coverage ≈ 0.7 ML) on the Ag(111) substrates with the vacancy islands exhibit the same coexistence of the hcp pattern and the 2D gas phase on the terraces as described above. Mostly, the vacancy islands exhibit only little corrugation in the STM images (Fig. 6.1a). These vacancy islands are not empty but the confined molecules form a 2D gas phase as observed on narrow terraces. In the following, two different STM modes are defined: In the 'imaging mode' an overview image is recorded with a scan range of 90–110 nm (tunneling parameters $I = 10$–20 pA, $U = 1.0$–1.6 V). In the 'nucleation mode' the image is recorded with a small scan range of 10–40 nm (tunneling parameters $I = 10$–200 pA, $U = 1.0$–2.0 V). Therefore the main difference between these two modes is the scan size. By scanning in the 'nucleation mode' in the center of the vacancy island, the gas phase in the vacancy island typically condenses to the hcp pattern. This interesting phase transition is shown in Fig. 6.1. In this figure the vacancy island is imaged in the 'imaging mode' before and after the tip-induced condensation due to the 'nucleation mode'. Before the scanning in 'nucleation mode', a dense 2D molecular gas phase is present inside the vacancy island, whereas afterwards the molecules are condensed to the hcp pattern. It is important to note, that these STM images obtained in the 'imaging mode' are recorded with exactly the same scanning and tunneling parameters. This excludes that the two phases are obtained due to imaging at different tunneling conditions. In order to investigate the conditions for the tip induced phase transition, experiments with various scan parameters have been performed. By scanning in the 'imaging mode' no condensation of the vacancy island could be achieved, although various scan velocities have been used ranging from 70–275 nm/s. Consequently, for a successful condensation of the gas phase to the hcp pattern, the vacancy island has to be imaged in the 'nucleation mode'. Higher voltages in the 'nucleation mode' are observed to facilitate the tip induced nucleation process, whereas changing the tunneling current did

---

[1]Similar to the 2D solid-gas coexistence of the honeycomb pattern which is discussed in detail in section 3.3.
[2]Terraces with a width below 20–30 nm

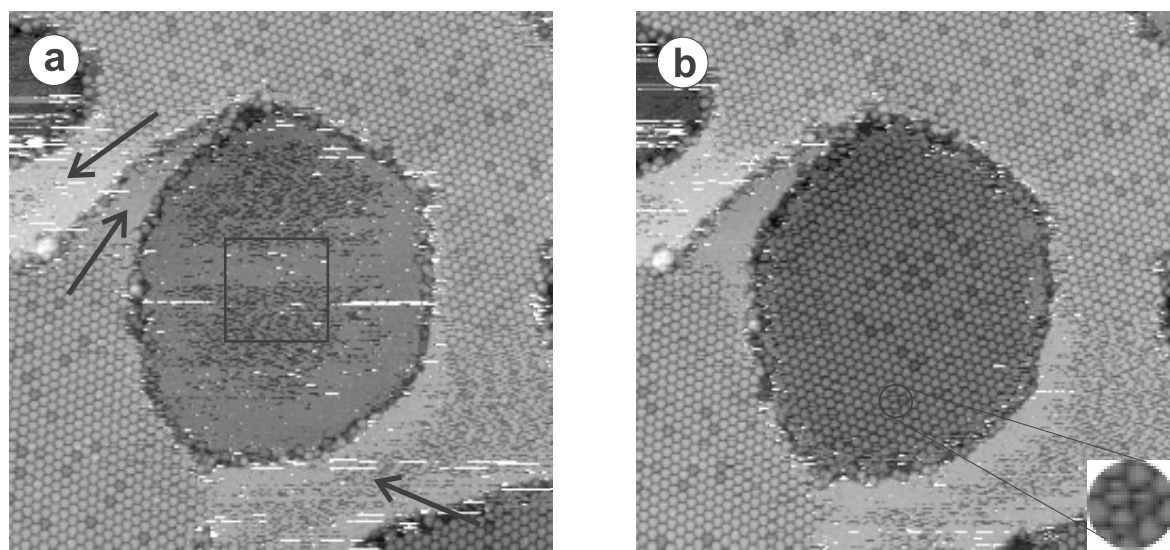not lead to a characteristic change in the condensation experiment.

Figure 6.1.: STM tip-induced nucleation. (a) STM image of a vacancy island filled with a molecular 2D gas phase. A typical scan area for the nucleation mode is shown by the square in the vacancy island. On large terraces the molecules form a hcp pattern which is in coexistence with a 2D gas phase (marked by the arrows). (b) The same vacancy island after the tip-induced condensation process by scanning in the 'nucleation mode'. The molecules inside the vacancy island condensed to the hcp pattern. Various molecules exhibited diffusion during scanning the image, e.g. the ones in the circle. The images (a) and (b) are taken with exactly the same scanning and tunneling parameters (scan range 90x90 nm; $I = 10$ pA, $U = 1.2$ V).

The tip-induced nucleation was not successful for all vacancy islands. Even at high voltages the tip-induced condensation process was not successful for vacancy islands smaller than 35 nm. A tendency was observed that larger islands condense more easily than small ones. However, the biggest vacancy island, which was not possible to condensate, had a diameter of 65 nm. In some experiments the molecules condensed in the 'nucleation mode', nevertheless no condensed phase was observed in the 'imaging mode', i.e. the vacancy island was still filled with gas phase when scanning in the 'imaging mode'. Therefore the successful ordering depends on more than just the size of the vacancy island. The condensation process is expected to depend also on the lattice registry at the border of the vacancy island and on the electric field of the tip and thus on its quality. Since the inter-molecular distance is much larger than the lattice constant of Ag, a misfit of the molecular overlayer with the vacancy island is possible, which probably destabilizes the whole layer.

The tip induced phase transition in the vacancy island caused by scanning in the 'nucleation mode' did only influence the molecules inside the vacancy island. The pattern on the terrace surrounding the vacancy island remains unchanged during the scanning in the 'nucleation mode'. This excludes a significant mass transport of molecules over the step edge. The STM tip is expected to act as a nucleation center, which triggers the nucleation process in the 2D gas phase. This assumption is further confirmed by additional experiments

regarding the condensation process. Experiments about the nucleation center revealed that the condensation propagates over the whole vacancy island if a stable nucleation center is achieved. This is experimentally shown by scanning in the 'nucleation mode' in one corner of the vacancy island and subsequent scanning in the 'imaging mode' without overlap with the previous scan area from the 'nucleation mode'. In such experiments the hcp pattern was observed in the vacancy island. Therefore the condensation propagates over the whole vacancy island, if a stable nucleation center is achieved. From the experimental findings it is expected that the size of a stable nucleation center is in the order of 30 nm.

At a first glance one might expect that the vacancy island in Fig. 6.1b is completely filled with molecules in the hcp pattern. But under careful inspection of the image, stable molecules are only observed in the center of the vacancy island, whereas the molecules around this center are mobile[3]. Therefore the vacancy island is not completely filled with molecules but the density corresponds to approximately 0.7 ML as measured by the micro balance. Time lapse imaging revealed that the vacancy islands which have been ordered by the tip-induced condensation remain in the hcp pattern and do not decay back into the gas phase during observation times up to 90 minutes. In the hcp pattern a certain amount of 'small' molecules appear, which have a different apparent height due to a different LDOS (section 3.2). However, time lapse imaging sequences revealed that during the condensation process or right afterwards no 'small' molecules appear in the vacancy island. But the number of 'small' molecules in the pattern increases with ongoing time. A striking feature of the 'small' moleules is that they appear only in the center of the vacancy island, where the molecules in the hcp pattern are stable. The density of 'small' molecules saturates below 10%, which is consistent with the density on large terraces. This spread out of the 'small' molecules could originate from a stress relaxation of the molecular layer on a time scale accessible by the STM.

The very interesting point about this tip induced condensation is that the phase transition of the molecules in the vacancy island can be reversed. After scanning a few images with negative sample bias no ordered layers are observed anymore. In these images with negative sample bias the silver step edges are decorated as in the images with positive bias, but on the terraces only a dense 2D gas phase is present. It is important to note that the terraces are filled with mobile molecules forming a 2D gas phase and are not empty (section 4.2). After switching back the bias voltage to positive sample bias, the hcp pattern appears immediately[4] on the terraces whereas in the vacancy island the 2D molecular gas phase remains, i.e. the initial situation is obtained as before the tip-induced condensation by scanning in the 'nucleation mode'. Therefore an additional STM mode is defined in analogy to the previous ones: In the 'erase mode' a few images are recorded with a scan range of 90–110 nm and tunneling parameters of $I = 10$–20 pA, $U = -1.2$ to -1.8 V. Thus a condensed vacancy island is reversed to the gas phase by using the 'erase mode'. Consequently, a controlled and reversible phase transition in the vacancy island between a 2D condensed and a 2D gas phase is possible using the 'nucleation mode', 'erase mode' respectively, and subsequent

---

[3]The molecules with a stripe in the fast scanning direction (left-right) are identified as mobile molecules. These stripes in the molecules arise from molecular jumps.

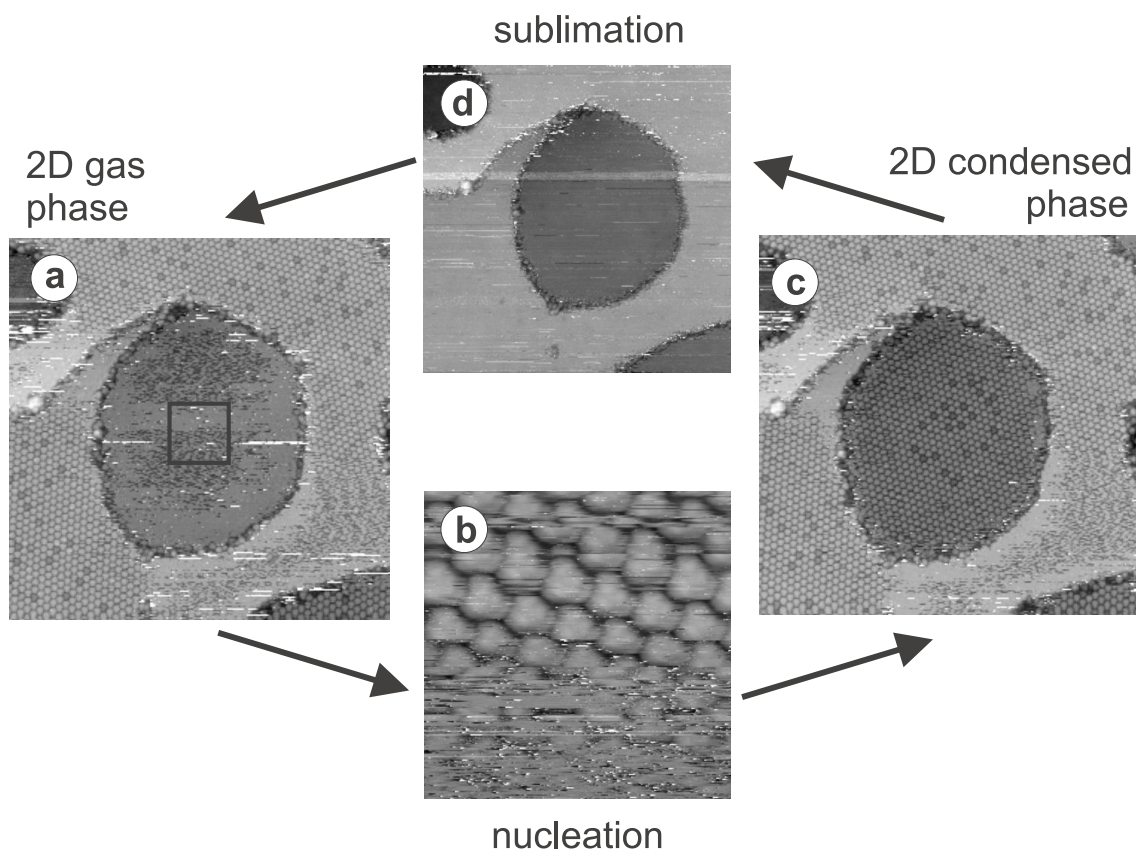[4]Immediately means faster than the time scale accessible by the STM.

Figure 6.2.: Reversible phase transition of the molecular layer in the vacancy island. By tip induced experiments it is possible to control the phase of this molecular layer between a 2D gas phase (a) and a 2D condensed phase (c). The condensation of the gas phase is achieved by scanning several images inside of the vacancy island with a small scan frame ('nucleation mode'). Such an image is shown in (b) where the nucleation to the hcp pattern started during scanning the image. STM images with negative sample bias (d) are recorded in order to sublime the condensed phase into the gas phase ('erase mode'). The gas phase (a) and the condensed phase (c) are taken with exactly the same scanning and tunneling parameters. This excludes that the two phases are obtained due to imaging at different tunneling conditions. Scan range: (a) and (c): 90x90 nm, $I = 10$ pA, $U = 1.2$ V; (b) 11x11 nm, $I = 10$ pA, $U = 1.2$ V; (d) 90x90 nm, $I = 10$ pA, $U = -1.2$ V

observation in the 'imaging mode' (Fig. 6.2). In Fig. 6.3 an experimental sequence of the controlled and reversible phase transition is shown. From Fig. 6.3b to Fig. 6.3d a change in the orientation of the hcp pattern occured. This is an additional evidence that the different images are not due to imaging artefacts but that phase transitions between the condensed phase and the gas phase take place. This tip-induced switching mechanism of the overlayer pattern could be repeated several times.

There are many examples of tip induced experiments reported in the literature. Besides the manipulation of single atoms [14] and molecules [15], the tip-induced chemical reaction of molecules [120], many experiments with tip induced adsorbate and island diffusion are re-
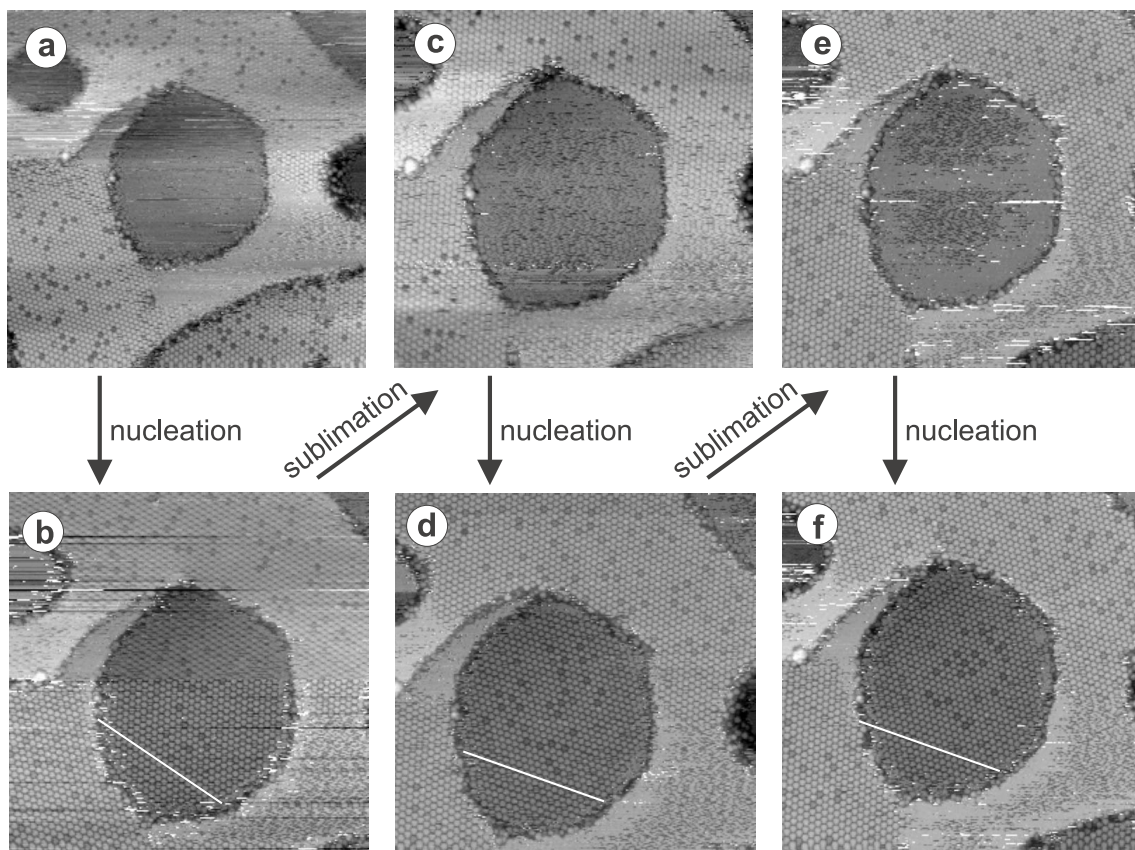
Figure 6.3.: Experimental sequence of the reversible phase transition between the 2D condensed phase and the 2D gas phase controlled by the STM tip. For the condensation of the 2D gas phase inside the vacancy island (e.g. from (a) to (b)) the 'nucleation mode' is used, whereas for the 2D sublimation (e.g. from (b) to (c)) the 'erase mode' is used. The orientation of the hcp pattern is marked by the white line and changed from (b) to (d). The images (a)-(f) are obtained in the 'imaging mode' (positive sample bias). Scan range: (a) 110x110 nm, (b)–(f) 90x90 nm.

ported [74, 79, 121–123]. But to my knowledge there is no example reported in the literature where experiments succeeded to reversible change the phase of a molecular overlayer from a condensed phase into a gas phase and vice versa. Remember that the condensed phase and the gas phase are imaged with exactly the same tunneling and scanning parameters and the phase transition is therefore not due to imaging under different tunneling conditions. Both phases, the gas phase and the condensed phase inside the vacancy island, exist under exactly the same conditions at room temperature. Consequently, one of these two phases is in a metastable state. Either the condensation of the gas phase is delayed (supersaturation) or the sublimation of the condensed phase is delayed ("Siedeverzug") [124]. It is assumed that the gas phase is metastable and the system can not overcome the activation energy for a stable nucleus [125, 126]. By scanning in the 'nucleation mode' the tip provides additional energy to overcome the activation energy to form a stable nucleus and nucleation of the vacancy island takes place.
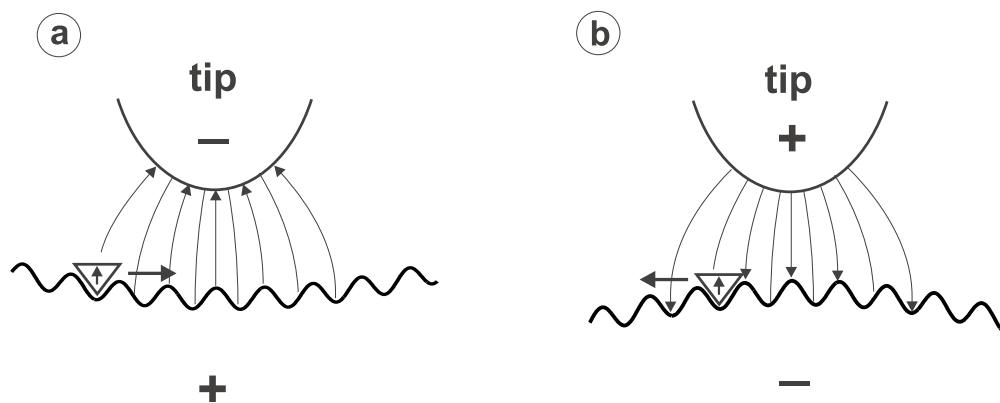
Figure 6.4.: Schematic diagram explaining the directional diffusion of the SubPc molecule due to its permanent dipole moment (marked by the vertical arrow) interacting with the inhomogeneity of the electric field of the tip. The potential energy curve leads to diffusion (a) towards the tip for positive sample bias whereas (b) negative sample bias leads to diffusion away from the tip.

In the following a microscopic model for the tip-induced phase transition is proposed. Local density variations within a 2D mobile phase could arise due to the electric field of the tip. It has been shown that the electric field of the tip induces a directional diffusion of alkali adatoms towards the tip or away from the tip depending on the polarity of the bias voltage [88, 127]. In case of the SubPc molecule the permanent dipole moment is pointing away from the Ag(111) surface, since the molecule adsorbs with the Cl towards the Ag substrate (section 4.1). This dipole moment experiences a force in the inhomogeneous electric field of the tip. Figure 6.4 shows schematically how the inhomogeneity of the electric field of the tip influences the diffusion of the molecules depending on the sign of the bias voltage. Due to the dipole moment of the SubPc pointing away from the surface, a positive sample bias will influence the diffusion in the direction towards the tip since the energy minimum is underneath the tip. Therefore a positive sample bias increases the molecular density underneath the tip and the molecules are trapped in the additional potential of the tip. Consequently, the tip acts as a nucleation center and a stable nucleus in the vacancy island is likely achieved. On the other hand, the dipole moment of the SubPc molecule is anti-parallel to the electric field of the tip for negative sample bias. Therefore, the induced diffusion away from the tip is enhanced, which leads to a decrease of the local coverage underneath the tip and to the sublimation of the condensed phase to the 2D gas phase. In addition internal molecular motions might be enhanced because of the anti-parallel dipole moment of the SubPc. For instance the wobbling of the whole molecule around the Ag-Cl bond is possibly excited. Such internal degrees of freedom are expected to lower the diffusion barrier in the case of molecules which span over several substrate unit cells [128]. This simple model based on the tip assisted diffusion gives therefore a qualitative explanation of the experimental observations. A further support for this model is the experimental finding that a higher positive sample bias facilitates the condensation process and higher negative sample bias the sublimation process.

7. Conclusions and Outlook

SubPc, a polar molecule with an aromatic π-electron system, shows an interesting phase behavior for the first molecular layer grown on Ag(111). At room temperature two different ordered superstructures, honeycomb and hcp, are observed in coexistence with a 2D lattice gas for increasing molecular coverage. The balance between inter-molecular interactions, molecule-substrate interactions and thermal energy is important for the diffusion of single molecules, island diffusion, nucleation and self-organization in general. In the case of SubPc/Ag(111) single molecules show mobility but tend to form ordered layers which are in coexistence with a 2D lattice gas. The complex phase behavior originates from a combination of attractive and repulsive inter-molecular interactions. However, the molecule-substrate interaction strongly influences the overlayers, since for each pattern, the hcp and the honeycomb, only two possible orientations are observed. For the honeycomb pattern these two different orientations have different chirality although the SubPc molecules themselves are achiral. In the honeycomb and the hcp pattern individual molecules are imaged with sub-molecular resolution as characteristic three lobes. Furthermore, in both patterns the molecules are expected to adsorb on the same adsorption site: an on-top site with the centers of the phenyl rings on hollow sites. However, the orientation of single SubPc molecules with respect to the ordered molecular layers (honeycomb and hcp) can be derived from the charge distribution of single SubPc molecules. Consequently, the inter-molecular interactions play an important role for the formation of the ordered layers. Not only single SubPc molecules diffuse but in some cases also whole overlayers exhibit mobility. For the honeycomb and the hcp patterns a change in orientation of the overlayer island occurred. A flipping process of the island between the two stable orientations of the overlayer pattern is observed. Appearing and disappearing vacancies show in addition the mobility of the SubPc layers. For the honeycomb pattern with its two chiral layers, this flipping process is even a phase transition between the layers with different chirality.

The STM tip-induced phase transition is another interesting feature of the SubPc layers on Ag(111). The STM tip was used to locally control a phase transition between the gas phase and the condensed hcp phase for the molecular overlayers in vacancy islands at room temperature. Surprisingly, both phases are stable at exactly the same conditions and moreover the phase of the confined overlayer could be reversible changed with the STM tip. Therefore one of these two phases is thermodynamically not favored, but is in a metastable phase due to a delay in condensation or in sublimation. This reversible switching mechanism of whole overlayer islands between different phases is a new phenomenon and is expected to base on the electric field of the tip experienced by the polar SubPc molecule. This mechanism is a potential method to reversible change the surface structure in the nanometer regime and thus also physical properties of polar molecular layers, e.g. optical, mechanical or electronic properties. An interesting feature about this switching mechanism is that the driving force

is the electric field and therefore it is potentially feasible to control the overlayer pattern simply by voltage pulses. By arrangement of the vacancy islands in a matrix, a memory device based on this switching mechanism of overlayers might be feasible in the long term.

In the case of the hcp pattern two slightly different binding types of the SubPc to the substrate are observed. This becomes evident in the STM images since some molecules are imaged with a different apparent height due to a different LDOS. Therefore these two binding mechanisms act as 'on-off' states. The 'on' state has a higher apparent height and thus a higher LDOS compared to the 'off' state. Experiments to induce this switching mechanism on purpose did not succeed but it points out that the SubPc molecules on Ag(111) could potentially be used as molecular switches. Thereby it is believed that this switching mechanism is induced by a slightly different adsorption geometry of the molecule due to a small horizontal rotation on the Ag(111).

From XPS, UPS and STM results in conjunction with calculations of the SubPc molecule it is concluded that the intact SubPc adsorbs with the Cl towards the Ag(111) substrate. The frontier orbitals of the SubPc molecule are only slightly influenced by the adsorption on the Ag(111) and therefore it is expected that the SubPc is mainly physisorbed. The additional chemical bond between the Ag and the Cl is concluded to be of minor importance for the π-electron system of the SubPc molecule.

In conclusions, the SubPc molecule shows interesting features on Ag(111) at room temperature, e.g. diffusion, nucleation, self-organization and phase transitions. The non-trivial phase behavior of the first molecular layer is a consequence of the attractive and repulsive inter-molecular interactions in conjunction with the molecule-substrate interaction. Single molecules and even whole ordered overlayers exhibit mobility.

Using a variable temperature STM it would be possible to investigate the complex phase behavior of SubPc/Ag(111) in more detail. Furthermore, it would be possible to study the tip-induced phase transition and the flipping process of molecular islands more quantitatively. In the condensed phase the orientation of individual SubPc molecules is visible and therefore molecular rotation is frozen. However, in the gas phase a rotation or other internal motions of the molecule can not be ruled out. In addition to possible changes of internal degrees of freedom upon diffusion and condensation, changes in conformation are also possible. One may foresee that such additional degrees of freedom may cause characteristic deviations from the ideal lattice gas behavior. Using temperature dependent STM techniques, the inter-molecular and molecule-substrate interactions can be explored in more detail. These interactions are the driving force for the complex phase behavior of SubPc on Ag(111). Such measurements could provide similar information about molecular adsorption, diffusion and 2D phase behavior as specific heat measurements have provided about phase transitions in bulk materials. The system presented here, SubPc adsorbed on Ag(111), appears to be a good model system to study such effects.
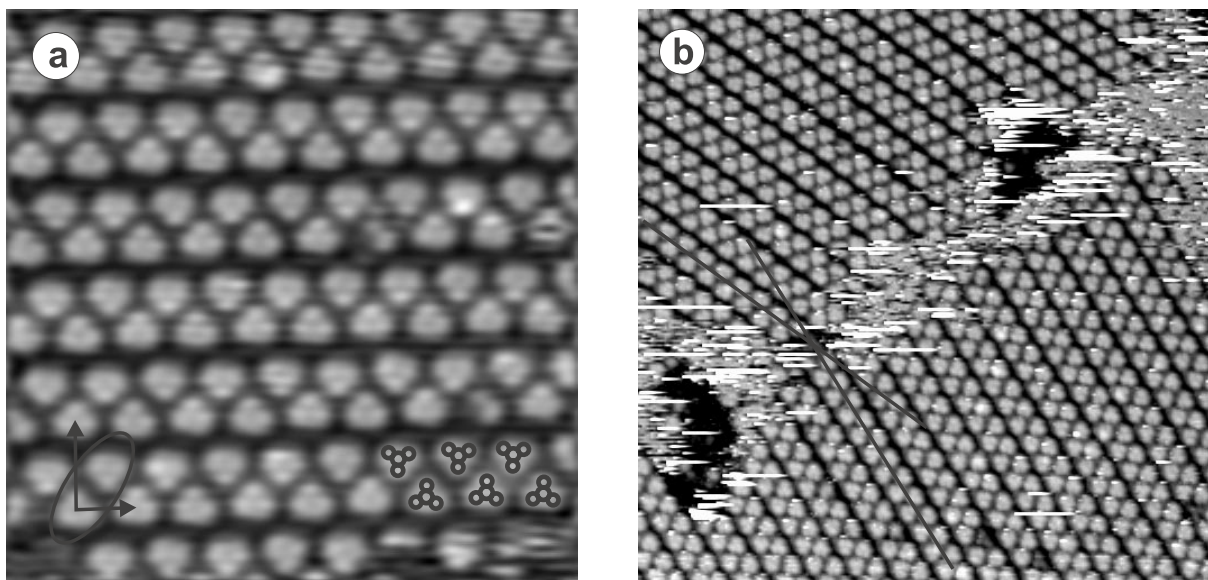
A. Double Row Pattern

Figure A.1.: STM images of the 2D double row pattern. (a) The molecules in one double row are arranged like in a zipper. The internal structure of the SubPc is outlined at the bottom right for one double row. The basis consisting of two SubPc and the corresponding Bravais vectors are indicated (scan range 22x22 nm, $I = 10$ pA, $U = 1.3$ V). (b) Domain boundary of the double row pattern. The mismatch angle is indicated by the black lines (scan range 56x56 nm, $I = 10$ pA, $U = 1.1$ V).

In a single preparation of a SubPc layer on Ag(111) a double row pattern has been observed. This pattern is not yet reproduced and therefore only presented in this appendix. The coverage of the molecular layer was slightly below 0.5 ML. Figure A.1 shows STM images of the double row pattern which has low symmetry and differs from the honeycomb and the hcp pattern. The molecules in one double row are arranged like in a zipper, where two adjacent double rows are spaced by a small distance. Like in the case of the honeycomb and the hcp pattern, individual molecules are resolved as triangular structures with the three characteristic protrusions. The basis consisting of two SubPc and the corresponding Bravais vectors for the double row pattern are drawn in Fig. A.1a. The angle between these two vectors is 86° and the length of the Bravais vectors are 20.2 Å, 30.2 Å respectively. This unit cell leads to a molecular density of 0.26 molecules/nm^2 which is only slightly higher than the one from the honeycomb pattern. Therefore the molecular density of the double row pattern is between the one of the honeycomb and the hcp pattern, which corresponds

well to the layer thickness measured by the quartz micro balance. As in the case of the hcp and honeycomb pattern, the arrangement of the SubPc molecules in the double row pattern can be explained by the charge distribution of the molecules. In each double row, the 'legs' pointing to the center of the 'zipper' are next to the electron-rich N-atoms of the phthalocyanine macro cycle. This leads to a relative small inter-molecular distance in the double row. On the other hand, the repulsion of the 'legs' leads to the observed gap between two adjacent double rows.

The double row pattern is in coexistence with a 2D gas phase as observed in the case of the honeycomb and the hcp pattern. Figure A.1b shows a domain boundary of the double row pattern. The angle between these two domains is approximately 20°. This domain boundary excludes that the double row pattern is caused by a tip artefact, e.g. due to a double tip. Some of the islands with the double row pattern are observed by scanning overview images in the order of 100 nm. However, in many overview images only 2D gas phase and no ordered islands are observed. By scanning images with a scan range of approximately 10 nm it was possible to nucleate islands underneath the STM tip. These nucleated islands could usually be imaged with scan ranges up to 50–60 nm, but disappeared when trying to image them with a scan range of 100 nm. The nucleation of the double row pattern is comparable to the nucleation of the hcp pattern in vacancy islands (Chapter 6).

Bibliography

[1] G.E. Moore, *Cramming more components onto integrated circuits*, Electronics **38** (1965).

[2] M. Schulz, *The end of the road for silicon?*, Nature **399**, 729–730 (1999).

[3] D.A. Muller, T. Sorsch, S. Moccio, F.H. Baumann, K. Evans-Lutterodt, and G. Timp, *The electronic structure at the atomic scale of ultrathin gate oxides*, Nature **399**, 758–761 (1999).

[4] A. Aviram and M. Ratner, *Molecular rectifiers*, Chem. Phys. Lett. **29**, 277–283 (1974).

[5] C. Joachim and J.K. Gimzewski, *An electromechanical amplifier using single molecule*, Chem. Phys. Lett. **265**, 353–357 (1997).

[6] S.J. Tans, A.R.M. Verschuren, and C. Dekker, *Room-temperature transistor based on a single carbon nanotube*, Nature **393**, 49–52 (1998).

[7] A. Bachtold, P. Hadley, T. Nakanishi, and C. Dekker, *Logic circuits with carbon nanotube transistors*, Science **294**, 1317–1320 (2001).

[8] J.-M. Lehn, *Supramolecular chemistry*, Science **260**, 1762–1763 (1993).

[9] J.-M. Lehn, *Supramolecular chemistry*, vol. 277, VCH, Weinheim (1995).

[10] C. Joachim, J.K. Gimzewski, and A. Aviram, *Electronics using hybrid-molecular and mono-molecular devices*, Nature **408**, 541–548 (2000).

[11] T.A. Jung, R.R. Schlittler, and J.K. Gimzewski, *Conformational identification of individual adsorbed molecules with the STM*, Nature **386**, 696–698 (1997).

[12] J.G. Kushmerick, D.B. Holt, J.C. Yang, J. Naciri, M.H. Moore, and R. Shashidhar, *Metal-molecule contacts and charge transport across monomolecular layers: Measurement and theory*, Phys. Rev. Lett. **89**, 86802 (2002).

[13] G.M. Whitesides, J.P. Mathias, and C.T. Seto, *Molecular self-assembly and nanochemistry: a chemical strategy for the synthesis of nanostructures*, Science **254**, 1312–1319 (1991).

[14] D.M. Eigler and E.K. Schweizer, *Positioning single atoms with a scanning tunneling microscope*, Nature **344**, 524–526 (1990).

[15] T.A. Jung, R.R. Schlittler, J.K. Gimzewski, H. Tang, and C. Joachim, *Controlled room-temperature positioning of individual molecules: molecular flexure and motion*, Science **271**, 181–184 (1996).

[16] M.F. Crommie, C.P. Lutz, and D.M. Eigler, *Confinement of electrons to quantum corrals on a metal surface*, Science **262**, 218–220 (1993).

[17] J.K. Gimzewski, E. Stoll, and R.R. Schlittler, *scanning tunneling microscopy of individual molecules of Copper Phthalocyanine adsorbed on polycrystalline silver surfaces*, Surf. Sci. **181**, 267–277 (1987).

[18] P.H. Lippel, R.J. Wilson, M.D. Miller, Ch. Wöll, and S. Chiang, *High-resolution imaging of Copper-Phthalocyanine by scanning tunneling microscopy*, Phys. Rev. Lett. **62**, 171–174 (1989).

[19] C.C. Leznoff and A.B.P. Lever (Eds.), *Phthalocyanines: Properties and Applications*, vol. 1–4, VCH, New York (1989).

[20] M.K. Engel, *Single-crystal and solid-state molecular structures of phthalocyanine complexes*, Rep. Kawamura Inst. Chem. Res. pp. 11–54 (1997).

[21] H. Kietaibl, *Die Kristall- und Molekülstruktur eines neuartigen phthalocyaninähnlichen Borkomplexes*, Monatsh. Chem. **105**, 405–418 (1974).

[22] M.K. Engel, J.Yao, H. Maki, H. Takeuchi, H. Yonehara, and C. Pac, *Synthesis, structural characterization and optical properties of several boron subphthlocyanines and boron β-Isoindigo complex*, Rep. Kawamura Inst. Chem. Res. **9**, 53–65 (1998).

[23] V.R. Ferro, L.A. Poveda, R.H. González-Jonte, J.M. Garcia de la Vega, T. Torres, and B. Del Rey, *Molecular electronic structure of subphthalocyanine macrocycles*, J. Porhpyrins Phthalocyanines **4**, 610–619 (2000).

[24] A. Meller and A. Ossko, *Phthalocyaninartige Bor-Komplexe*, Monatsh. Chem. **103**, 150–155 (1972).

[25] M.J. Frisch et al., *Gaussian 98 Revision A.7*, Gaussian Inc., Pittsburgh PA (1998).

[26] H. Yanagi, D. Schlettwein, H. Nakayama, and T. Nishino, *Site-specific physisorption and chemical reaction of subphthalocyanine molecules on silicon(111)-(7x7)*, Phys. Rev. B **61**, 1959–1964 (2000).

[27] G. Binnig and H. Rohrer, *Scanning tunneling microscopy*, Helvetica Physica Acta **55**, 726–735 (1982).

[28] R. Young, J. Ward, and F. Scire, *Observation of metal-vacuum-metal tunneling, field emission, and the transition region*, Phys. Rev. Lett. **27**, 922–924 (1971).

[29] G. Binnig, H. Rohrer, Ch. Gerber, and E. Weibel, *Surface studies by scanning tunneling microscopy*, Phys. Rev. Lett. **49**, 57–61 (1982).

[30] G. Binnig, H. Rohrer, Ch. Gerber, and E. Weibel, *(111) facets as the origin of reconstructed Au(110) surfaces*, Surf. Sci. **131**, L379–L384 (1983).

[31] A.M. Baró, G. Binnig, H. Rohrer, H. Stoll, A. Baratoff, and F. Salvan, *Real-space observation of the 2x1 structure of chemisorbed oxygen on Ni(110) by scanning tunneling microscopy*, Phys. Rev. Lett. **52**, 1304–1307 (1984).

[32] G. Binnig, H. Rohrer, Ch. Gerber, and E. Weibel, *7x7 reconstruction on Si(111) resolved in real space*, Phys. Rev. Lett. **50**, 120–123 (1983).

[33] C.J. Chen, *Introduction to Scanning Tunneling Microscopy*, Oxford University Press, New York (1993).

[34] R. Wiesendanger and H.-J. Güntherodt (Eds.), *Scanning Tunneling Microscopy III*, Springer-Verlag, Berlin Heidelberg, 2nd ed. (1996).

[35] D. Drakova, *Theoretical modelling of scanning tunneling microscopy, scanning tunneling spectroscopy and atomic force mircroscopy*, Rep. Prog. Phys. **64**, 205–290 (2001).

[36] J. Bardeen, *Tunneling from a many-particle point of view*, Phys. Rev. Lett. **6**, 57–59 (1961).

[37] J. Tersoff and D.R. Hamann, *Theory and application for the scanning tunneling microscope*, Phys. Rev. Lett. **50**, 1998–2001 (1983).

[38] J. Tersoff and D.R. Hamann, *Theory of the scanning tunneling microscope*, Phys. Rev. B **31**, 805–813 (1985).

[39] N.D. Lang, *Spectroscopy of single atoms in the scanning tunneling microscope*, Phys. Rev. B **34**, 5947–5950 (1986).

[40] W.-D. Schneider (ed.), *Scanning Tunneling Spectroscopy*, Journal of Electron Spectroscopy and Related Phenomena **109**, 1–224, special issue (2000).

[41] T.A. Jung, F.J. Himpsel, R.R. Schlittler, and J.K. Gimzewski, *Chemical information from scanning probe microscopy and spectroscopy*, Springer-Verlag, Berlin Heidelberg (1998), in R. Wiesendanger (ed.), *Scanning Probe Microscopy - Analytic Methods*, NanoScience and Technology.

[42] S. Zöphel, J. Repp, G. Meyer, and K.H. Rieder, *Determination of binding sites in ordered phases of CO/Cu(211) employing molecular level manipulation*, Chem. Phys. Lett. **310**, 145–149 (1999).

[43] J.K. Gimzewski, T.A. Jung, M.T. Cuberes, and R.R. Schlittler, *Scanning tunneling microscopy of individual molecules: beyond imaging*, Surf. Sci. **386**, 101–114 (1997).

[44] H. Ohtani, R.J. Wilson, S. Chiang, and C.M. Mate, *Scanning tunneling microscopy observations of benzene molecules on the $Rh(111)$-$(3x3)(C_6H_6+2CO)$ Surface*, Phys. Rev. Lett. **60**, 2398–2401 (1988).

[45] N.D. Lang, *Vacuum tunneling current from an adsorbed atom*, Phys. Rev. Lett. **55**, 230–233 (1985).

[46] N.D. Lang, *Theory of single-atom imaging in the scanning tunneling microscope*, Phys. Rev. Lett. **56**, 1164–1167 (1986).

[47] N.D. Lang, *Apparent size of an atom in the scanning tunneling microscope as a function of bias*, Phys. Rev. Lett. **58**, 45–48 (1987).

[48] D.M. Eigler, P.S. Weiss, E.K. Schweizer, and N.D. Lang, *Imaging Xe with a low-temperature scanning tunneling microscope*, Phys. Rev. Lett. **66**, 1189–1192 (1991).

[49] W. Mizutani, M. Shigeno, K. Kajimura, and M. Ono, *Tunneling through a deformed potential*, Ultramicroscopy **42–44**, 236–241 (1992).

[50] P. Sautet, *Images of adsorbates with the scanning tunneling microscope: theoretical approaches to the contrast mechanism*, Chem. Rev. **97**, 1097–1116 (1997).

[51] H. Hertz, Ann. Physik **31**, 983 (1887).

[52] A. Einstein, *Über einen die Erzeugung und Verwandlung von Licht betreffenden heuristischen Gesichtspunkt*, Ann. Physik **17**, 132 (1905).

[53] J. Wider, *Untersuchungen zum Ad- und Absorptionsverhalten von Sauerstoff auf Rh(111)*, diploma thesis, Institut für Physik der Universität Zürich (1997).

[54] S. Hüfner, *Photoelectron spectroscopy, second edition*, Springer Verlag, Berlin (1996).

[55] M.P. Seah and W.A. Dench, *Quantitative electron spectroscopy of surfaces: a standard data base for electron inelastic mean free paths in solids*, Surf. Interface Anal. **1**, 2–11 (1979).

[56] T.M Schaub, *Untersuchung nichtperiodischer Oberflächen im Ultrahochvakuum mittels Rastertunnelmikroskopie*, Ph.D. thesis, Institut für Physik der Universität Basel (1994).

[57] D.E. Bürgler, C.M. Schmidt, J.A. Wolf, T.M. Schaub, and H.-J. Güntherodt, *Ag films on Fe/GaAs(001): from clean surfaces to atomic Ga structures*, Surf. Sci. **316**, 295–305 (1996).

[58] C.M Schmidt, *Magnetic Interlayer Exchange Coupling in Fe/Cr/Fe(001) Trilayers is Correlated to Nanometer Scale Lateral Interface Structure*, Ph.D. thesis, Institut für Physik der Universität Basel (1998).

[59] F. Meisinger, *Rastersondenmikroskopie an magnetischen Systemen*, Ph.D. thesis, Institut für Physik der Universität Basel (1999).

[60] A.A. Baski and H. Fuchs, *Epitaxial growth of silver on mica as studied by AFM and STM*, Surf. Sci. **313**, 275–288 (1994).

[61] A. Zangwill, *Physics at surfaces*, Cambrige University Press, Cambridge (1988).

[62] H. Yanagi, K. Ikuta, H. Mukai, and T. Shibutani, *STM-induced flip-flop switching of adsorbed subph-thalocyanine molecular arrays*, Nano Lett. **2**, 951–955 (2002).

[63] R. Viswanathan, J.A. Zasadzinski, and D.K. Schwartz, *Spontaneaous chiral-symmetry breaking by achiral molecules in a Langmuir-Blodgett-Film*, Nature **368**, 440–443 (1994).

[64] F. Charra and J. Cousty, *Surface-induced chirality in a self-assembled monolayer of discotic liquid crystal*, Phys. Rev. Lett. **80**, 1682–1685 (1998).

[65] J.V. Barth, J. Weckesser, G. Trimarchi, M. Vladimirova, A. de Vita, C. Cai, H. Brune, P. Günter, and K. Kern, *Stereochemical effects in supramolecular self-assembly at surfaces: 1-D versus 2-D enantiom-rophic ordering of PVBA and PEBA on Ag(111)*, J. Am. Chem. Socc. **124**, 7991–8000 (2002).

[66] E.I. Altman and R.J. Colton, *Nucleation, growth, and structure of fullerene films on Au(111)*, Surf. Sci. **279**, 49–67 (1992).

[67] E.I. Altman and R.J. Colton, *The interaction of C_{60} with noble metal surfaces*, Surf. Sci. **295**, 13–33 (1993).

[68] E. Giudice, E. Magnano, S. Rusponi, C. Boragno, and U. Valbusa, *Morphology of C_{60} thin films grown on Ag(100)*, Surf. Sci. Lett. **405**, L561–L565 (1998).

[69] R. Fasel, P. Aebi, R.G. Agostino, D. Naumović, J. Osterwalder, A. Santaniello, and L. Schlapbach, *Orientation of adsorbed C_{60} molecules determined via X-ray photoelectron diffraction*, Phys. Rev. Lett. **76**, 4733–4736 (1996).

[70] R. Gomer, *Diffusion of adsorbates on metal surfaces*, Rep. Prog. Phys. **53**, 917–1002 (1990).

[71] J.V. Barth, *Transport of adsorbates at metal surfaces: From thermal migration to hot precursors*, Surf. Sci. Rep. **40**, 75–149 (2000).

[72] A. Patrykiejew, S. Skolowski, and K. Binder, *Phase transitions in adsorbed layers formed on crystals of square and rectangular surface lattice*, Surf. Sci. Rep. **37**, 207–344 (2000).

[73] G.L. Kellogg, *Field ion microscopy studies of single-atom surface diffusion and cluster nucleation on metal surfaces*, Surf. Sci. Rep. **21**, 1–88 (1994).

[74] Y.W. Mo, *Direct determination of surface diffusion by displacement distribution measurement with Scanning Tunneling Microscopy*, Phys. Rev. Lett. **71**, 2923–2926 (1993).

[75] J.V. Barth, T. Zambelli, J. Wintterlin, R. Schuster, and G. Ertl, *Direct observation of mobility and interactions of oxygen molecules chemisorbed on the Ag(110) surface*, Phys. Rev. B **55**, 12902–12905 (1997).

[76] T. Zambelli, J. Trost, J. Wintterlin, and G. Ertl, *Diffusion and atomic hopping of N atoms on Ru(0001) studied by Scanning Tunneling Microscopy*, Phys. Rev. Lett. **76**, 795–798 (1996).

[77] M. Schunack, T.R. Linderoth, F. Rosei, E. Lægsgaard, and F. Besenbacher, *Long jumps in the surface diffusion of large molecules*, Phys. Rev. Lett. **88**, 156102 (2002).

[78] M. Böhringer, W.-D. Schneider, and R. Berndt, *Scanning tunneling microscope-indcuced molecular motion and its effect on the image formation*, Surf. Sci. **408**, 72–85 (1998).

[79] M. Böhringer, W.-D. Schneider, R. Berndt, K. Glöckler, M. Sokolowski, and E. Umbach, *Corrugation reversal in scanning tunneling microscope images of organic molecules*, Phys. Rev. B **57**, 4081–4087 (1998).

[80] B. Lehner, M. Hohage, and P. Zeppenfeld, *Novel Monte Carlo scheme for the simulation of adsorption and desorption processes*, Chem. Phys. Lett. **336**, 123–128 (2001).

[81] K. Wandelt, *Properties and influence of surface defects*, Surf. Sci. **251/252**, 387–395 (1991).

[82] X. Chen, E.R. Frank, and R.J. Hamers, *Spatially and rotationally oriented adsorption of molecular adsorbates on Ag(111) investigated using cryogenic scanning tunneling microscopy*, J. Vac. Sci. Technol. B **14**, 1136–1140 (1996).

[83] R. Smoluchowski, *Anisotropy of the electronic work function of metals*, Phys. Rev. **60**, 661–674 (1941).

[84] C. Uebing and R. Gomer, *A Monte Carlo study of surface diffusion coefficients in the presence of adsorbate-adsorbate interactions. I. Repulsive interactions*, J. Chem. Phys. **95**, 7626–7635 (1991).

[85] C. Uebing and R. Gomer, *A Monte Carlo study of surface diffusion coefficients in the presence of adsorbate-adsorbate interactions. II. Attractive interactions*, J. Chem. Phys. **95**, 7636–7640 (1991).

[86] C. Uebing and R. Gomer, *A Monte Carlo study of surface diffusion coefficients in the presence of adsorbate-adsorbate interactions. III. Repulsive nearest-neighbor and attractive next-nearest neighbor interactions*, J. Chem. Phys. **95**, 7641–7647 (1991).

[87] T.T. Tsong, *Effects of an electric field in atomic manipulations*, Phys. Rev. B **44**, 13703–13710 (1991).

[88] J.A. Stroscio and D.M. Eigler, *Atomic and molecular manipulation with the Scanning Tunneling Microscope*, Science **254**, 1319–1326 (1991).

[89] Ch. Girard, Ph. Lambin, A. Dereux, and A.A. Lucas, *Van der Waals attraction between two C_{60} fullerene molecules and physical adsorption of C_{60} on graphite and other substrates*, Phys. Rev. B **49**, 11425–11432 (1994).

[90] R.M. Feenstra, A.J. Slavin, G.A. Held, and M.A. Lutz, *Edge melting of the Ge(111) surface studied by scanning tunneling microscopy*, Ultramicroscopy **42–44**, 33–40 (1992).

[91] J.C. Dunphy, P. Sautet, D.F. Ogletree, O. Dabbousi, and M.B. Salmeron, *Scanning-tunneling-microscopy study of the surface diffusion of sulfur on Re(0001)*, Phys. Rev. B **47**, 2320–2328 (1993).

[92] J. Trost, J. Wintterlin, and G. Ertl, *Atomic scale imaging of a 2D fluid-solid equilibrium for Cs and O coadsorbed on a Ru(0001)*, Surf. Sci. Lett. **329**, L583–L587 (1995).

[93] C. Nagl, R. Schuster, S. Renisch, and G. Ertl, *Regular mixing in a two-dimenstional lattice system: the coadsorption of N and O on Ru(0001)*, Phys. Rev. Lett. **81**, 3483–3486 (1998).

[94] J.K. Gimzewski, C. Joachim, R.R. Schlittler, V. Langlais, H. Tang, and I. Johannsen, *Rotation of a single molecule within a supramolecular bearing*, Science **281**, 531–533 (1998).

[95] G. Ertl and J. Küppers, *Low energy electrons and surface chemistry*, VCH, Weinheim, 2nd ed. (1985).

[96] K. Binder and D.P. Landau, *Square lattice gases with two- and three-body interactions: a model for the adsorption of hydrogen on Pd(100)*, Surf. Sci. **108**, 503–525 (1981).

[97] G.-C. Wang, T.-M. Lu, and M.G. Lagally, *Phase transitions in the chemisorbed layer W(110)p(2x1)-O as a function of coverage. I. Experimental*, J. Chem. Phys. **69**, 479–489 (1978).

[98] P.K. Wu, M.C. Tringides, and M.G. Lagally, *Ordering kinetics of a chemisorbed overlayer: O/W(110)*, Phys. Rev. B **39**, 7595–7610 (1989).

[99] K.E. Johnson, R.J. Wilson, and S. Chiang, *Effects of adsorption site and surface stress on ordered structures of oxygen adsorbed on W(110)*, Phys. Rev. Lett. **71**, 1055–1058 (1993).

[100] I. Vattulainen, J. Merikoski, T. Ala-Nissila, and S.C. Ying, *Adatom dynamics and diffusion in a model of O/W(110)*, Phys. Rev. B **57**, 1896–1907 (1998).

[101] I. Vattulainen, S.C. Ying, T. Ala-Nissila, and J. Merikoski, *Memory effects and coverage dependence of surface diffusion in a model adsorption system*, Phys. Rev. B **59**, 7697–7707 (1999).

[102] P. Nikunen, I. Vattulainen, and T. Ala-Nissila, *Non-equilibrium effects in profile evolution measurements of surface diffusion*, Surf. Sci. Lett. **447**, L162–L168 (2000).

[103] D. Briggs, R.A. Marbow, and R.M. Lambert, *An XPS and UPS study of chlorine chemisorption on Ag(110)*, Chem. Phys. Lett. **53**, 462–464 (1978).

[104] R. Hesper, L. H. Tjeng, and G. A. Sawatzky, *Strongly reduced band gap in a correlated insulator in close proximity to a metal*, Europhys. Lett. **40**, 177–182 (1997).

[105] M. R. C. Hunt, P. Rudolf, and S. Modesti, *Localization of substrate-induced modification in the electronic structure of C_{60} at fullerene-metal interfaces*, Phys. Rev. B **55**, 7882–7888 (1997).

[106] H. Lüth, *Surfaces and interfaces of solid materials*, Springer, Berlin Heidelberg, 3rd ed. (1995).

[107] M. Pedio, K. Hevesi, N. Zema, M. Capozi, P. Perfetti, R. Gouttebaron, J.-J. Pireaux, R. Caudano, and P. Rudolf, *C_{60}/metal surfaces: adsorption and decomposition*, Surf. Sci. **437**, 249–260 (1999).

[108] M. Schunack, E. Lægsgaard, I. Stensgaard, I. Johannsen, and F. Besenbacher, *A chiral metal surface*, Angew. Chem. Int. Ed. **40**, 2623–2626 (2001).

[109] F. Rosei, M. Schunack, P. Jiang, A. Gourdon, E. Lægsgaard, I. Stensgaard, C. Joachim, and F. Besenbacher, *Organic molecules acting as templates on metal surfaces*, Science **296**, 328–331 (2002).

[110] R.J. Hamers, R.M. Tromp, and J.E. Demuth, *Scanning tunneling microscopy of Si(001)*, Phys. Rev. B **34**, 5343–5357 (1986).

[111] A. Lo and R.T. Skodje, *Diffusion and evaporation kinetics of large islands and vacancies*, J. Chem. Phys. **111**, 2726–2734 (1999).

[112] A. Bogicevic, S. Liu, J. Jacobsen, B. Lundqvist, and H. Metiu, *Island migration caused by the motion of the atoms at the border: Size and temperature dependence of the diffusion coefficient*, Phys. Rev. B **57**, R9459–R9462 (1998).

[113] J.M. Soler, *Cluster diffusion by evaporation-condensation*, Phys. Rev. B **53**, R10540–R10543 (1996).

[114] S.V. Khare, N.C Bartelt, and T.L. Einstein, *Diffusion of monolayer adatom and vacancy clusters: Langevin analysis and Monte Carlo simulations of their Brownian motion*, Phys. Rev. Lett. **75**, 2148–2151 (1995).

[115] C. DeW. Van Siclen, *Single jump mechanisms for large cluster diffusion on metal surfaces*, Phys. Rev. Lett. **75**, 1574–1577 (1995).

[116] J.-M. Wen, S.-L. Chang, J.W. Burnett, J.W. Evans, and P.A. Thiel, *Diffusion of large two-dimensional Ag clusters on Ag(100)*, Phys. Rev. Lett. **73**, 2591–2594 (1994).

[117] K. Morgenstern, G. Rosenfeld, B. Poelsema, and G. Comsa, *Brownian motion of vacancy islands on Ag(111)*, Phys. Rev. Lett. **74**, 2058–2061 (1995).

[118] J.P. Rabe and S. Buchholz, *Commensurability and mobility in two-dimensional molecular patterns on graphite*, Science **253**, 424–427 (1991).

[119] R. Lüthi, E. Meyer, H. Haefke, L. Howald, W. Gutmannsbauer, and H.-J. Güntherodt, *Sled-type motion on the nanometer scale: Determination of Dissipation and cohesive energies of C_{60}*, Science **266**, 1979–1981 (1994).

[120] S.-W. Hla, L. Bartels, G. Meyer, and K.-H. Rieder, *Inducing all steps of a chemical reaction with the scanning tunneling microscope tip: towards single molecule engineering*, Phys. Rev. Lett. **85**, 2777–2780 (2000).

[121] J. Li, R. Berndt, and W.-D. Schneider, *Tip-assisted diffusion on Ag(110) in scanning tunneling microscopy*, Phys. Rev. Lett. **76**, 1888–1891 (1996).

[122] J.E. Freund, M. Edelwith, J. Grimminger, R. Schloderer, and W.M. Heckl, *STM-induced formation of Ag islands on Ag(111)*, Appl. Phys. A **66**, S787–S790 (1998).

[123] F. Dulot, J. Eugène, B. Kierren, and D. Malterre, *STM-tip induced surface diffusion of copper on copper(100)*, Appl. Surf. Sci. **162–163**, 86–93 (2000).

[124] K. Huang, *Statistical Mechanics*, J. Wiley, New York, 2nd ed. (1987).

[125] J.A. Venables, *Atomic processes in crystal growth*, Surf. Sci. **299/300**, 798–817 (1994).

[126] H. Brune, *Microscopic view of epitaxial growth: nucleation and aggregation*, Surf. Sci. Rep. **31**, 121–229 (1998).

[127] N. Mingo and F. Flores, *Lateral forces and atomic desorption induced by the electric field created by STM tips on metal surfaces*, Surf. Sci. **395**, 342–355 (1998).

[128] J.S. Raut and K.A. Fichthorn, *Diffusion mechanisms of short-chain alkanes on metal substrates: Unique molecular features*, J. Chem. Phys. **108**, 1626–1635 (1998).

List of Publications

Publications

- H. Suzuki, S. Berner, M. Brunner, H. Yanagi, D. Schlettwein, T.A. Jung, and H.-J. Güntherodt, *Characterization of molecular overlayers on metal surface in dynamic equilibrium by scanning tunneling microscope*, Thin Solid Films **393** (2001) 325-328

- S. Berner, M. Brunner, L. Ramoino, H. Suzuki, H.-J. Güntherodt, and T.A. Jung, *Time evolution analysis of a 2D solid-gas equilibrium: A model system for molecular adsorption and diffusion*, Chem. Phys. Lett. **348** (2001) 175-181

- M. de Wild, S. Berner, H. Suzuki, H. Yanagi, D. Schlettwein, S. Ivan, A. Baratoff, H.-J. Güntherodt, and T.A. Jung, *A novel route to molecular self-assembly: Self-intermixed monolayer phases*, ChemPhysChem **10** (2002) 881-885

- M. de Wild, S. Berner, H. Suzuki, L. Ramoino, A. Baratoff, and T.A. Jung, *Molecular assembly and self-assembly: Molecular Nanoscience for future technologies*, Chimia **56** (2002) 500-505

- M. Brunner, S. Berner, H. Suzuki, and T.A. Jung, *Production Method for atomic and molecular patterns on surfaces and nanostructured devices*, PCT Patent Application Nr. WO 02/086200 A1 (2002)

- S. Berner, M. de Wild, L. Ramoino, H. Suzuki, H. Yanagi, D. Schlettwein, S. Ivan, A. Baratoff, H.-J. Güntherodt, and T.A. Jung, *Adsorption and 2D phase behavior of a large polar molecule: SubPc on Ag(111)*, to be submitted

- S. Berner, M. de Wild, L. Ramoino, S. Schintke, A. Baratoff, H.-J. Güntherodt, and T.A. Jung, *2D Molecular phase transition in the nanometer scale controlled by the Scanning Tunneling Microscope tip*, manuscript in preparation

Conference Presentations

- S. Berner, M. Brunner, H. Suzuki, T.A. Jung, and H.-J. Güntherodt, *Molecular patterning in UHV: From deposition to STM experiments*, Talk at the "Workshop on Scanning Probe Microscopies and Organic Materials IX", Hannover (Germany), October 9-11, 2000

- S. Berner, M. Brunner, H. Suzuki, T.A. Jung, and H.-J. Güntherodt, *Deposition system for single molecule STM experiments*, Poster at the "4th Hasliberg Workshop on Nanoscience", Hasliberg (Switzerland), October 16-20, 2000

- S. Berner, M. Brunner, L. Ramoino, H. Suzuki, H. Yanagi, D. Schlettwein, T.A. Jung, and H.-J. Güntherodt,*Two dimensional molecular motion confined by decorated terrace edges: dynamic ecquilibrium in a 2 dimensional 'molecular corrall or bottle'*, Talk at the "17th SAOG Meeting", University of Fribourg (Switzerland), January 25th, 2001

- S. Berner, M. Brunner, L. Ramoino, H. Suzuki, T.A. Jung, and H.-J. Güntherodt, *Two dimensional molecular solid-gas equilibrium observed by Scanning Tunneling Microscopy*, Talk at the "Jahrestagung der Schweizerischen Physikalischen Gesellschaft", EMPA Dübendorf (Switzerland), May 2-3, 2001

- S. Berner, M. Brunner, L. Ramoino, H. Suzuki, T.A. Jung, and H.-J. Güntherodt, *Direct observation of a molecular 2D solid-gas equilibrium by STM*, Talk at the "11th International Conference on Scanning Tunneling Microscopy/Spectroscopy and Related Techniques", Vancouver (Canada), July 15-20, 2001

- S. Berner, M. Brunner, L. Ramoino, H. Suzuki, H.-J. Güntherodt, and T.A. Jung, *Two dimensional molecular solid-gas equilibrium observed by Scanning Tunneling Microscopy*, Poster at the "20th European Conference on Surface Science", Krakow (Poland), September 4-7, 2001

- S. Berner, M. de Wild, L. Ramoino, S. Schintke, H. Suzuki, A. Baratoff, H.-J. Güntherodt, and T.A. Jung, *Reversible layer phase transition triggered by the STM tip*, Talk at the "NANO-7/ECOSS-21 (7th International Conference on Nanometer-scale Science and Technology and 21st European Conference on Surface Science)", Malmö (Sweden), June 24-28, 2002

Acknowledgements

Many people contributed to this PhD thesis. I am grateful to all of them!

I thank Prof. H.-J. Güntherodt for giving me the opportunity and the financial support to work in his group.

I am grateful to my supervisor Dr. Thomas Jung. He was involved in all stages of this work: From the planning and realization of the molecular deposition system to the discussion and interpretation of the experimental data.

I thank Prof. P. Oelhafen for the acceptance of being a referee for this thesis.

I would like to thank the whole crew of the NANOLAB, Dr. Frank Meisinger, Michael de Wild, Dr. Hitoshi Suzuki, Luca Ramoino, Dr. Silvia Schintke, Alex Heuri, Diego Haldemann and Stefan Vock, for the fruitful collaboration and the good atmosphere. In particular I would like to thank Dr. Frank Meisinger for the introduction to the huge UHV system and Michael de Wild, who I learnt to know as Michael Brunner, not only for the time we spent in the lab but also for the time outside of it.

I would like to thank Dr. Alexis Baratoff for his theoretical support in numerous discussions. I was always impressed by his big knowledge. I thank Prof. C. Bruder for his theoretical support concerning the solid-gas coexistence.

I acknowledge Stanislav Ivan, Wilfried Michaelis, Dr. Derck Schlettwein and Dr. Hisao Yanagi for the calculations and the discussions concerning the SubPc molecule. I thank Dr. H. Kliesch and Prof. D. Wöhrle for synthesizing and providing the SubPc molecules.

I would like to express my gratitude to the mechanical workshops for transforming my ideas into reality. Without the big efforts of Sylvester Jakob and Heinz Breitenstein and the work from P. Cattin and his team the deposition system would not have been possible.

I thank H.-R. Hidber and his team from the electronic workshop for taking care of all electronic problems.

I would like to thank A. Kalt, B. Kammermann, J. Vetter and G. Weaver from the secretaries for the administrative work.

I am grateful to Dr. Roland Bennewitz who carefully read the manuscript.

I thank Remo Hofer for his numerous support on computer problems and for answering all my questions concerning "SXM".

I acknowledge the people from the whole Güntherodt and Meyer group for the friendly atmosphere and the numerous discussions during coffee break. Special thanks to Dr. Alex Bouhelier, Adriaan Bredekamp, Dr. Mark Lantz, Leo Merz and Julien Toquant for the numerous "Settlers of Catan" we played.

This work was financially supported from the Swiss National Science Foundation, the TOPNANO21 program and the NCCR on Nanoscale Science.

Last but not least I would like to thank my family for the huge support during my PhD work. A special thanks to Karin who had sometimes to suffer under this work...

Curriculum Vitae

Simon Berner

22.04.1973	geboren in Bern
1980-1985	Besuch der Primarschule in Erlinsbach
1985-1989	Besuch der Bezirksschule in Aarau
1989-1993	Besuch der Kantonsschule in Aarau
Jan. 1993	Maturität Typus C
Okt. 1993	Beginn des Studiums in Physik an der Universität Zürich mit grossem Nebenfach Mathematik und kleinem Nebenfach Informatik
Apr. 1995	1. Vordiplom
Okt. 1996	2. Vordiplom
Okt. 1996 – Juli 1997	Hilfsassistent im Physikpraktikum für Mediziner und Biologen an der Universität Zürich
Juli – Sept. 1997	zweimonatiges Praktikum am Synchrotron des Brookhaven National Lab (USA)
Okt. 1997 – Okt. 1998	Diplomarbeit in der Forschungsgruppe von Prof. J. Osterwalder am Physik-Institut der Universität Zürich mit dem Thema: *"Unterdotieren von Kuprat-Supraleitern mittels ultraviolettem Licht"*
Jan. 1999	Diplomexamen in Experimentalphysik, Abschluss mit "Auszeichnung für die Prüfungsnoten"
März 1999 – Juli 2002	Doktorarbeit und Assistenztätigkeit unter der Leitung von Dr. T.A. Jung in der Gruppe von Prof. H.-J. Güntherodt am Institut für Physik der Universität Basel

Folgenden Dozentinnen und Dozenten verdanke ich meine Ausbildung:

C. Amsler (ZH), A. Baratoff (BS), R. Bennewitz (BS), H. Bitto (ZH), P. Bösiger (ZH), D. Brinkmann (ZH), R. Durrer (ZH), S. Egli (ZH), R. Engfer (ZH), T. Greber (ZH), H.-J. Güntherodt (BS), M. Hegner (BS), M. Hieber (ZH), H.-J. Hug (BS), R. Holzner (ZH), E. Holzschuh (ZH), W. Jaus (ZH), T.A. Jung (BS), W. Kündig (ZH), M. Mali (ZH), P.F. Meier (ZH), E. Meyer (BS), Ch. Okonek (ZH), J. Osterwalder (ZH), F. Ould-Saada (ZH), B.D. Patterson (ZH), H.S. Pruys (ZH), G. Rasche (ZH), J. Roos (ZH), C. Schönenberger (BS), V. Schroeder (ZH), H.C. Sigg (ZH), S. Spanier (ZH), N. Straumann (ZH), D. Wyler (ZH)

BS: Universität Basel
ZH: Universität Zürich